Spring 1-1-2016

A Comparison of Spring Stiffness Profiles for Use in a Passive-Elastic Leg Exoskeleton

John Kearns III
University of Colorado Boulder, kearnsiii@gmail.com

A COMPARISON OF SPRING STIFFNESS PROFILES FOR USE IN A PASSIVE-ELASTIC LEG EXOSKELETON

by

John Kearns III
B.S. California Polytechnic State University, 2012

A thesis submitted to the
Faculty of the Graduate School of the University of Colorado
in partial fulfillment of the requirement for the degree of Master of Science

Department of Mechanical Engineering
2016

This thesis entitled:
A Comparison of Spring Stiffness Profiles for Use in a Passive Leg Exoskeleton

Written by John Kearns III
has been approved for the Department of Mechanical Engineering

_____
Mark Rentschler, Ph.D.

_____
Alena Grabowski, Ph.D.

Date_____

The final copy of this thesis has been examined by the signatories, and we find that both the content and the form meet acceptable presentation standards of scholarly work in the above mentioned discipline.

IRB protocol # 13-0641

John Kearns III (M.S., Mechanical Engineering)

A Comparison of Stiffness Profiles for Use in a Passive-Elastic Leg Exoskeleton

Thesis directed by: Professor Mark Rentschler, Ph.D.

Abstract

Several research groups have pursued the development of a device capable of improving a human's running ability. In 2009, Grabowski and Herr developed a passive-elastic leg exoskeleton that reduced the metabolic demand of hopping by 19 to 28% across a range of hopping frequencies. Hopping is used as an analogue to running because it exhibits similar biomechanical behavior and is more easily studied. Grabowski and Herr's exoskeleton implemented bow springs that had a stiffness that decreased with increasing compression. No study has addressed if this form of non-linearity is the most optimal, or if other spring behaviors could be more effective. In the present study, three exoskeleton spring types were developed with linear, progressively increasing, and progressively decreasing stiffness profiles. The metabolic effort of hopping in place was studied for each stiffness type and compared to hopping with no exoskeleton in three subjects. It was hypothesized that a linear spring profile that matches the near-linear stiffness profile of the human leg would result in the lowest metabolic power compared to the other profiles. Instead, the exoskeleton exhibiting gradually decreasing stiffness was most effective, reducing metabolic power for one subject by up to 32%. Analysis of ground reaction forces suggests that the stiffness profile that results in the lowest metabolic cost would be one that is initially stiff to absorb the energy of impact, and then adopts a stiffness profile which is tuned to allow the leg to adopt a near-linear stiffness while the leg is compressed.

Acknowledgements

Dr. Alena Grabowski and Dr. Mark Rentschler, thank you so much for giving me the opportunity to work on this project, and for supporting my efforts with sage advice and a wealth of experience. Thanks also to the entire AMTL lab group for their expertise, friendliness, and unceasing enthusiasm for puzzling over design problems. Dr. Paolo Taboga and Owen Beck have my heartfelt gratitude for their assistance and expertise in the Applied Biomechanics Lab. I would like to express my sincere thanks to Craig Joy and Greg Potts of the Trades Teaching Lab and the Idea Forge for their manufacturing expertise, and their willingness to share it. Thanks also to Brett Alexander for enthusiastically assisting me with the testing process. Finally, my heartfelt thanks to all my family and friends for their support throughout my academic career.

Table of Contents

Index of Tables

Table of Figures

Chapter 1: Introduction

During bouncing gaits such as running and hopping, prior studies have shown that the muscles and tendons of the leg store and return energy in such a way that they can be effectively modeled as a spring-mass system, in which the mass of the body oscillates on a mass-less linear spring (Cavagna, 1970; Blickhan, 1989). During the first half of stance phase, the tendons store elastic energy, and during the second half of stance, this energy is returned to accelerate the body mass. The muscles contract eccentrically and concentrically and optimize the energy storage and return in the tendon and thus require metabolic energy. The goal of developing a passive-elastic leg exoskeleton is to reduce the metabolic energy requirements of the leg muscles by optimizing the in-parallel elastic energy storage and return. This study introduces a spring leg exoskeleton which can absorb some of the kinetic energy during the first half of stance phase as spring potential energy, and then release that energy once again during the second half of the stance phase.

This project's parent study showed that a passive-elastic exoskeleton in parallel with the legs can reduce the metabolic energy required for hopping (Grabowski and Herr, 2009). This study expands on the results of its predecessor by seeking to assess what mechanism and spring behavior best reduces the workload placed on the body during running. Once this is firmly established, there are a variety of applications for devices that can effectively absorb and return elastic energy. These include therapeutic, rehabilitative, and augmentative approaches to running.

In the first place, a device which reduces the effort of running can be used in conjunction with patients who are limited by respiratory or muscular illness, and have difficulty exercising enough to stay healthy. By reducing the effort involved in running, exercise can be made more accessible to people with a variety of illnesses. Furthermore, leg exoskeletons can allow injured patients to re-accustom their bodies to running while reducing the forces borne by their legs. Reducing the metabolic effort and forces experienced during running, but preserving the motions involved, could help atrophied muscles regain flexibility and gently ease them into the rigor of use. Finally, the ability to enhance a human's ability to run long distances at minimal effort can be useful for many professions. From a military perspective, leg exoskeletons can improve a soldier's ability to travel distances on foot while laden with gear. The same concept applies to rescue workers who must carry heavy equipment loads across difficult terrain, traveling quickly to respond to medical emergencies. These examples show that a passive-elastic leg exoskeleton has the potential to benefit a wide section of the human population, from chronic illness patients to healthy people with physically demanding employment or hobbies. To deliver the best benefit possible, however, it is necessary to assess the best design for such a device.

Chapter 2: Background

2.1 Running Gait Mechanics

It has been well established that the overall mechanics of the body during bouncing gaits, including the complicated interactions of muscles and tendons in the leg, as well as multiple degrees of freedom in the joints, demonstrate overall behavior that is well-modeled as a simple spring-mass system (Blickhan, 1989; Farley, 1991; McMahon, 1987). In studies such as this one, hopping is examined as an analogue for running because it is a proxy for running, but occurs in one dimension and doesn't have a leg swing phase. Although the legs contact the ground simultaneously instead of in alternating fashion, the behavior of the legs is similar between the two gaits (Farley, 1998; Ferris, 1997). Experimental evidence shows that leg stiffness is independent of both speed and body mass for running, implying that the "inherent properties of the musculoskeletal system" determine the leg stiffness (Ferris, 1998).

Studies have shown that people modulate their leg stiffness to account for the stiffness of the in-series ground surface. If leg stiffness were constant, it follows that the spring-mass system would exhibit noticeably different behavior when running on varying surfaces; running on compliant surfaces would cause the body's mass to move more, and vice versa. Instead, when a human runs or hops on different surfaces, leg stiffness changes to maintain *overall* stiffness. Spring elements in series follow the reciprocal rule:

When $k_{surface}$ changes, the body adjusts k_{leg} to preserve a constant k_{total}. This is true for wide variations of surface stiffness; the surface stiffness can vary by up to three orders of magnitude without measurably affecting the body's ability to maintain the overall system stiffness (Ferris, 1997; Kerdok, 2002).

Computer modeling and combined ultrasound imaging and motion studies suggest complicated interactions between muscle groups and tendons. As a human transitions from walking to running, the peak calf muscle fiber velocity drastically decreases, facilitating a greater peak force (Farris, 2012). The muscle applies greater force, but more and more of the total elastic deformation occurs in the tendons as frequencies increase (Biewener, 1998). Furthermore, the angles of the leg joints change through a stride cycle, which affects the elastic deformation of tendons (Holt, 2014); an important element in determining overall stiffness (Krishnaswamy, 2011).

Farley et al. found that the largest determining factor in overall leg stiffness is the stiffness of the ankle joint, with lesser contributions from the knee (Farley, 1998). This study used experimental evidence to show that leg stiffness is predominantly sensitive to ankle stiffness, with the stiffness and position of the other joints playing minor stabilizing roles. In fact, the sensitivity of overall leg stiffness to an individual joint seemed to increase dramatically with the joint's proximity to the ground. As a result, many subsequent studies have focused on augmenting the ankle when trying to improve hopping and walking performance (Collins, 2015; Ferris, 2006; Malcolm, 2013).

One of the most common means of understanding how difficult a physical activity is involves studying the metabolic rates of the person during the activity. Comparing the rates of oxygen consumption and carbon dioxide production is a reliable way of measuring sub-maximal metabolic effort (Brooks, 2000). The net metabolic cost of an activity is the gross metabolic cost minus the cost of standing.

2.2 Prior Work

The following sections will examine prior work done in the area of braces and exoskeletons that attempted to augment human performance in a variety of ways. The term “exoskeleton” is used broadly in the biomechanics community, but is generally defined as a device that attaches to the human body and uses mechanical and possibly electromechanical components to assist or augment the body’s ability to perform mechanical tasks.

2.2.1 Powered Exoskeletons

The most straightforward means of categorizing leg exoskeletons is by their designer’s approach to power. Electronically powered leg exoskeletons generally face a different set of design challenges than unpowered or passive exoskeletons, and each have a different set of strengths and weaknesses. Two prominent examples of notable powered leg exoskeletons are the Berkeley Lower Extremity Exoskeleton, commonly abbreviated to BLEEX, and the Hybrid Assistive Limb (HAL), produced by the Cyberdyne Corporation (Figure 1). These two devices use different approaches to augment performance. The BLEEX uses linear actuators to directly support the physical loads

being placed on the body, while the HAL applies joint torques to assist, but not structurally support, the leg.

Figure 1. The Berkeley Lower Extremity Exoskeleton (left), and Cyberdyne's HAL exoskeleton (right). Both of these exoskeletons assist human locomotion and are powered by a battery they house in their own structures, but they interact with their users in different ways. [A] [B]

The BLEEX (shown in Figure 1, left) is an exoskeleton developed by the Berkeley Robotics and Human Engineering Laboratory in 2006. It uses hydraulic actuators to bear the load of the legs. It includes a backpack with a battery, making it energetically autonomous. It allows for the legs to move with three degrees of freedom at the hip, one

at the knee, and three at the ankle; it only provides power to flex each of these joints, however, allowing free rotation at the hip and ankle during walking.

BLEEX uses a large array of encoders and accelerometers to detect the position, velocity, and acceleration of the user's leg. With this information, its control system operates bidirectional hydraulic actuators to bear the vertical loads of walking (Cenciarini, 2011). As of today, the Ekso Bionics company, formerly Berkeley Bionics, has developed the BLEEX into a commercial product, called the Ekso, first released in 2012. There is currently no peer-reviewed material that discusses the Ekso's technical capabilities; however, the BLEEX was capable in 2006 of supporting a 75 kg load while walking at 0.9 m/s (Zoss, 2006).

The HAL (Figure 1, right) represents a different approach to powered exoskeletons. Rather than support an external load independently, the HAL was developed to augment the torque output of the leg joints. The HAL differs from the BLEEX in that it does not transfer force directly to the ground, but rather applies extra torque at each joint, allowing for both augmentative and rehabilitative applications (Herr, 2009). HAL uses EMG electrodes placed on the surface of the skin to detect muscle activation, as well as accelerometers and potentiometers to detect limb positions. DC motors operate at each exoskeletal joint to assist the walking gait (Kawamoto, 2003). Like the Ekso, HAL is a current commercial product with limited technical data available; however, the company website (www.cyberdyne.jp) reports that the exoskeleton allows users to lift

objects of up to 70 kg, and increases leg press capability by up to 80 kg. No studies have been carried out to assess the HAL's benefit to walking.

The HAL and the BLEEX are emblematic of design concerns that powered exoskeletons face. Both are heavy – weighing 20 kg or more – and only assist walking. The added weight of a battery is not only an additional load that the exoskeleton must bear, but it can also disturb the user's balance by altering the distribution of weight on their torso (Zoss, 2005). Although both of these exoskeletons have enormous potential to improve human quality of life by assisting walking and load-carrying, there is an opportunity for lighter, longer-lasting, faster-moving exoskeletons to offer benefits that these exoskeletons cannot.

In 2013, a study was conducted at Ghent University in Belgium to assess the effectiveness of a powered ankle exoskeleton which assisted planar flexion of the foot. This exoskeleton achieved positive results, reducing the metabolic cost of walking by 6±2% from the cost of walking without an exoskeleton. However, the study also discovered that the ankle flexes enough during walking that an unpowered exoskeleton could be implemented and offer significant benefit (Malcolm, 2013). This paved the way for another powered exoskeleton – this one autonomous and powered by an on-board power supply (Mooney, 2014) – but also for another ankle orthosis that used a spring in conjunction with a mechanical clutch to accomplish the same task without requiring any power input whatsoever. This ankle orthosis, developed by Collins et al. in 2015, is discussed in the next section.

2.2.2 Unpowered Exoskeletons

A number of exoskeleton inventors have attempted to improve running performance by artificially extending the length of the wearer's leg, creating a structure that operates in series, rather than in parallel, with the user's legs (Dick, 1991; Herr, 1997). However, although these devices offer some benefit, such as improved jumping height, none have been able to significantly improve the metabolic cost of running (Herr, 2009). Two exoskeletons have reduced the metabolic cost of walking or hopping without using powered means.

Collins et al. (2015) designed and implemented a passive ankle exoskeleton that reduced the metabolic cost of walking by 7.2% compared to walking without the exoskeleton (Figure 2). This is the only known passive device that reduces the metabolic cost of walking. The reduction in metabolic cost is comparable to those reported by the powered ankle exoskeletons developed in Malcolm, 2013, and Mooney, 2014. Achieving the same performance without requiring any power input or bulky battery infrastructure offers a great benefit in weight and convenience. Collins et al. also developed an exoskeleton clutch that reliably disengages and then re-engages with precise timing to allow forward locomotion. This is one of the critical hurdles that unpowered exoskeletons need to overcome in order to be useful in the large scale.

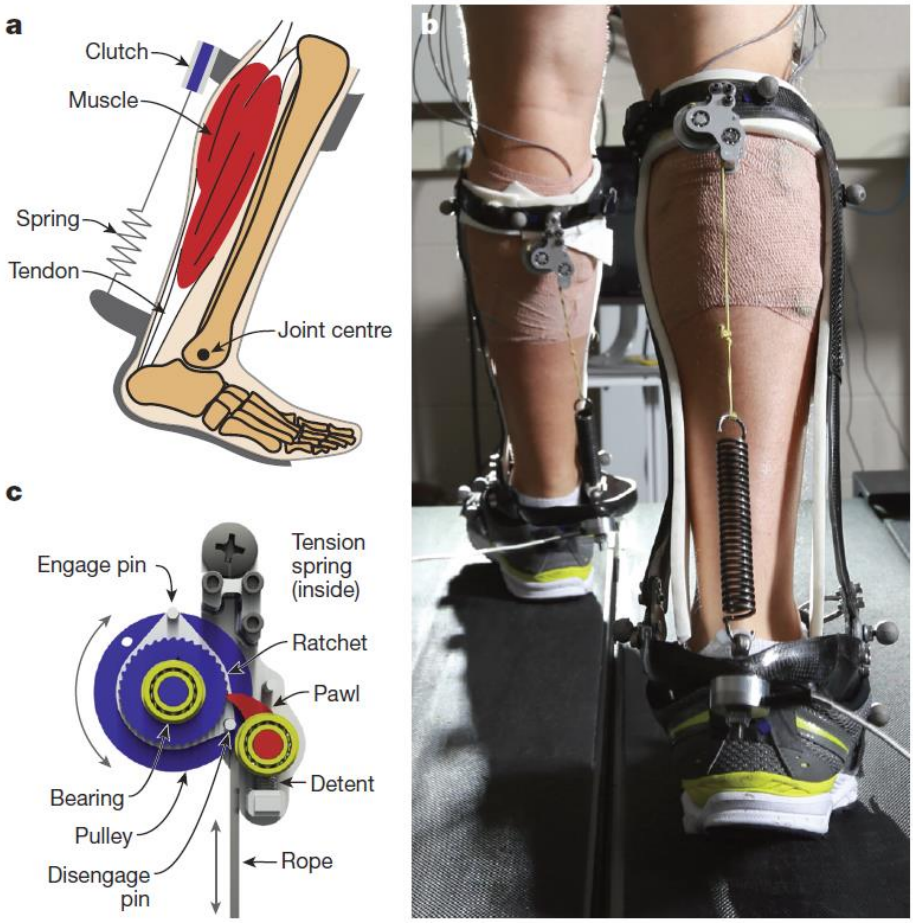

Figure 2. The unpowered ankle exoskeleton presented by Collins et al. **a** This exoskeleton is implemented in parallel with the calf muscles and Achilles tendon, using a coil spring in tension and a disengage mechanism at the upper end of the coil. **b** The device is shown in use on a treadmill, attaching at the ankle above a shoe and just below the knee. **c** A detail of the passive clutch mechanism, showing the ratchet and pawl as well as the pins that engage and disengage the pawl to allow walking (Collins, 2015).

In contrast to the walking exoskeleton developed by Collins et al., another unpowered exoskeleton, developed in 2009, focused on improving human running and hopping performance. The exoskeleton developed by Grabowski and Herr (2009) implemented fiberglass bow springs in parallel with the entire leg. This exoskeleton is shown in Figure 3.

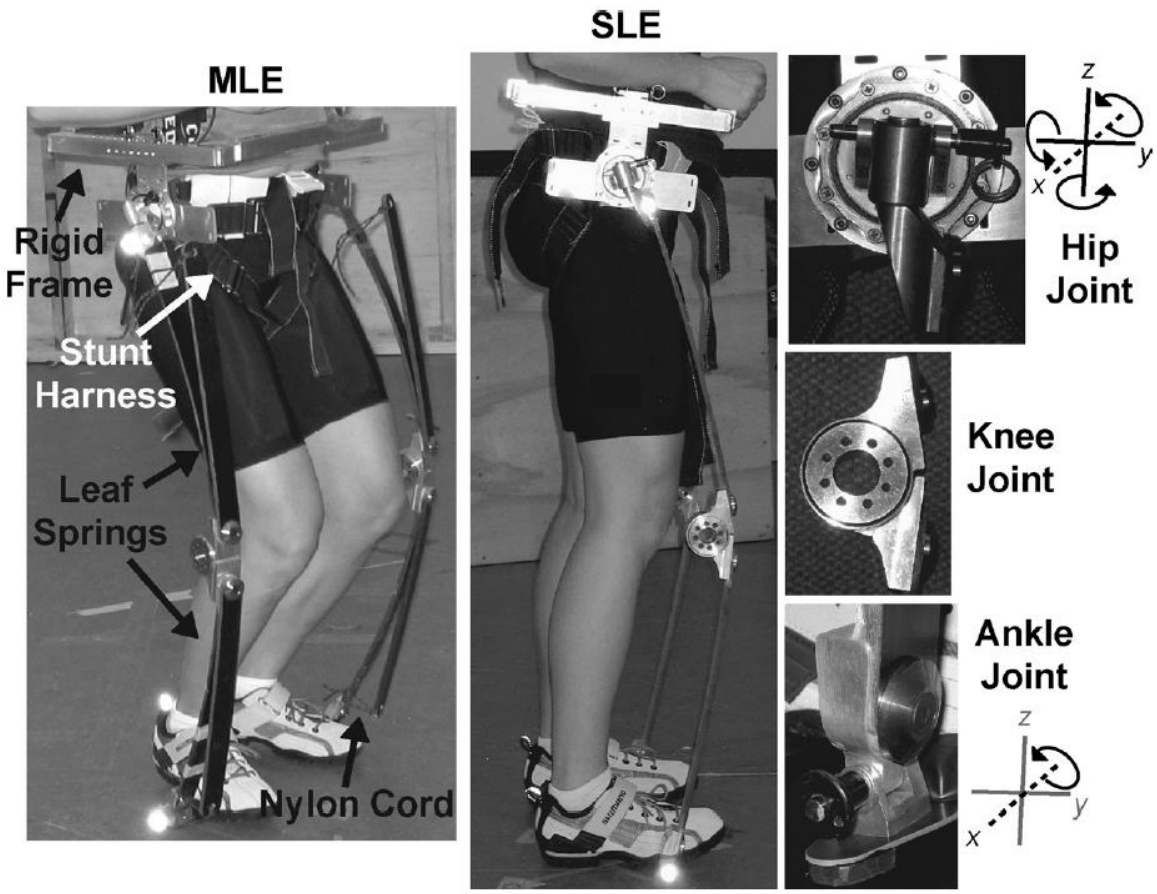

Figure 3. The passive-elastic leg exoskeleton developed by Grabowski and Herr. The exoskeleton design used fiberglass leaf springs held at a 165 degree angle which deflected in a predictable manner when compressed. The Single Leaf Exoskeleton (SLE) used only one leaf spring.

Grabowski and Herr attached the exoskeleton to the user via a modified rock climbing harness. This harness was attached to a rigid aluminum frame that served as one end point of the leg springs. Modified bike shoes provided the other end point of the springs. The exoskeletal hip joint had three degrees of freedom, which allowed hip flexion and extension, abduction and adduction, and internal/external rotation. At the exoskeletal ankle, a metal pin allowed ankle flexion and extension.

Grabowski and Herr used two springs. The first, called the Single Leaf Exoskeleton, was a set of two fiberglass leaf springs held at a 165-degree angle by a rigid knee joint (Figure 3). Applying vertical force to the springs deformed them into a bow shape. This shape lengthened the moment arm of the applied force compressing the springs. Consequently, the bow spring took progressively less force to deform it, as deformation increased. This progressively decreasing stiffness profile is shown in Figure 4. To create a more linear profile, the Multiple Leaf Exoskeleton was (MLE) implemented. The MLE had a second set of bow springs that were engaged once the first set had been compressed enough to exhibit nonlinearity. This allowed the exoskeleton to remain stiff and nearly linear through the full range of compression.

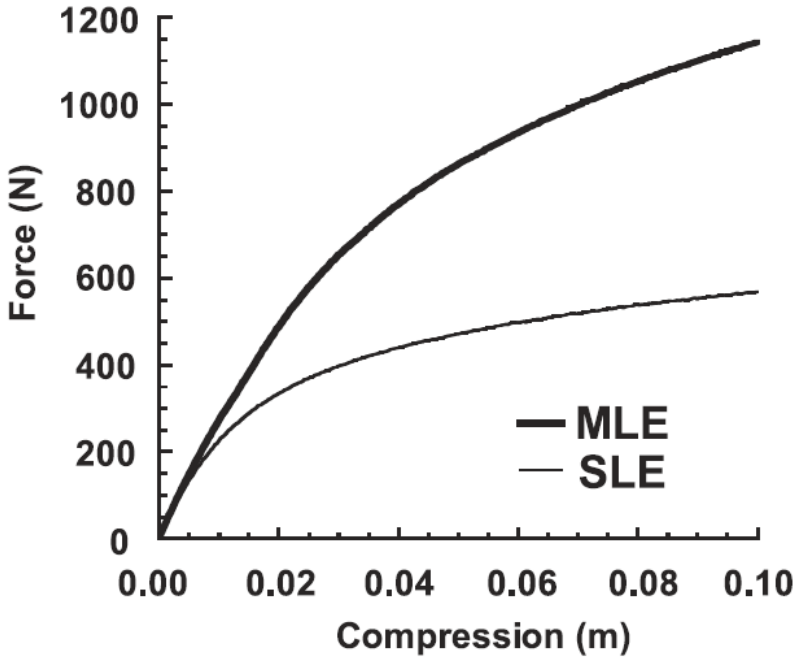

Figure 4. The stiffness profiles of the SLE vs. the MLE. Implementation of the second set of bow springs allowed the exoskeleton to remain stiffer through a larger range of compression (Grabowski, 2009).

When 10 subjects hopped in place on both feet with the SLE, they reduced net metabolic power by an average of 24% when compared to hopping without an exoskeleton across hopping frequencies from 2.2 to 2.6 Hz. The MLE, however, reduced net metabolic power by an average of only 6% compared to hopping without an exoskeleton. The result of the SLE was a major improvement over any previous exoskeleton performance, particularly for an unpowered device. But the poorer performance of the MLE was not fully explained. It was suggested in the discussion that the mathematical model for estimating the correct stiffness of the bow springs overestimated the optimal values, and that the MLE's initial linear stiffness was too great. However, less stiff MLE bow springs were not implemented during the study.

2.3 Goals of This Study

Grabowski and Herr, 2009, demonstrated that a passive-elastic leg exoskeleton placed in parallel with the legs substantially reduced the metabolic cost of hopping. The goals of the current study are to determine the effects of different stiffness profiles on the net metabolic cost of hopping. Whereas Grabowski et al. tested two stiffness profiles, both were nonlinear and with decreasing stiffness, the current study was designed to examine three stiffness profiles: one nonlinear with decreasing stiffness similar to Grabowski et al., one linear, and one nonlinear with increasing stiffness (Figure 5).

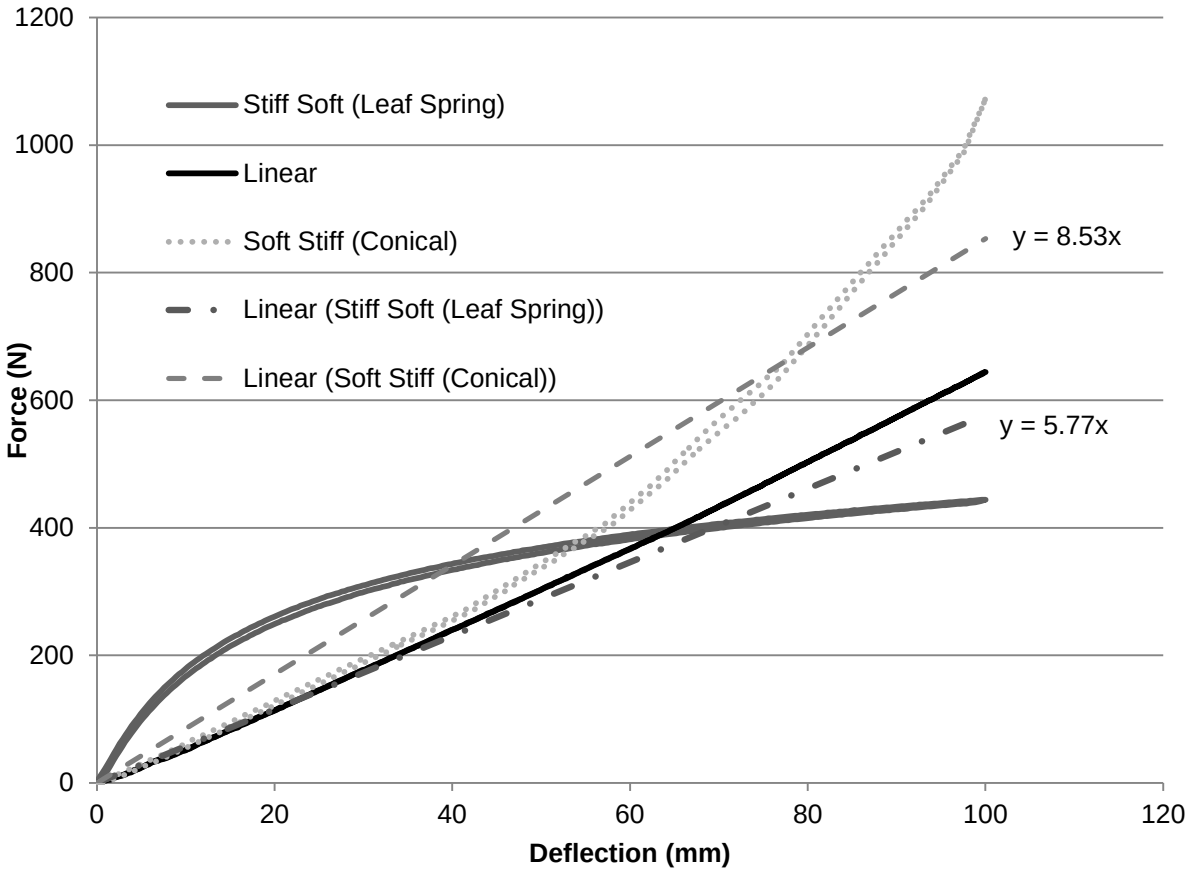

Figure 5. Examples of the three stiffness profiles for a 75 kg person (Subject 3) — nonlinear decreasing (Stiff-Soft), linear, and nonlinear increasing (Soft-Stiff) stiffnesses measured by an Instron testing machine. Linearization of the Stiff-Soft and Soft-Stiff exoskeletons has been provided for comparison. The mathematical model for determining optimal stiffness for an exoskeleton user is discussed in Chapter 3.4.

Because springs in parallel have additive stiffness, an exoskeletal spring with a stiffness profile that closely matches the total biological stiffness (k_{total}) would presumably decrease the muscular effort and minimize metabolic cost. Previous studies suggest the leg is well approximated by a linear stiffness spring across most hopping frequencies, but at higher hopping frequencies it becomes slightly nonlinear with increasing stiffness (Farley, 1998). It was hypothesized that the linear stiffness spring profile would reduce the net metabolic cost of hopping compared to the other stiffness profiles and hopping without an exoskeleton. To test this hypothesis, a passive-elastic leg exoskeleton was

built, similar to that of Grabowski et al., as well as three different spring profile mechanisms that could be implemented interchangeably in the exoskeleton. The details of this exoskeleton's design follow in the next section.

Chapter 3: Exoskeleton Design

The leg exoskeleton is designed to allow the separate spring mechanisms to be switched out and rapidly fit to the wearer's body size and leg length. The design has three general components (Figure 6). The first component is the frame, which snugly attaches around the wearer's hips. It is important to have a snug fit so that the weight of the wearer can be transmitted through the exoskeleton to the ground. It is also important that the frame fits comfortably. If the exoskeleton is too uncomfortable to wear, it will never be a viable product for human use. Any movement or slack in the harness system is detrimental to the effectiveness of the exoskeletal springs to store and return elastic energy and could negatively impact the efficiency of the exoskeleton.

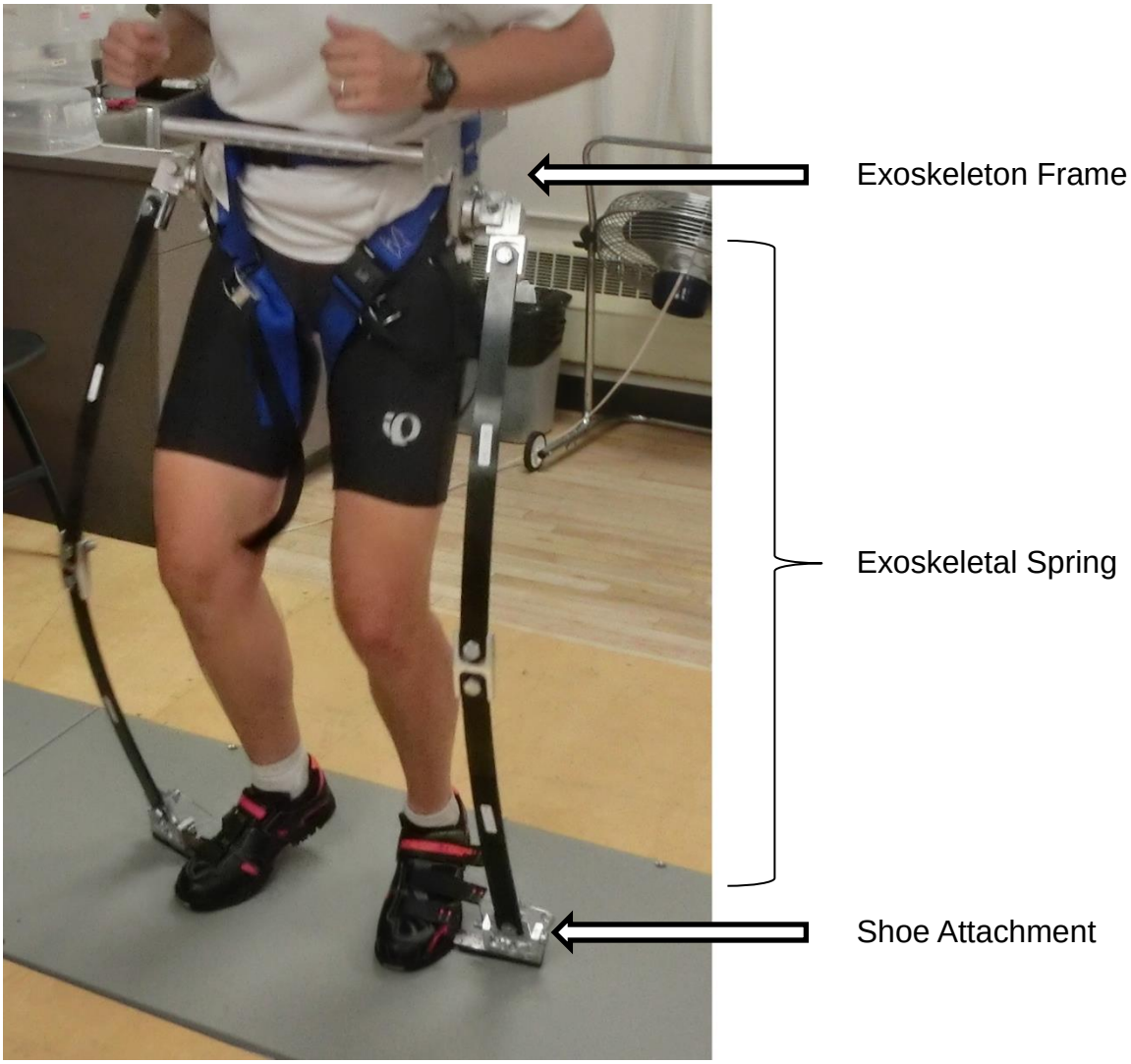

Figure 6. The three components of the leg exoskeleton: the frame, the spring, and the shoe attachment.

The second component is the exoskeletal spring, which is positioned between the frame at the top and the foot attachment at the bottom. The exoskeleton structure depends on the spring stiffness that is being implemented. The stiff-soft springs are a set of fiberglass bow springs, while the linear and soft-stiff springs use telescoping rods and plungers to compress different coil springs. The exoskeletal springs are designed to

meet the desired spring profile types, fit to the user, and are adjustable and interchangeable.

The third component of the exoskeleton is the shoe attachment, which provides a semi-rigid attachment between the exoskeleton's distal end and the wearer's feet. The shoe attachment must fit the patient, transmit force from the ground to the exoskeleton, and be reliable and robust.

Each of the exoskeleton components are discussed in detail in the following pages. Detailed part and assembly drawings are located in Appendix B.

3.1 Exoskeleton Support Structure

3.1.1 Hip Frame

The purpose of the hip frame is to transfer force from the exoskeletal springs to the user's body. It is comprised of two things: a rigid platform to which the spring mechanisms attach, and a harness that is comfortable for the user to wear. In this iteration of the exoskeleton hip frame, the comfort experienced by different users was variable, depending on their hip size and geometry. Foam or rubber pads were inserted to reduce any uncomfortable pressure on the user's legs and hips. Future iterations of the exoskeleton will seek to improve user comfort. The total weight of the hip frame is 2.4 kg.

The original design of the hip frame included two frame bars and two sets of telescoping rods that defined a rectangle around the user's hips, parallel to the transverse plane (Figure 7). The two frame bars were located at the user's sides, level with their iliac crest of the pelvis. A separate piece, called the hip plate, was attached by screws to each frame bar and had slots for the nylon harness straps. Each plate also contained the "hip bearing," the first of three mechanisms that allow the exoskeleton to rotate freely with the user's leg.

The original hip frame's telescoping rods were attached with screws to the frame bars. Each exterior rod had holes drilled through its diameter in a regular pattern along its length, while the interior rod had a single hole. When interior and exterior holes were aligned, a linch pin could be driven through, securing the hip plates a certain distance from each other. However, these linch pins were uncomfortable for the user. When it became clear that the nylon straps were capable of tightening the frame to the hips more securely and with better size resolution, the linch pins were abandoned, and the hole array became superfluous.

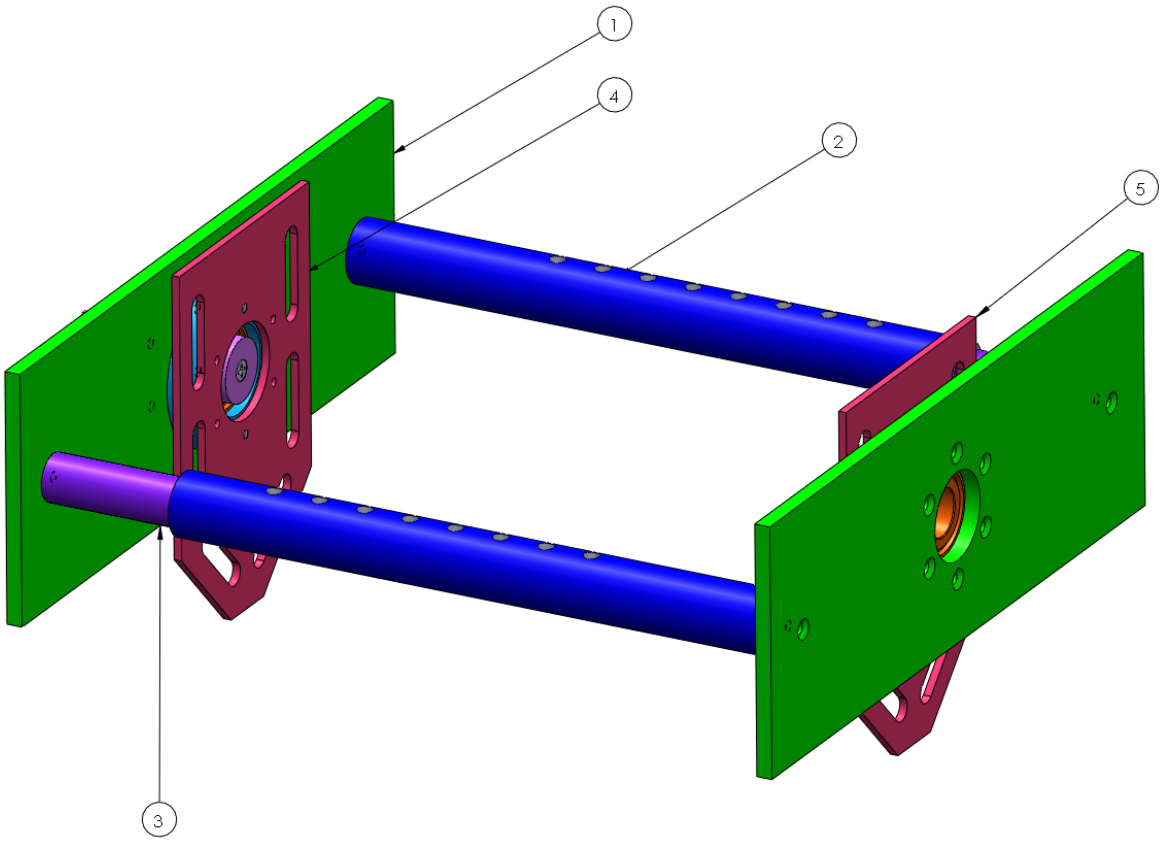

Figure 7. Original Frame Bar design. The first iteration of the frame bar (1) was rectangular, and the telescoping rods (2 and 3) allowed the frame to be cinched against the user's waist. At this time, the frame bars and hip plates (4 and 5) were still separate pieces.

During preliminary testing, it was discovered that the frame bar, as designed, did not hold the hip bearing in the correct place relative to the user's legs. Because the exoskeleton was designed to mimic the hip joint, the ideal placement of the bearing is at the pivot point of the leg, lateral to the head of the femur. In the frame bar design, the bearing was located too high (proximally) on the body, which reduced the overall effectiveness and comfort of the device.

To address this, the hip frame was altered to its current state, the T Bar design. In the T Bar design, the hip plate has been removed, and its function has been integrated into the crosspieces (Figure 8). Furthermore, the crosspieces have been altered to a T-shape which reduces their bulk and moves the bearings to a more distal position, directly lateral from the head of the femur. This design change improved the fit of the exoskeleton, reduced bulk, and also allowed the harness to be tightened more comfortably around the body. Figure 9 shows the final hip frame design fitted to a hopping subject.

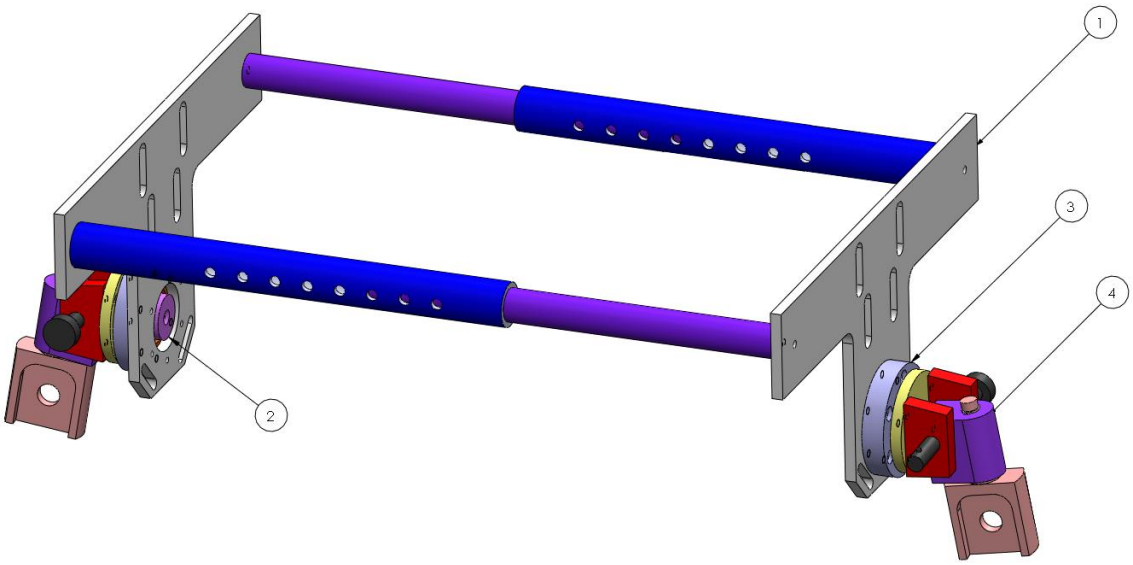

Figure 8. Final design of the hip frame (contrast with Figure 7). In this version the hip plates have been combined with the frame bar to make a T-shape (1) and the bearings have been moved to a more distal location (2 and 3). This assembly also shows the hip joint (4), discussed below, attached to the frame bar. Figure 9 shows a subject wearing the exoskeleton hip frame.

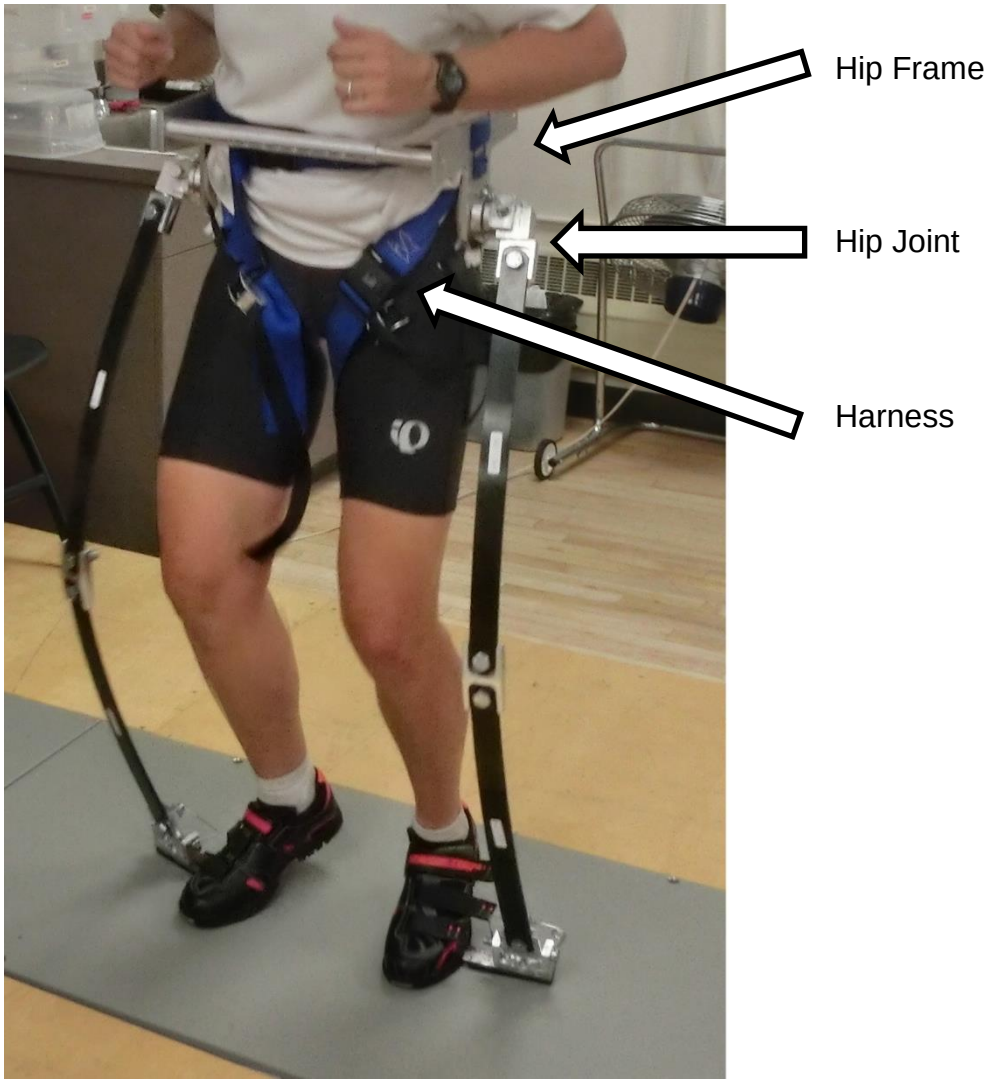

Figure 9. A subject using the stiff-soft exoskeleton during a hopping trial. The image shows the position of the hip frame, hip joint, and harness around the user.

The hip frame connects to the exoskeleton mechanism through a series of machined parts that allow the exoskeleton to rotate freely with the leg along three degrees of freedom (see Figure 10). Because it mimics the behavior of the biological hip, it is referred to as the “hip joint assembly.” All of the hip joint assembly’s custom parts were machined from 6061 Aluminum.

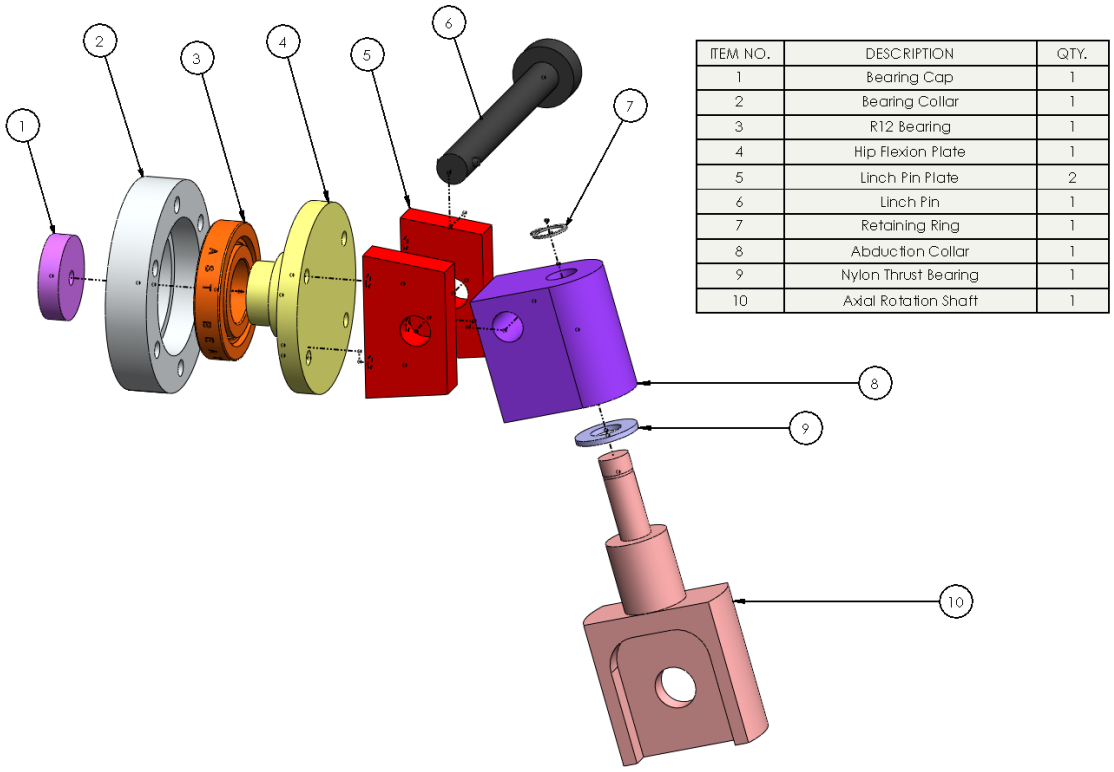

ITEM NO.	DESCRIPTION	QTY.
1	Bearing Cap	1
2	Bearing Collar	1
3	R12 Bearing	1
4	Hip Flexion Plate	1
5	Linch Pin Plate	2
6	Linch Pin	1
7	Retaining Ring	1
8	Abduction Collar	1
9	Nylon Thrust Bearing	1
10	Axial Rotation Shaft	1

Figure 10. The exploded hip joint assembly. The R12 bearing (3) is seated inside the bearing collar (2). The inner race of the bearing is fit to the inner diameter of the Hip Flexion Plate (5). This assembly provides three degrees of freedom: 1) Hip flexion through the R12 Bearing. 2) Hip abduction through the Abduction Collar (8). 3) Hip axial rotation through the Axial Rotation Shaft (10).

The first item of the hip rotation assembly is an R12-size ball bearing set in a press-fit bearing collar, which allows hip flexion and extension. The stepped circular hip flexion plate (Item 4, Figure 10) is fastened into the bearing via a shoulder machined into the plate, and a cap that tightens around the other side of the bearing's inner race (Item 1, Figure 10).

Mounted on the hip flexion plate are two linch pin plates (Item 5, Figure 10), with collinear holes that hold a linch pin (Item 6, Figure 10) in place. Linch pins are commonly used in the exoskeleton because they allow hardware to be swapped in and

out quickly while keeping a semi-rigid connection. Another component, the abduction collar (Item 8, Figure 10), is set on the linch pin between the two linch pin plates. The abduction collar has a clearance hole for the linch pin which allows it to rotate freely and allows for hip abduction and adduction, activities that allow the user to balance while in the exoskeleton.

Finally, the abduction collar has a vertical stepped hole through its lateral half. This hole fits a nylon bushing and the stepped rotation shaft. This design accommodates interior and exterior rotation of the leg, the final degree of freedom necessary for the exoskeleton to follow the leg's motion. A retaining ring at the proximal end of the axial rotation shaft holds it in place.

The harness that fastens the hip frame to the user's body has undergone several iterations to improve its fit and comfort. The first iteration used a climbing harness, modified to attach to the user more tightly. A climbing harness was chosen because they are designed to cradle a human's pelvis and comfortably provide upward force. However, climbing harnesses may fit loosely to their wearers and are designed to catch a fall rather than suspend someone vertically. A loosely-fitting harness would increase the slop in the system and negatively impact the device's performance. Additionally, extra straps and buckles were bulky and necessitated a change to a simpler design.

The most recent iteration of the exoskeleton harness is shown in Figure 11. It has one strap (Top, in blue, Figure 11) that encircles the user's waist, bringing the rectangular

cage of the frame in close to the hips. Two more straps per leg secure the hip frame to the body. The first leg strap (Middle, in blue, Figure 11) attaches to the hip frame just below the waist strap and goes around the inner leg, allowing the exoskeleton to exert a vertical force on the user's pelvic cradle. The second strap (Bottom, in black, Figure 11) attaches at the bottom of the hip frame, below the leg flexion bearing. It goes around the thigh and prevents any moment exerted on the T arm of the hip frame from twisting the frame away from the legs.

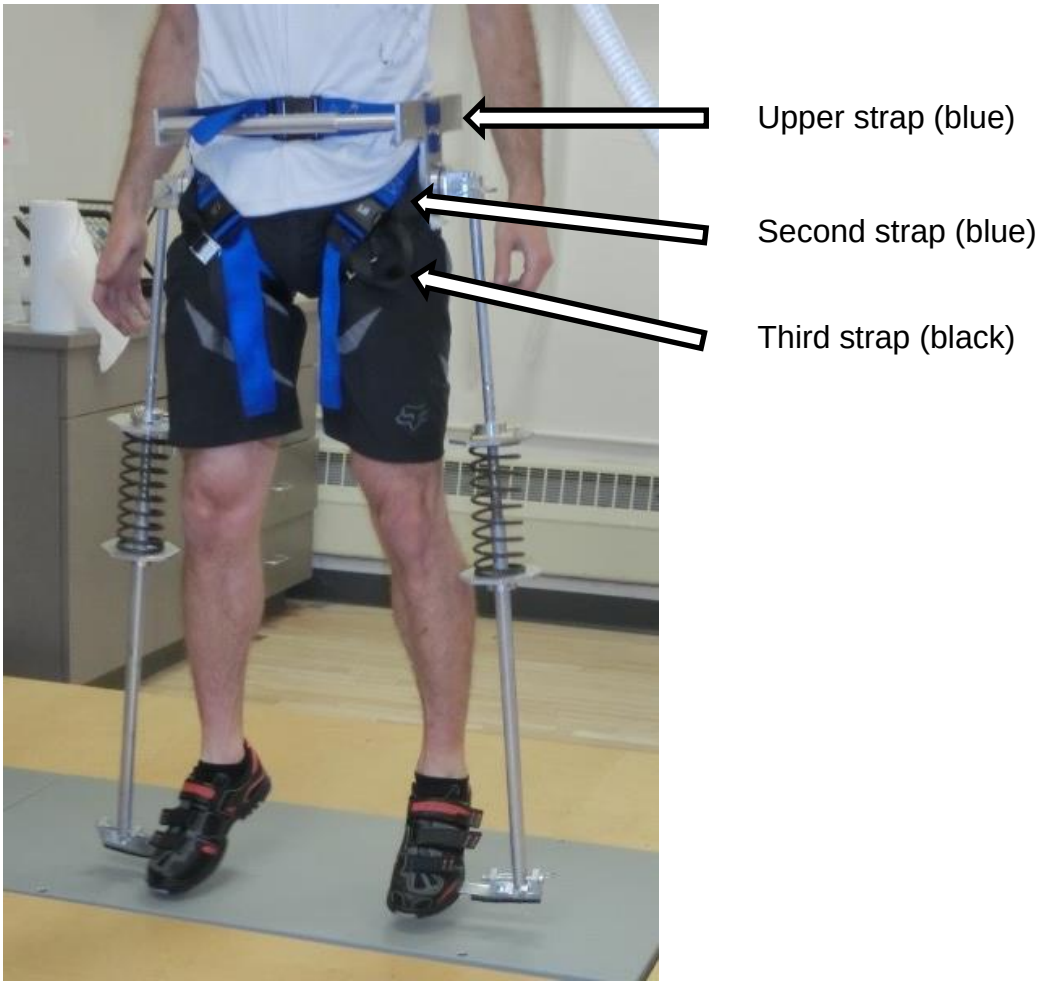

Figure 11. Hip frame and leg harness in use. One strap circles the waist and holds the pivot points tight against the hips. A second strap runs from above where the bearing is seated, around the leg, bearing most of the vertical force during hopping. A third strap (black) runs from below the bearing around the leg, preventing the hip frame from twisting around the hip from the applied moment.

3.1.2 Shoe Attachment

At the spring's distal end, the exoskeleton fastens to the user's feet using modified Gavin brand Spin Cycle/Mountain Bike shoes (Figure 12). These are effective because they are cheap, they have a rigid sole, and they offer a durable means of attaching hardware to the sole of the shoe. The total weight of both modified shoes is 2.6 kg.

Figure 12. Gavin mountain cycling shoe with shoe attachment inserted into the sole, and bolts and screws present. A rubber pad has been adhered to the bottom of the spring steel plate, so that the bottom of the pad is even with the bottom of the sole when the shoe rests on the ground.

Located on the underside of the bike shoes, directly below the ball of the foot, is the site of the intended attachment from the bike shoe to pedal cleat. Cleats are fastened to the shoe sole via a sliding metal bracket within the shoe's sole, which has tapped M6 holes.

These shoes were modified by cutting a slice through the rubber of the sole lateral of the sliding bracket and by inserting a long strip of 4130 spring steel. This steel strip was anchored by screwing it into the sliding bracket.

The spring steel extends laterally from the ball of the foot to provide a platform for the exoskeleton to attach to. It should extend just far enough for the exoskeleton mechanism to be vertical when the user stands with feet shoulder width apart. This prevents any force couple acting on the springs during operation. The proper extension varies between 4 and 6 inches, depending on the user's leg geometry. The best way to account for this variation is by drilling a linear array of M6 holes in the spring steel. When more or less protrusion is required, the spring steel plate can be slid out or in from the shoe until the next set of M6 holes lines up with the cleat attachment site in the shoe. See Appendix B and the spring steel plate documentation for more details.

The spring steel plate extends laterally from the shoe's sole, with the force of the exoskeleton acting at its tip. This makes it vulnerable to bending under the applied moment. To rectify this, an epoxy adhesive was used to adhere a hard neoprene rubber pad below the plate (Figure 12). This pad is ideally the thickness of the shoe's sole. A 3/8" thick rubber sheet was used, but it required trimming for the spring steel to lie flat. This pad also doubles as a means of protecting the hopping surface from the hard edges of the spring steel.

At the end of the steel plate is the attachment point for the spring mechanism. Three machined aluminum pieces are fastened by screws to make a u-shaped assembly (Figure 13). The uprights of the “u” shape are pierced by a 0.375” diameter hole to allow another linch pin to slide through. This linch pin secures the distal end of the spring mechanism to the shoe attachment. The degree of rotational freedom provided by the linch pin holds the exoskeleton to the foot while allowing ankle plantar flexion and dorsiflexion as the user hops.

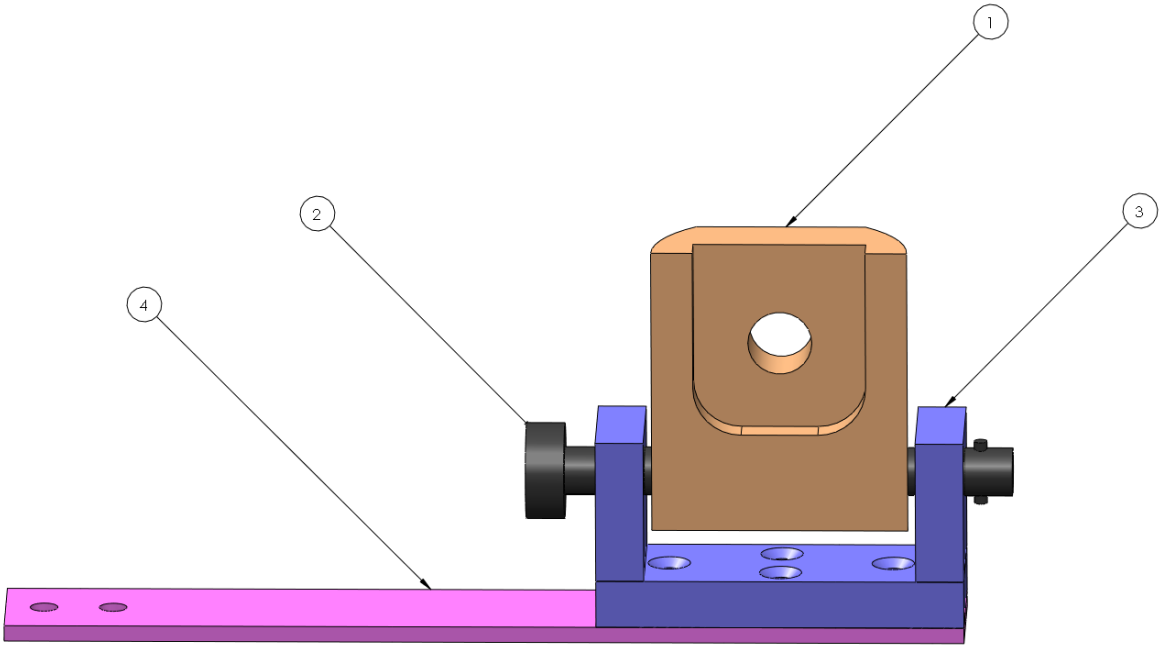

Figure 13. The ankle joint assembly. A 0.50-inch bolt holds the spring deflection joint (1) to the lower fiberglass bow spring. The deflection joint pivots around the linch pin (2), which is held in place by the ankle joint assembly (3). The spring steel platform (4) is inserted into the sole of the bike shoe and fastened into the cleat with two M6 screws.

3.2 Progressively decreasing stiffness design

The bow spring design is the simplest of the exoskeleton mechanisms. It has few parts, none of which move against each other. Instead, it relies on strips of fiberglass that deflect elastically to store and return energy. These fiberglass bow springs are made from Gordon Composites GC-67-UB fiberglass, and cut into strips using the CNC WaterJet precision cutting machine owned by the CU Physics Precision Instrument Shop. The total weight of the pair of bow springs is 2.0 kg.

The fiberglass springs are cut to have a constant width of 1.25 inches. Their lengths vary to accommodate the varying leg lengths of users, from 15.5 to 19.5 inches. Each user requires a particular set of springs that are selected based on the user's weight and leg length. Also, because the bow springs deform according to the moment placed on them, longer springs are softer than shorter ones. To provide the correct stiffness for all users, varying thicknesses of fiberglass were used, ranging from 0.250 to 0.320 inches. Sheets were provided in this thickness by Gordon Composites, and did not vary by more than 0.005 inches. At either end, the springs are rounded, and a 0.50 inch diameter hole is drilled for them to attach to the exoskeleton hip frame and shoes. For an explanation of how the appropriate stiffness is determined for each subject, please see Chapter 3.4.

At its proximal maximum, the bow springs attach to the hip frame at the axial rotation shaft (Figure 14). This machined aluminum part rotates in the stepped shaft of the abduction collar to allow internal and external rotation of the leg. It also features

mirrored slots at its lower end with holes for a 0.50” bolt. The upper bow springs are secured here, and stretch down to the knee joint.

Figure 14. Progressively decreasing stiffness mechanism CAD model and in use.

The knee joint is another machined aluminum part. Its function is to hold the two bow springs of the exoskeleton at a rigid 165-degree angle from each other. This angle allows the springs to deflect in a predictable and consistent manner. Each knee joint has two more 1.25-inch wide slots with 0.50-inch diameter bolt holes for securing both fiberglass bow springs (Figure 15). The obtuse angle occurs halfway between each slot. On the “backside” of the knee joint, slots have been machined to provide a parallel surface for the nuts to tighten against. Outside these slots, the knee joint’s sidewalls act as ribs to reinforce the structure of the joint while under compression from the springs. See the knee joint part drawing in Appendix A for more details.

Figure 15. The top half of a bow spring, showing the knee joint (left), which holds the two bow springs at a 165-degree angle, and the assembled axial rotation shaft and abduction collar (right), which attach the bow spring to the hip and allow the leg to rotate. These two components are part of the hip joint assembly (Figure 10).

At the distal end of the compression mechanism, a final machined aluminum part connects the lower bow spring to the shoe (Figure 16). This part, the ankle joint, has a final 1.25” slot and 0.50” hole to secure the spring. Below that, a 3/8” hole passes through its width. A linch pin holds the joint between the two risers of the shoe attachment’s ankle joint assembly, allowing the ankle to flex while the spring deflects.

Figure 16. The bottom half of a bow spring, showing the knee joint (right), and the ankle joint (left).

3.3 Linear and progressively increasing stiffness designs

The linear and progressively increasing spring designs use the same mechanism, in conjunction with coil springs of different types, to achieve their respective stiffness profiles. The linear spring implements a coil spring of constant diameter, which provides a constant stiffness throughout the compression range. The progressively increasing design uses a conical coil spring, with wide coils on one end narrowing to small coils on the other (Figure 18). The wider coils compress more easily, and deform easily for small amounts of compression. Once the wider coils have compressed, the stiffer, narrower coils are activated, creating a smooth, steadily increasing profile. See section 3.4 for a discussion of spring stiffnesses.

The mechanism that compresses the springs uses two telescoping rods, each with a wide plate that compresses the coil spring between them (Figures 17 and 18). Each rod supports a wide plate that acts as a platform to support one end of the spring. The coil spring mechanism is shown in use in Figure 19.

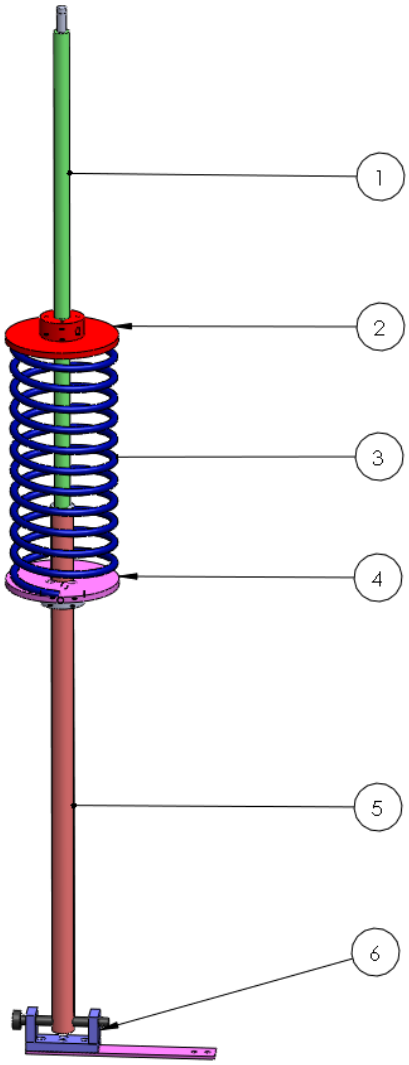

Figure 17. Coil spring exoskeleton mechanism, shown as a CAD assembly. The inner telescoping rod (1) is fixed by a removable linch pin to the upper spring plate (2). The two spring plates compress (2 and 4) compress the coil spring (3). The outer telescoping rod (5) is fixed by set screws to the lower spring plate (4). At the distal end of the outer telescoping rod, a linch pin secures the ankle joint assembly (6) to the exoskeleton spring. The hip joint of the coil spring exoskeleton is interchangeable with the hip joint of the bow spring mechanism.

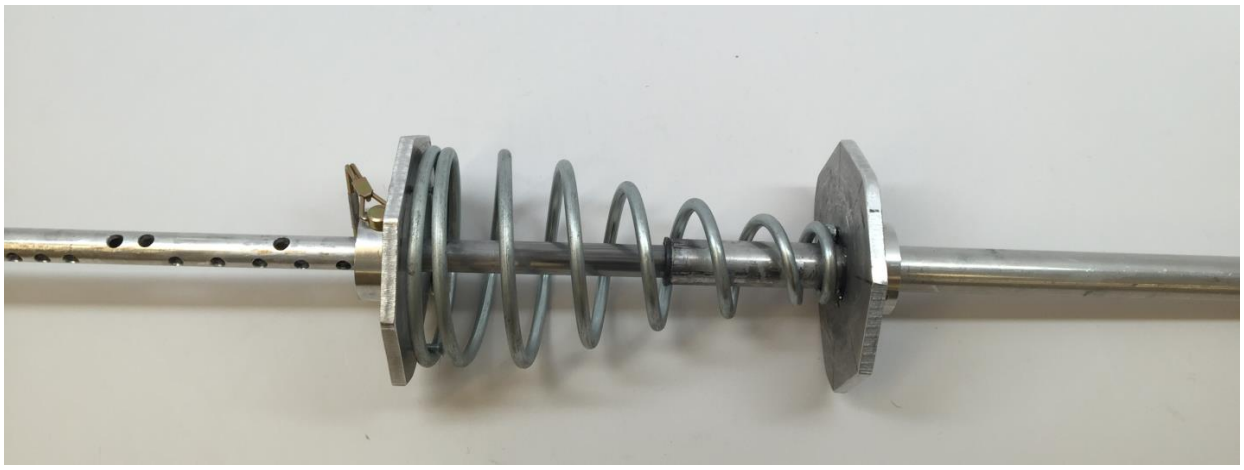

Figure 18. View of telescoping rods with conical coil spring. The two spring plates compress the coil spring between them as the telescoping rods are pressed towards one another.

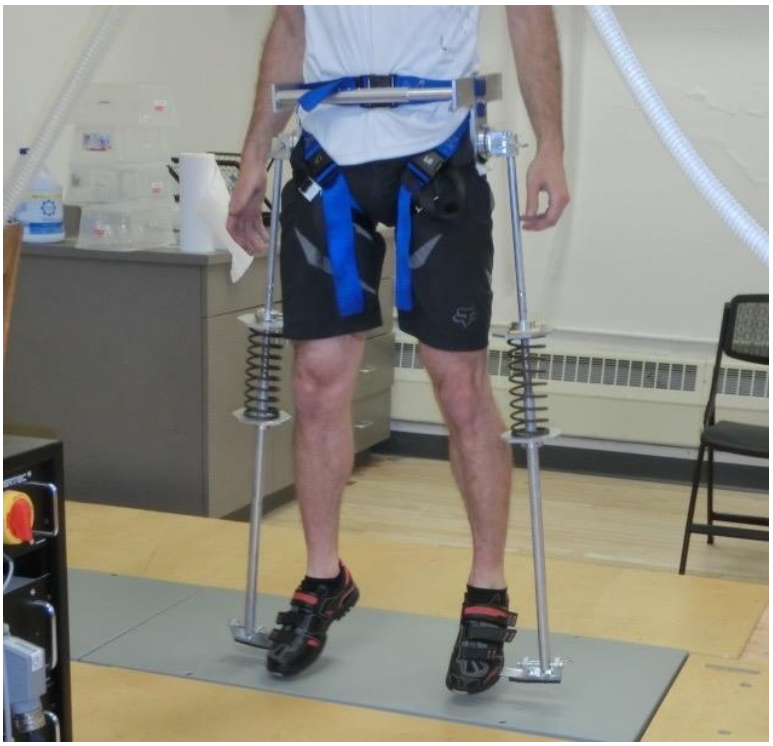

Figure 19. Coil spring assembly in use. The bow spring has been exchanged for the coil spring assembly; however, the same hip joint is used for both designs.

The inner and outer rods slide freely past each other with a nominal diametral clearance of 0.010 inches. This dimension is supplied by the vendor, OnlineMetals.com, which

gives the inside diameter of the outer rod as 0.635” and the outside diameter of the inner rod as 0.625”. In the quantities purchased for this project, these dimensions did not vary by more than three thousandths, allowing easy slip between the two parts.

To assist the rods in sliding against each other, nylon bushings are installed at the interface between. The tip of the inner rod is turned down to allow a cylindrical nylon bushing to be adhered to the shoulder using a metal-polymer epoxy (Figure 20). At the end of the outer rod, the inner diameter is widened for a nylon shoulder bearing to be adhered to the inside (Figure 21). These inserts reduce friction between the rods and reduce losses in the system as the user hops. Additionally, an all-purpose lubricant is applied to the rods to further reduce any frictional losses.

Figure 20. Upper (inner) telescoping rod. The hole arrays in the center are drilled to accommodate the varying leg lengths of exoskeleton users. In the final iteration, the spring compression plate has been trimmed on one side to avoid brushing against the user’s legs during hopping. Screws have been installed in the spring plate to guide the coil springs and prevent them from moving laterally during hopping. At right, the tip of the aluminum rod has been turned down, and a nylon bushing adhered in place to reduce the friction between the telescoping rods.

Figure 21. Lower (outer) telescoping rod. At left, the 0.375 inch hole has been drilled for the linch pin of the ankle attachment assembly. At right, the inside diameter of the hollow aluminum rod has been widened. A nylon shoulder bushing has been adhered inside to reduce friction between the rods.

At either end, the plunger mechanism attaches to the hip frame simply. A cylindrical insert at the end of the upper rod provides the stepped shaft that can rotate within the axial rotation collar (see previous sections), and a 0.375” hole at the end of the lower rod allows the linch pin to attach the rod to the shoe assembly. The total weight of the telescoping rods structure is 2.8 kg for both sides.

3.4 Spring Stiffnesses

This section contains a breakdown of how the estimates for optimal spring stiffness were developed, a discussion of the three different stiffness types and how they are modeled, and the real values of stiffness used for each mechanism and subject.

A mathematical model has been developed to estimate the appropriate spring stiffness for each subject, using the individual's body mass to determine an approximate linear stiffness. The ideal linear stiffness *k* is calculated using the governing equation of a simple spring-mass system, which represents the subject's mass (*m*) oscillating at the end of a spring of stiffness (*k*). If *x* is the vertical position of the oscillating mass, and *g* is the acceleration due to gravity, the spring-mass equation of motion is:

$$mx'' = -kx + mg$$

The initial conditions for position (*x*) and velocity (*x'*) are:

$$x(0) = 0, \qquad x'(0) = u$$

This system has the particular solution:

$$x(t) = \frac{u}{\omega_0 \sin(\omega_0 t)} + \frac{mg}{k}(1 - \cos(\omega_0 t))$$

Where ω_0 is the natural frequency of the system.

$$\omega_0 = \sqrt{k/m}$$

For a hopping frequency of 2.0 Hz, empirical data give the contact time (t_c) and the aerial time (t_a) of the hop. The knowledge of t_a allows for the calculation of the initial condition *u*, the velocity of the body on contact with the ground. With this, the particular solution can be solved numerically to give a value of *k.* This method is an approximation

that presumes a hopping frequency of 2.0 Hz, chosen as a comfortable starting point for any exoskeleton user. This yields an estimate of *k* that can be refined through experimental trials.

The *k* estimates determined using this method proved to be too stiff, and were reduced after preliminary testing. Experimental trials with Subject 1 hopping on a range of stiffnesses established that the optimal *k* reduction was 10%. To achieve this reduction, thinner fiberglass sheets were used to make the bow springs, and less stiff coil springs were selected for each subject. The sheet thicknesses and spring stiffnesses were only available in discrete intervals, so an exact reduction of 10% was not always possible. Real values ranged from 8% to 15% reduction for Subjects 1 and 3. For Subject 2, whose body mass was comparatively smaller, the estimate of *k* was reduced even further until Subject 2 could hop in the exoskeleton. Subject 2 required the stiff-soft (bow springs) to be reduced by nearly 50% before testing was possible. These data are given in Table 1.

It was a simple matter to find linear springs that corresponded to the preliminary estimates of *k*. Several spring manufacturers offer a wide range of linear springs with the correct geometry to fit the exoskeleton. Locating conical springs was more difficult, and only one spring was found that fit the correct range of stiffnesses. As a result, all subjects used the same soft-stiff spring, which is why its stiffness was slightly higher than the *k* estimate dictated. The bow springs were not ordered, but cut from Gordon Composites GC-67-UB fiberglass sheets of thicknesses between 0.250 and 0.320

inches, with each sheet varying by up to 0.005 inches. The bow spring stiffness was dependent on both the thickness of the sheet and the length of the individual leafs. The length of each leaf was adjusted to match the user's legs, and the thickness was then adjusted to achieve the desired stiffness.

To compare the nonlinear stiffnesses to the optimal linear stiffness *k*, a regression model was used. A linear regression from the origin was selected as the model that best approximates how each spring behaved throughout its entire compression curve. Each spring type was validated using an Instron testing machine to confirm that it had the correct stiffness profile. Figure 22 shows the three different stiffness profiles used by Subject 1 during hopping, and how their linearized forms matched the ideal values. Table 1 gives the linearized stiffness data for each subject in the study. The stiff-soft (bow spring) and linear springs are close to 90% of the estimated *k* value, while the soft-stiff has an increased stiffness because of the aforementioned rarity of conical springs.

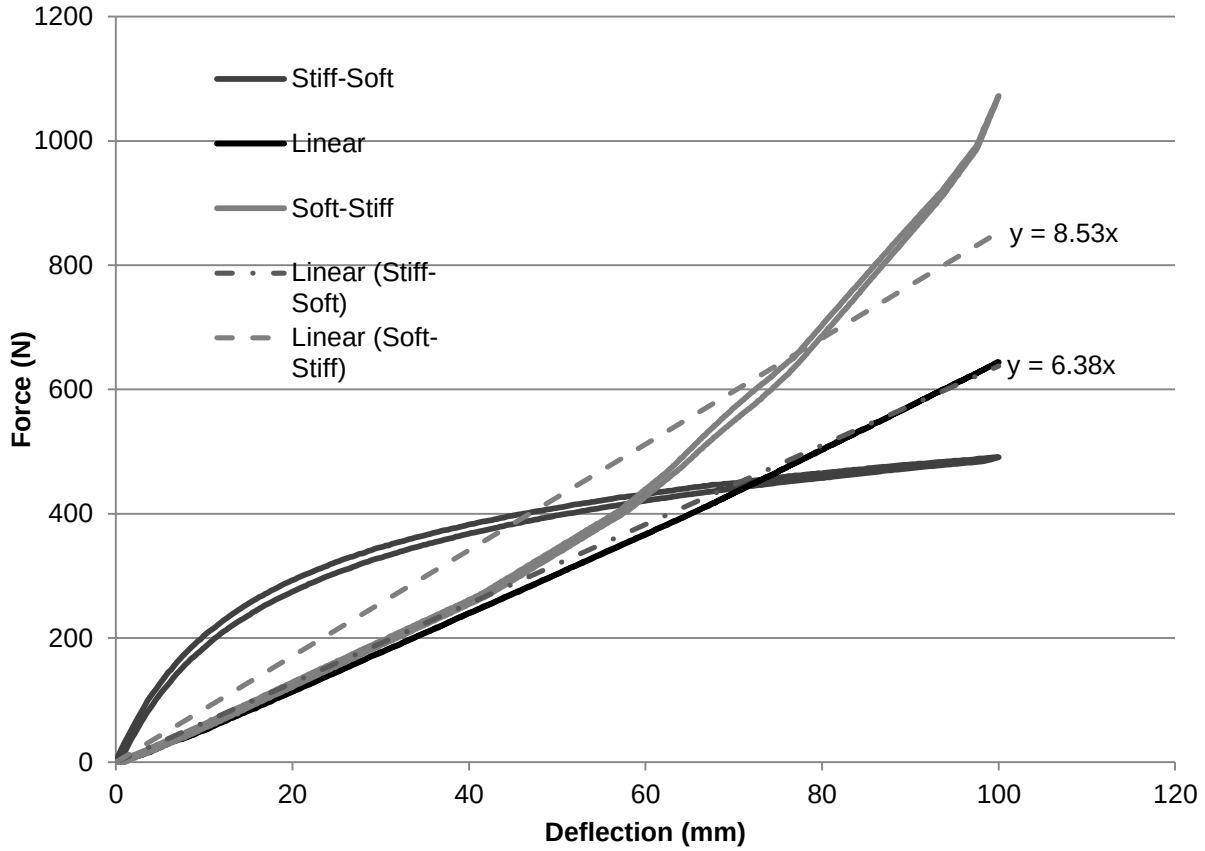

Figure 22. Linear approximations of the three spring mechanisms used by Subject 1. A linear regression with a (0,0) intercept was selected as the best means of modeling the non-linear stiffnesses in comparison to the ideal linear *k.* Only the linear regression of the Soft-Stiff spring (y = 8.53x) is easily visible. The regression of the Stiff-Soft spring (y=6.38x) coincides with the Linear spring.

Table 1. Experimental values of the three spring stiffnesses used by each subject in the study, in kN/m. The Ideal column represents the estimated *k*, determined using the spring-mass model outlined above.

Subject	Ideal	Stiff-Soft (Leaf)	Linear	Soft-Stiff (Conical)
1	7.15	6.38	6.25	8.53
2	6.17	3.18	6.02	8.53
3	6.81	5.78	6.25	8.53

Chapter 4: Methods

Before the study took place, the Institutional Review Board of CU Boulder reviewed the experimental methods to ensure safe and ethical experimentation using human subjects (IRB protocol # 13-0641). Each subject gave informed written consent before participating in the exoskeleton study. Subjects were informed that at any point during the testing procedure they could decide not to participate in the study. All testing was voluntary, and all information was collected with the subjects' permission. To prevent the release of personal information, subjects are numbered 1, 2, and 3.

Three healthy runners took part in the study. Each subject participated in three days of trials, with approximately two hours of testing per day. The testing sessions were limited to 6 trials per session and separated by at least two days to prevent any potential fatigue.

An indirect calorimetry system (Parvo Medics TrueOne 2400) was used to measure rates of oxygen consumption and carbon dioxide production. This system must be calibrated correctly prior to use. The first step is the gas calibration. The system includes a tank of calibration gas, with known quantities of oxygen and carbon dioxide. During gas calibration, the gas from this tank is circulated through the gas mixing chamber while a measurement is being taken. The machine compares the readings from the instruments inside the mixing chamber to the known quantities of the calibration gas, and automatically calibrates the gas detector.

The second step is the flow meter calibration. A large syringe with a total volume of three liters connects to the inlet of the mixing chamber. Once flow meter calibration has been initiated, the operator must completely and smoothly pump the syringe 10 times. The first five pumps are not recorded, but the second five pumps should be at different volumetric flow rates to ensure the flow meter is calibrated across the range of expected flows. The monitor on the system will show a guide for what flow rates each pump should achieve for proper calibration. Calibration was performed before testing each day.

Once the calibration is complete, metabolic data can be collected. Clicking on Metabolic Measurement will prompt the system to collect preliminary data: the subject's height, weight, and age. Once these have been entered, the monitor will show a live readout of the gas entering the mixing chamber. The two quantities used for the purposes of this experiment are the volumetric flow rates of oxygen and carbon dioxide, or $\dot{V}O2$ and $\dot{V}CO2$. The Respiratory Exchange Ratio (RER), or the ratio of exhaled carbon dioxide to inhaled oxygen, can be useful in assessing the substrate (i.e., carbohydrate, fat, or protein) that is being metabolized during physical activity, and should also be monitored. Oxidation of fat yields fewer carbon dioxide molecules than it consumes oxygen molecules, so an RER for a subject burning only this fuel is 0.7. Oxidation of simple carbohydrates typically yields an RER of 1.0. A higher RER is correlated with increased effort by the body, requiring the use of carbohydrate energy stores. If the RER rises above 1.0 for an extended period of time, this is an indicator that the subject is utilizing both aerobic and anaerobic metabolic pathways. If the RER stays over 1.0, measures of

oxygen consumption and carbon dioxide production do not accurately quantify the entire metabolic energy required for the task, and the trial should be halted.

All subjects fasted and drank only water for at least two hours prior to testing so that we could assume a mixed diet for measuring volumetric oxygen and carbon dioxide flow rates. Additionally, a person's metabolic rate frequently changes throughout the course of a day. Subjects can be tested at any time of day; however, all trials on the same subject should be at the same time to reduce day-to-day variability.

AMTI force platforms were used to measure forces. They must also be calibrated to take accurate data. These platforms record the ground reaction forces of the hopper in three orthogonal directions, as well as the moments around each axis of the platform. For this experiment, only the magnitudes of the vertical forces were used for analysis. Calibrating the force platforms to collect data requires only that the associated amplifiers be zeroed, as well as the data stream in the AMTI NetForce recording software. When no load is being applied to the force platforms, the amplifiers may be easily calibrated with the press of a zeroing button. Similarly, in the AMTI NetForce software, the data may be easily zeroed before any trial. This should be done once before testing begins each day.

Before testing each day, the testing area was prepared for the subject, as shown in Figure 23. The breathing apparatus, consisting of a mouthpiece, an inlet hose, and an outlet hose, was suspended from the ceiling directly above the force plate at the height

of the subject's mouth. This height usually needed slight adjustment so that the subject remained comfortable throughout the testing process. Both inlet and outlet hoses were fastened to heavy objects (in Figure 23, the wooden chairs) on either side of the force plate. This prevented the hoses from moving unnecessarily and shaking loose while the subject hops. In particular, movement of the outlet hose directly in front of the gas mixing chamber can cause air to be moved into the gas mixing chamber, which alters the reading of the volumetric flow rate.

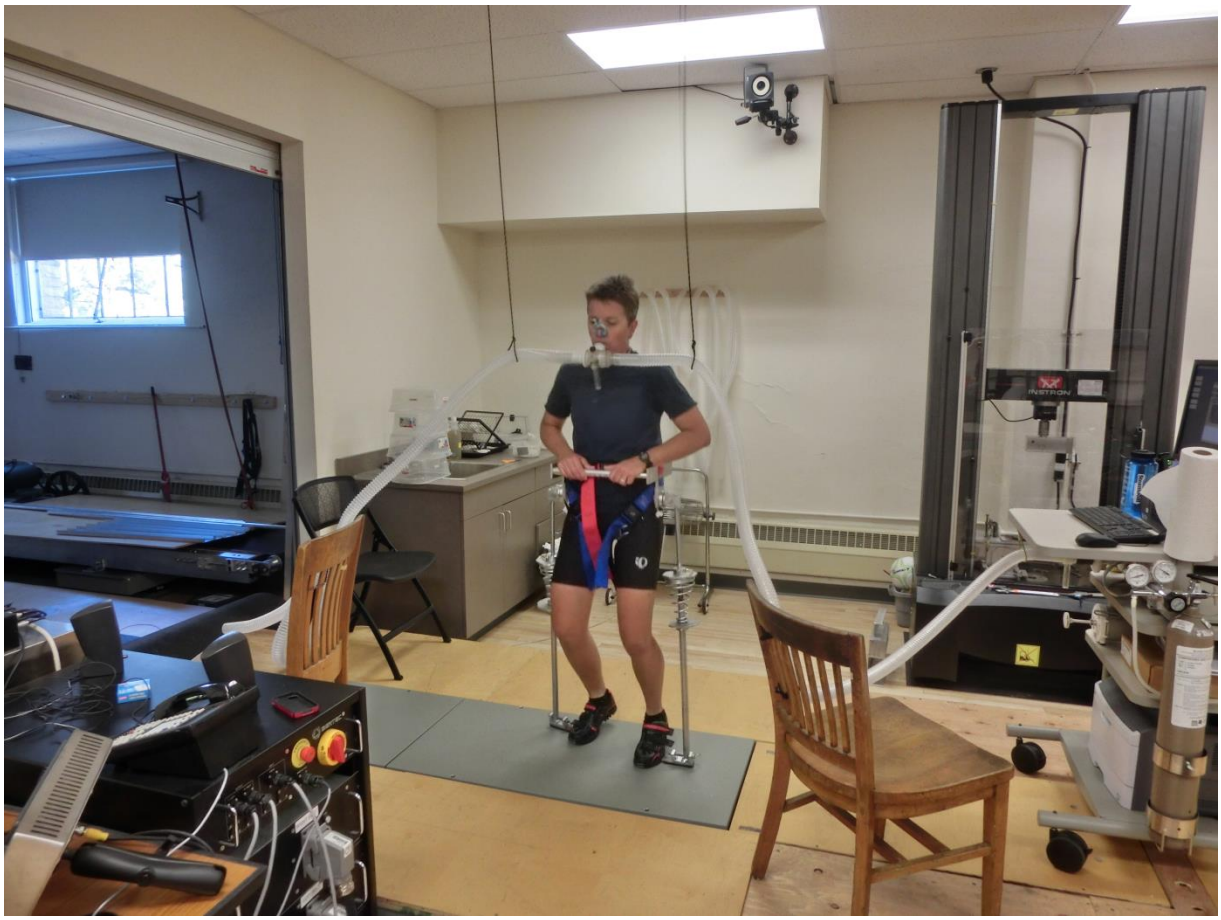

Figure 23. Exoskeleton testing setup. The subject wears a mouthpiece with an inlet and an outlet hose. The outlet hose, at right, leads to the Parvo Medics TrueOne system. The subject hops on the gray AMTI force platform.

On the first day, subjects hopped with the stiff-soft (bow spring) exoskeleton and without the exoskeleton. On the second day, subjects hopped in the linear exoskeleton and without. On the third day, subjects hopped in the soft-stiff (conical spring) exoskeleton and completed their no exoskeleton trials. The trials within each session were randomized, with a different order of trials for each patient within a session.

During the first trial of each session, subjects stood in place and minimized extraneous movement so that the individual's baseline oxygen production and carbon dioxide consumption could be measured. In all subsequent trials of a session, subjects hopped in place for five minutes while a metronome dictated their hopping frequency. Subjects performed trials for each of three exoskeleton devices, and without an exoskeleton, at the hopping frequencies of 2.2, 2.4, 2.6, and 2.8 Hz. Each subject participated in a total of sixteen trials. Each trial lasted five minutes to allow the subject to reach metabolic steady state, which typically took about 90 seconds. The rates of oxygen consumption and carbon dioxide production from minutes 2:30 to 4:30 were used for analysis. Throughout all trials, the test proctor paid careful attention to the subject's metabolic rates, ensuring that the activity was not too demanding for the subject to reach a comfortable steady state.

The volumetric rates of oxygen inhalation and carbon dioxide exhalation are averaged over minutes 2:30 to 4:30 in each trial. Metabolic power was calculated using a standard equation (Brockway, 1987). This formula takes into account the ratio of oxygen

to carbon dioxide for common fuels used in respiration, and can accurately predict the metabolic power requirement of an activity using simple arithmetic relationships.

$$P = 16.51\left(\frac{kJ}{L}\right) * VO2\left(\frac{L}{min}\right) + 4.58\left(\frac{kJ}{L}\right) * VCO2(\frac{L}{min})$$

(Brockway, 1987)

The metabolic power from the first trial of each day, in which the subject remained still, is the baseline metabolic power. The metabolic power calculated from the gas volumetric rates during hopping is the gross metabolic power. Subtracting the baseline metabolic power form the gross metabolic power yields the net metabolic power, which is the measurement of the effort needed for a particular activity.

The AMTI force platform sampled ground reaction forces of the subject's hopping during each trial. Forces were sampled at 1000 Hz for 10-15 second intervals, twice per trial. The force plate monitors forces in three axes and the moments about each axis; for this study, only the vertical forces were examined.

At the end of each day of testing, the metabolic data and force data were logged and duplicated. The testing area was cleaned, the exoskeleton was disassembled and any necessary maintenance performed, and the respiration apparatus was cleaned and disinfected for use by another subject.

Chapter 5: Results

5.1 Net Metabolic Power

The net metabolic power of hopping for each of the three separate subjects, wearing each of the 3 exoskeletons and no exoskeleton, at each of the four hopping frequencies, are displayed in Figures 24 through 31. Each individual experienced different minima and maxima of net metabolic power. This is likely due to a combination of several factors, some of which are the type of physical activity to which each subject is accustomed, and the geometry of the subject's legs. However, several trends recurred across all subjects, which support several conclusions about the comparative effectiveness of each exoskeleton type. This section begins with an analysis of each subject's data and moves on to a discussion of the overall results. For all metabolic cost results, the uncertainty of the Parvo Medics indirect calorimetry system data is ±2% of the measurement. Section 5.2 discusses a repeatability study performed to ensure that the metabolic cost data were consistent across trials and accurately represented a subject's net metabolic cost.

5.1.1 Subject 1

Subject 1 is unique among the three test subjects because the exoskeleton was built using this subject as a model, and Subject 1 had the most extensive experience using and testing the exoskeleton. As a result, the exoskeleton fit Subject 1 better in several regards, and the data should be interpreted with this in mind. Subject 1 experienced the greatest reductions in metabolic cost while using the exoskeleton, but it would be reasonable to expect that, if the exoskeleton hip frame were improved to fit the other subjects as well, metabolic cost reductions could be improved for each user to achieve results of similar magnitude.

Subject 1's metabolic cost results are shown in Figures 24 and 25. Subject 1 experienced a general decrease in net metabolic power as the hopping frequency increased. This rule held for the no exoskeleton case, the soft-stiff case, and the linear case. In the stiff-soft case, Subject 1's net metabolic cost was low across every frequency, and declined still further at 2.8 Hz.

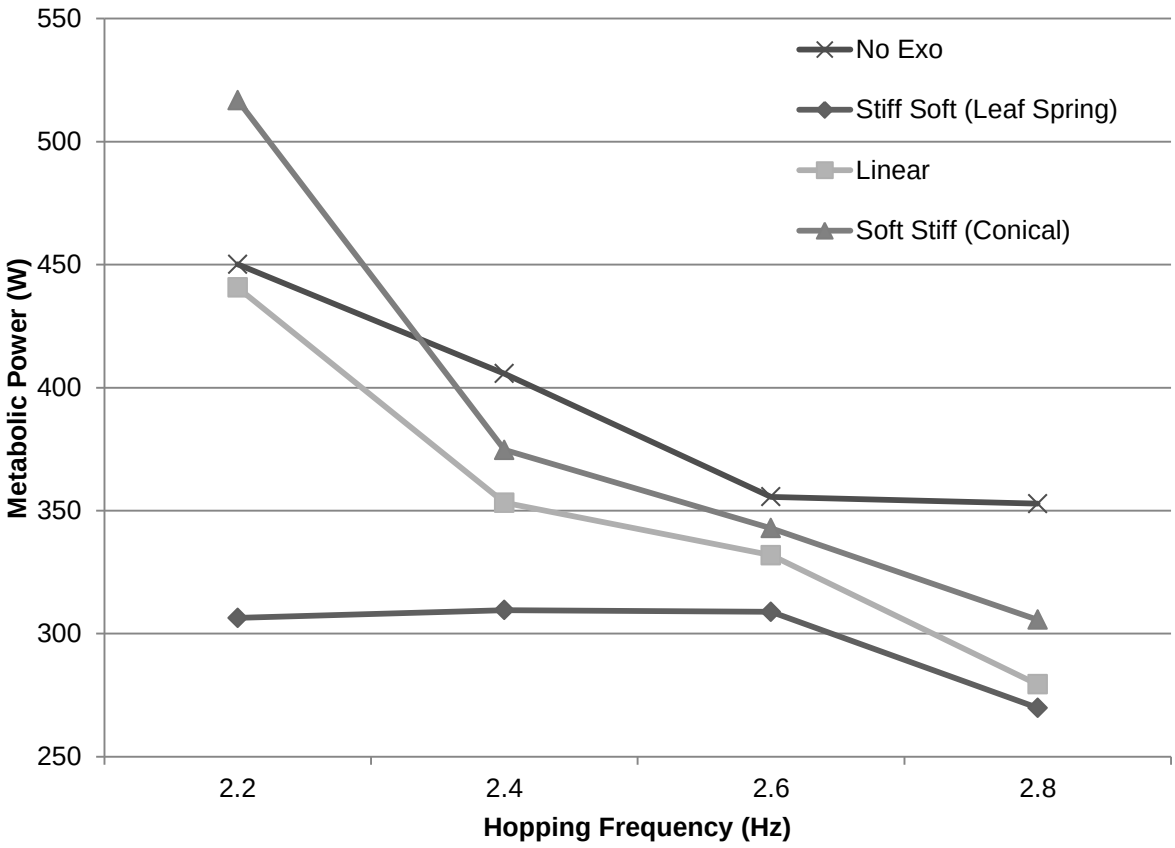

Figure 24. Subject 1's net metabolic power for hopping in each condition.

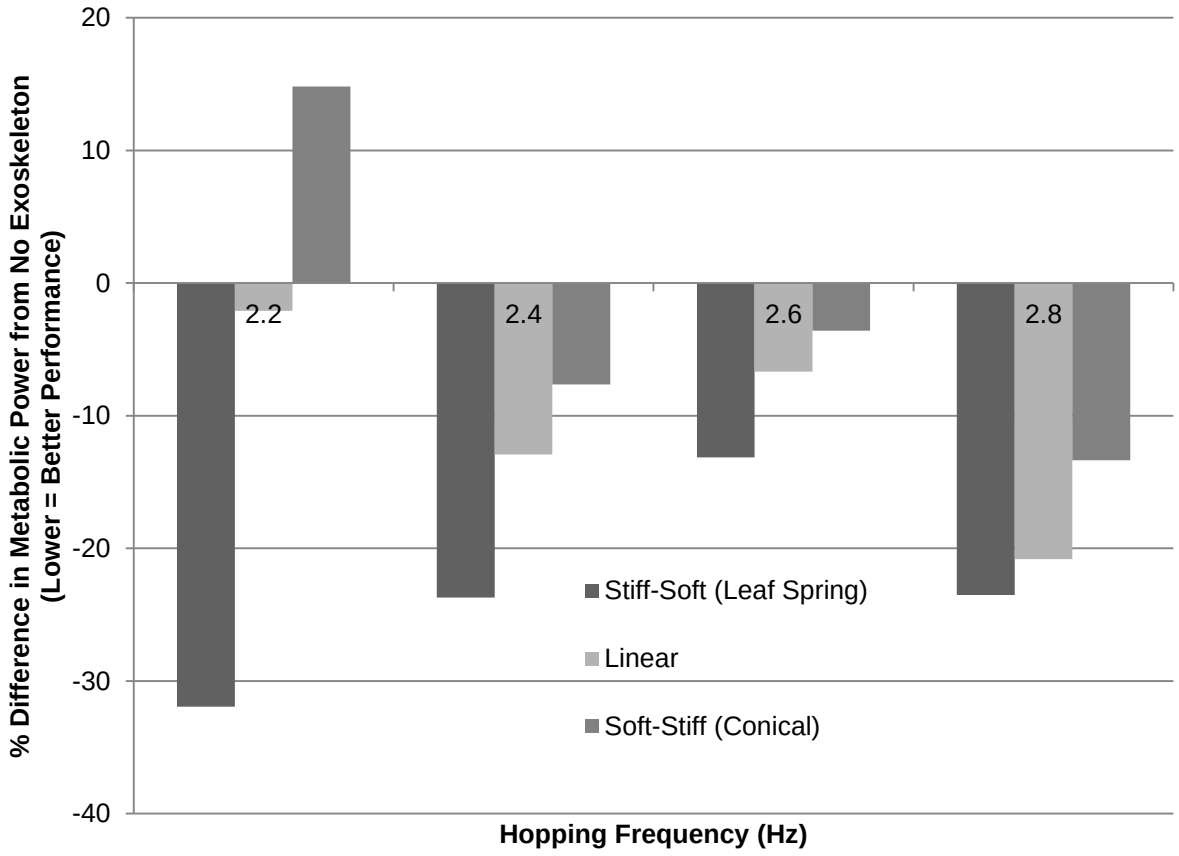

Figure 25. Subject 1's difference in net metabolic power for hopping in each condition compared to hopping without an exoskeleton.

While using the bow spring exoskeleton (stiff-soft), Subject 1 hopped with a low metabolic demand at all frequencies, but the exoskeleton's effectiveness was greatest at the lower frequencies. Because of the trend for metabolic demand to decline with increasing frequencies, the other spring stiffnesses approached the stiff-soft exoskeleton's performance at 2.8 Hz. At 2.2 Hz, the stiff-soft stiffness reduced Subject 1's net metabolic power by 32% compared to hopping without an exoskeleton. This was the largest reduction of net metabolic power that occurred in the study. The stiff-soft exoskeleton reached a minimum of a 13% reduction in metabolic power at 2.6 Hz compared to hopping without an exoskeleton, still offering a benefit to the user.

Subject 1 followed similar patterns while hopping in the linear and conical springs. Using each, Subject 1 exhibited steadily decreasing net metabolic power with increasing frequency. Net metabolic power decreased slightly faster with increasing frequency than hopping without an exoskeleton, which leveled off at higher frequencies. For each condition, metabolic power was lowest while Subject 1 hopped at the highest frequency, 2.8 Hz. At 2.8 Hz, hopping in the linear exoskeleton reduced net metabolic power by 21%, nearly matching the stiff-soft exoskeleton reduction of 24%. This typifies a theme, common to all subjects, of a marked increase in effectiveness for the linear and soft-stiff mechanisms at higher frequencies. The data suggest that these mechanisms could catch and possibly even exceed the stiff-soft exoskeleton's performance at even higher hopping frequencies, which are not unusual for competitive runners. While many frequent runners typically prefer stride frequencies of between 2.6 and 2.8 Hz (Cavagna, 1997), an elite athlete coach has observed that he rarely sees competitive runners with stride frequencies below 3 Hz (Daniels, 2014). In one well-known study of the 10 kilometer running event at the 2007 World Championships, it was found that the top three men's finalists had stride frequencies which ranged from 3.1 to 3.3 Hz over the course of the race, rising even higher at the finish (Enomoto, 2008).

5.1.2 Subject 2

Of the three users, Subject 2 had the most difficulty hopping in the exoskeleton. This is most directly a result of physical factors. Subject 2 was significantly smaller and lighter than Subject 1, who had been used as the template for building the exoskeleton. As a result, the hip frame was the poorest fit for Subject 2 of the three test subjects. Furthermore, the issue that all subjects faced — difficulties compressing the stiffer springs at lower frequencies — was magnified for Subject 2's lower body mass. Finally, Subject 2's experience and feedback suggested that the optimal *k* estimation model, which was developed to determine optimal spring stiffness for a given subject, overestimated correct stiffness values for patients with lesser body mass. Although the estimated spring stiffnesses, especially of the bow spring mechanisms, were appropriate for the more massive subjects, they gave values that were too stiff for Subject 2 to operate. Subject 2's bow springs were softened by a significant amount (from 5.6 kN/m to 3.18 kN/m) before they were considered usable (see Section 3.4). Figures 26 and 27 show Subject 2's net metabolic power while hopping with each spring type.

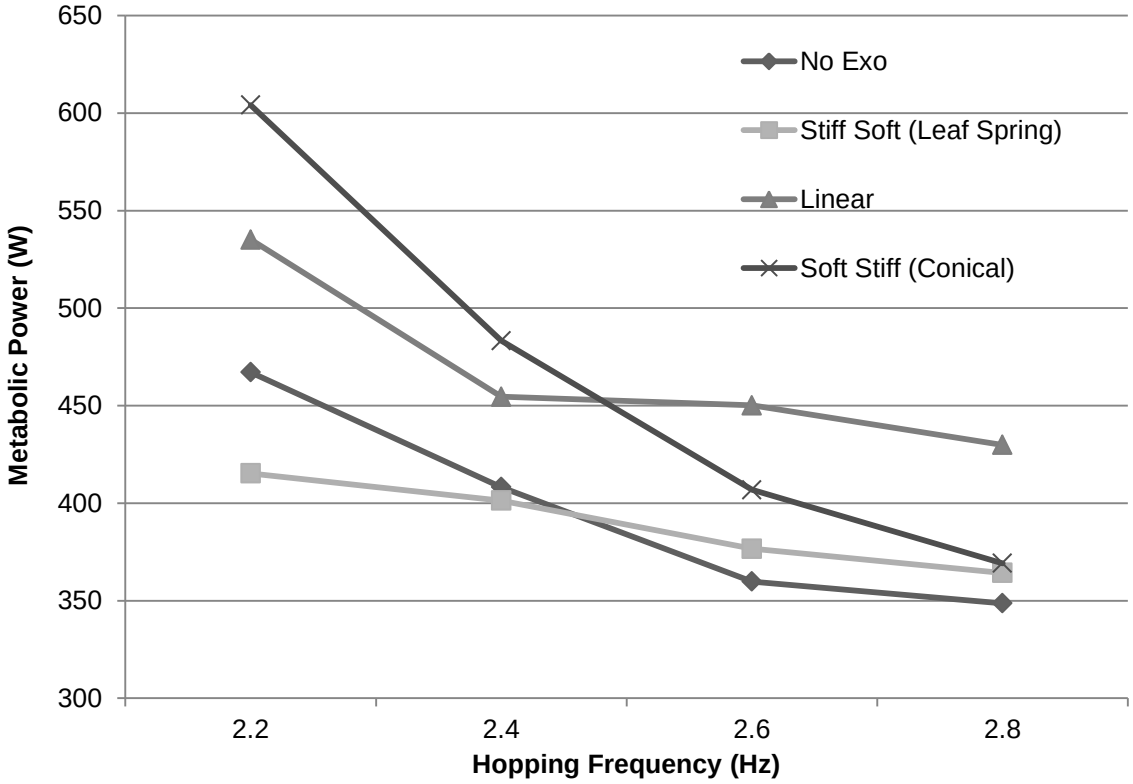

Figure 26. Subject 2's net metabolic power for hopping in each condition.

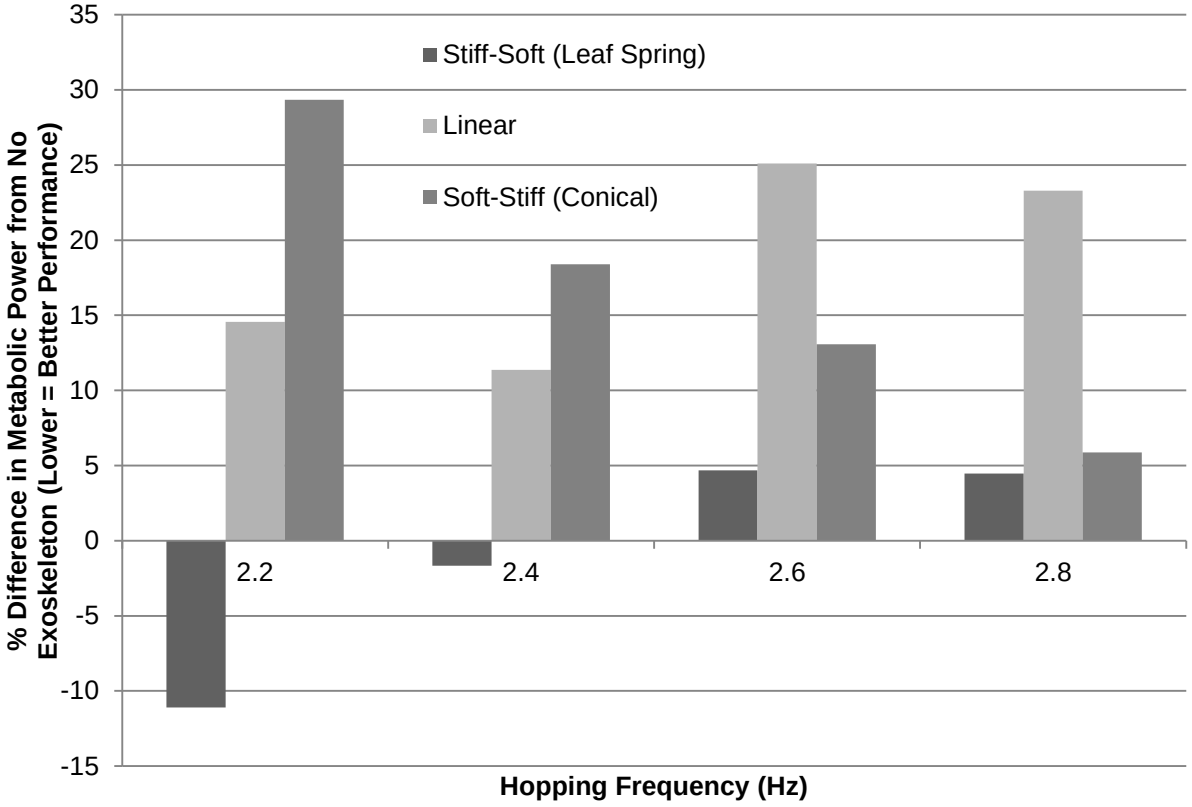

Figure 27. Subject 2's difference in net metabolic power for hopping in each condition compared to hopping without an exoskeleton.

For most trials, hopping with the exoskeleton did not reduce metabolic power compared to hopping without an exoskeleton; only using the bow spring exoskeleton at 2.2 and 2.4 Hz yielded a metabolic power reduction. For the linear and soft-stiff (conical) exoskeletons, net metabolic power decreased as frequency increased, similar to the trends observed in the other subjects' data. In contrast, the stiff-soft (bow spring) exoskeleton's effectiveness decreased with increasing frequency.

For Subject 2, the linear spring increased the net metabolic power for hopping at every frequency, with no indication of a frequency-dependent trend. This may be related to the

difficulty of fitting the hip frame to Subject 2's body comfortably and snugly. Each of the other conditions was affected by differing circumstances: the stiff-soft (bow spring) spring, whose stiffness was drastically reduced to allow Subject 2 to hop comfortably, was the only one that yielded a metabolic power reduction. The soft-stiff (conical) spring is drastically softer when compression is minimal, which is why it became less detrimental for Subject 2 at higher frequencies; at higher frequencies, the hopping period is shorter and the vertical hopping distance is smaller, so Subject 2 never compressed the springs enough for them to become stiff. In comparison to these cases, the linear spring used by Subject 2 was significantly stiffer across the range of compression (see Table 1). No linear spring was available at the softness dictated by Subject 2's comfort level, so the spring that equated to the model's approximation of appropriate stiffness was used. This evidence suggests that the model should be tuned to better account for each user's body mass in the next iteration of the exoskeleton.

5.1.3 Subject 3

Subject 3 possessed similar leg length and body mass to Subject 1. This allowed the springs and exoskeleton to be more easily tuned to Subject 3, who found the springs more comfortable and easy to compress than Subject 2. Figures 28 and 29 show Subject 3's net metabolic power for each spring type.

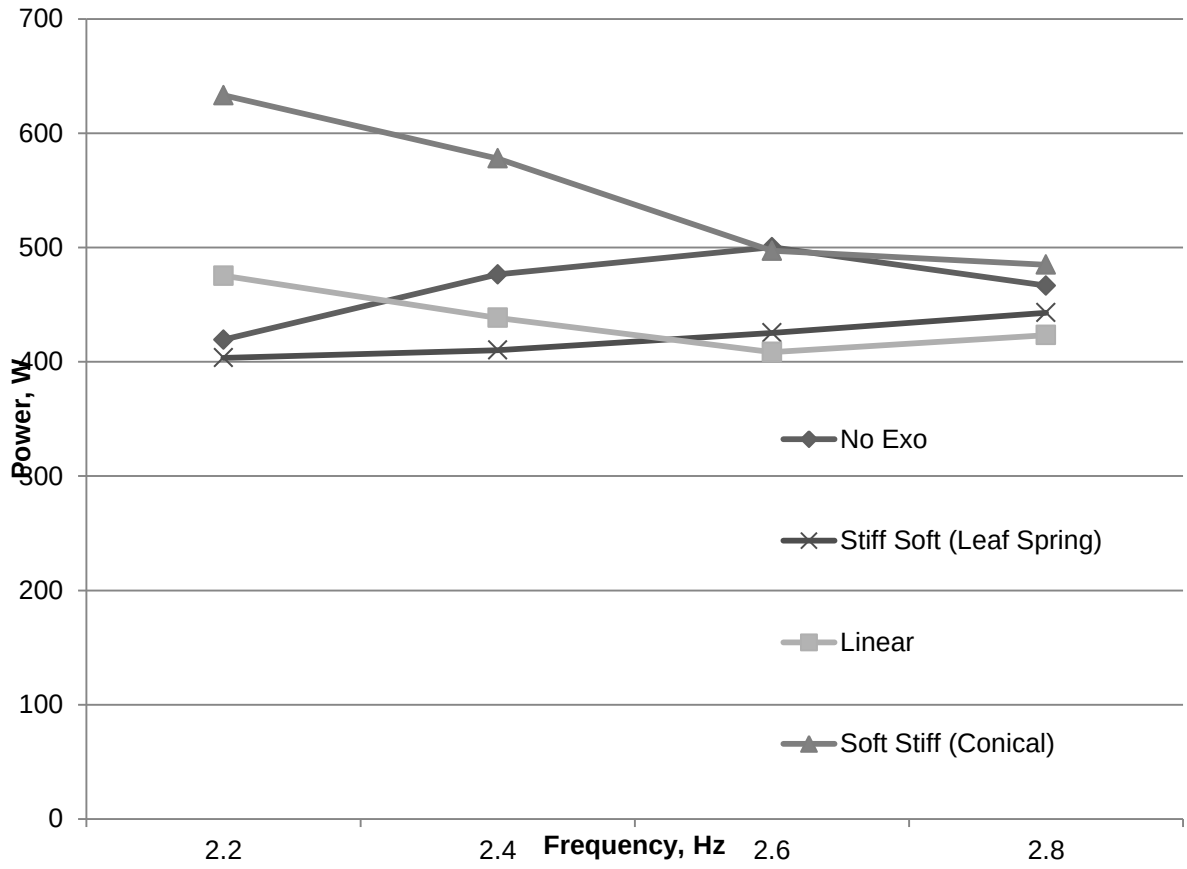

Figure 28. Subject 3's net metabolic power for hopping in each condition.

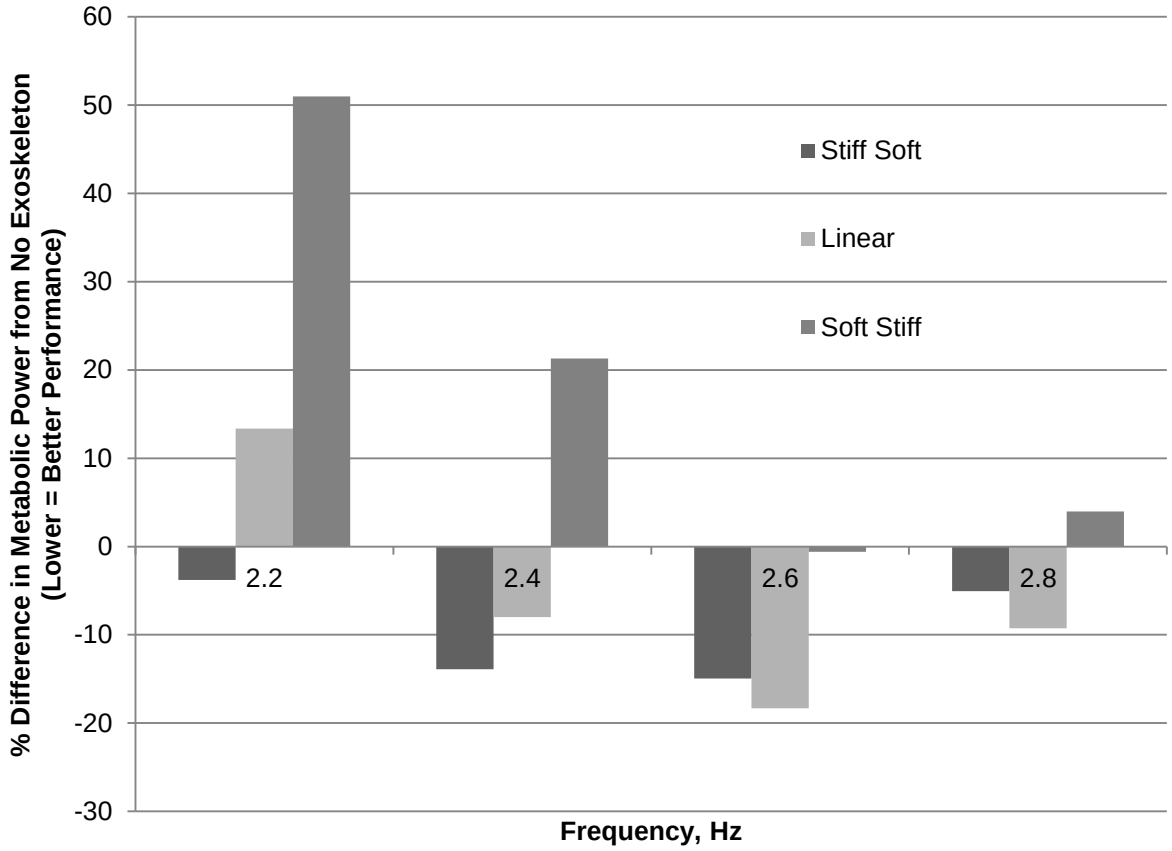

Figure 29. Subject 3's difference in net metabolic power for hopping in each condition compared to hopping without an exoskeleton.

Subject 3's data are distinct from the other subjects' presented in this study for several reasons. In the first place, this individual's net metabolic power for hopping without an exoskeleton did not decrease with increasing frequency as the others did. Instead, it peaked at 2.6 Hz. However, both the linear and soft-stiff (conical) cases exhibited the general trends of decreasing metabolic power as frequency increased, which occurs in the other subject's data. Hopping with the stiff-soft (bow spring) case actually seemed to follow the pattern of the no exoskeleton case, increasing metabolic power with increasing frequency. This suggests that the stiff-soft exoskeleton was affecting Subject

3’s leg behavior in a different way than the other exoskeleton types. This phenomenon is discussed further in section 5.3: Force-Displacement Results, and in Chapter 7: Discussion.

Subject 3 was also the only participating subject whose net metabolic power for hopping was most reduced by the linear exoskeleton mechanism (at 2.6 Hz, linear: 18% reduction; stiff-soft: 15% reduction). Subjects 1 and 2 both experienced the greatest reduction in metabolic power for hopping while using the stiff-soft (bow spring) exoskeleton. The measurement uncertainty of the Parvo metabolic testing system is approximately 2%, so this result is not explained by measurement error; however, further testing would be appropriate to fully establish this relationship.

5.1.4 Mean Metabolic Power for All Subjects

The combined net metabolic power for all subjects is shown in Figures 30 and 31, and in Table 2. The mean data support several conclusions. First, the stiff-soft (bow spring) exoskeleton was more effective at reducing the metabolic power for hopping at every frequency. Its greatest reduction of average metabolic power was 15%, occurring at 2.2 Hz. Second, subjects experienced greater reduction in metabolic power for all exoskeleton spring types as hopping frequency increased. The magnitude of this gradual improvement is greater for the less effective spring types, so that they all converge to a similar performance level at the highest frequency. This suggests that future trials at an even higher frequency, for example 3.0 Hz, could show if the trend continues and the less effective exoskeleton types improve even more. The 2.2 through 2.8 Hz frequencies were selected because they are representative of a broad range of running frequencies; however, frequencies higher than 2.8 Hz are not uncommon, especially among competitive athletes.

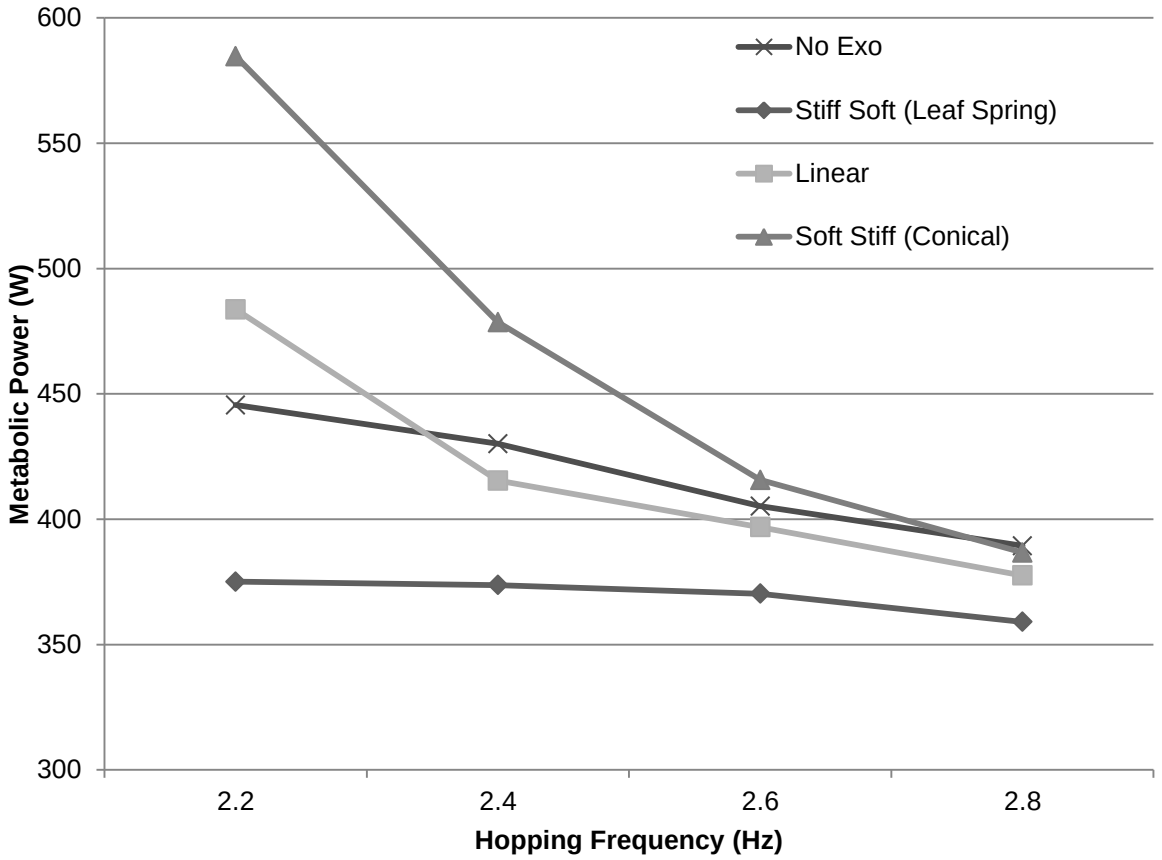

Figure 30. Mean net metabolic power for hopping in each condition, for all subjects.

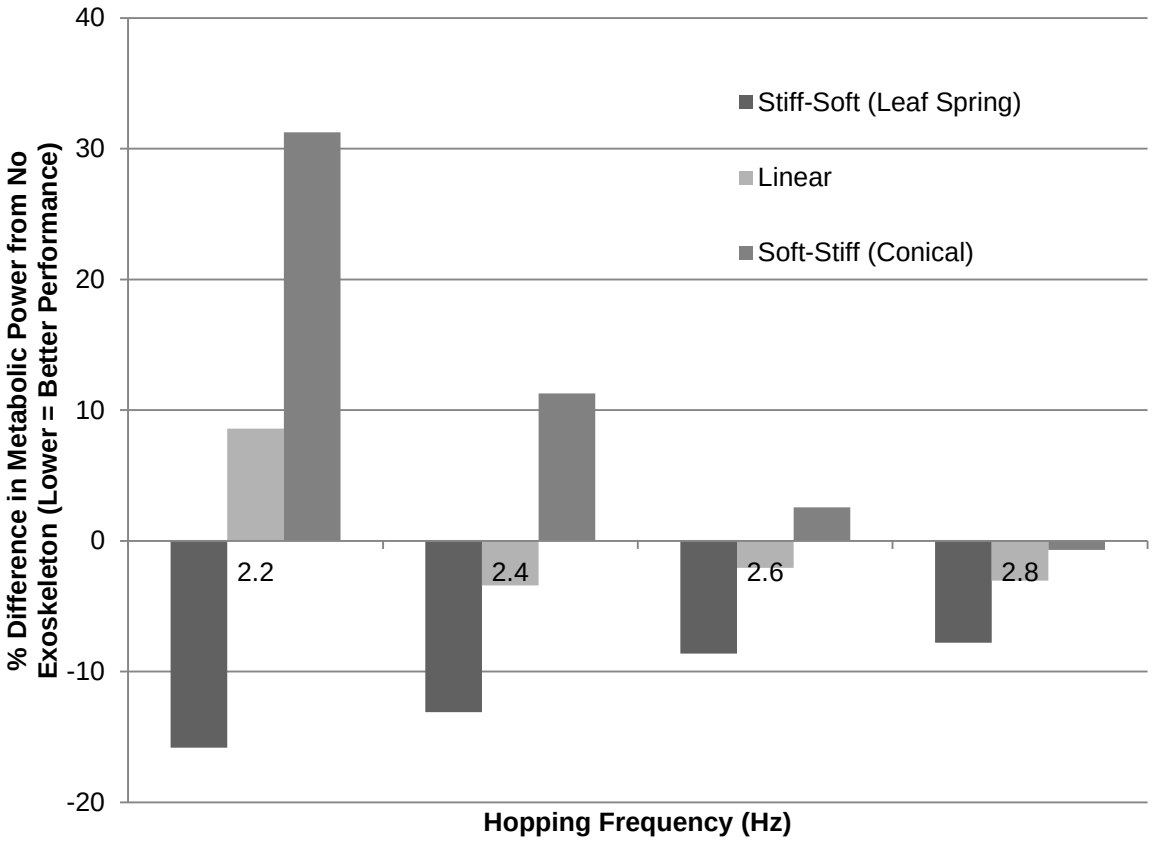

Figure 31. Mean difference in net metabolic power for hopping in each condition, compared to hopping without an exoskeleton.

Table 2. Performance of each exoskeleton type, in % difference compared to hopping without an exoskeleton. Data is for all subjects averaged together. Negative numbers indicate trials that improved the metabolic power compared to no exoskeleton case.

Freq (Hz)	2.2	2.4	2.6	2.8
Stiff Soft (%)	-15.8	-13.1	-8.6	-7.9
Linear (%)	8.6	-3.4	-2.1	-3.0
Soft Stiff (%)	31.2	11.3	2.6	-0.1

5.2 Consistency of Metabolic Data

A small study was carried out to ascertain the consistency of data from each trial. In this process, Subject 3 hopped four times at the same frequency, using the same mechanism, on two separate days spaced five days apart. A person's metabolism changes significantly throughout the day, so the time of day was held the same across trials, a method that was applied to each subject throughout the entire study. The results of this study are shown in Table 3.

Table 3. Repeatability study results. Subject 3 hopped in the stiff-soft (bow spring) exoskeleton at 2.6 Hz in four trials. These trials occurred at the same time on two separate days spaced five days apart, to investigate the repeatability of individual trial results.

Trial	Power (W)	Mean P for 4 Trials (W)	% Difference from Mean
1	425.4	420.4	1.2
2	407.1		-3.1
3	422.5		0.5
4	426.4		1.4

The measurement uncertainty for the Parvo metabolic data collection system is ±2%. Compared to this, Subject 3's data showed low deviation between trials, supporting the statement that the data collected for the study as a whole are an accurate representation of each subject's real metabolic rates. This small consistency study was

limited in scope due to time constraints, but the small variation in Subject 3's trials support this conclusion.

5.3 Force-Displacement Behavior

Indirect calorimetry is effective for demonstrating which exoskeleton types best reduce the physical effort of activity. However, the data collected from the force plates allow an examination of how each mechanism is affecting the legs, and offer insight into why each exoskeleton performs the way it does. This section discusses how the force-displacement analysis is developed and reports its results.

Force plate data are collected in two intervals of approximately 15 seconds during each 5-minute hopping trial. The load cells in the AMTI force plate are sampled at 1000 Hz, providing detailed data of the normal forces acting on the body throughout the stance phase of hopping. A MATLAB script, given in Appendix A, uses the force data to develop and plot a curve of the overall leg stiffness of the subject. Beginning with vertical force data and the subject's body mass, it calculates the vertical acceleration of the subject's center of mass. It then integrates acceleration twice to model the subject's vertical displacement throughout the course of a hop. By comparing the applied normal force to the displacement of the center of mass, an "overall leg stiffness" curve can be created, which shows how the leg system behaves over the course of a hop. The script normalizes data to leg length and body weight, and averages 20 separate hops to eliminate small deviations between each hop and examine the overall mechanics.

As an example of what these force-displacement curves look like, Figure 32 shows the force displacement data for all subjects hopping without the use of an exoskeleton. The hops have been normalized to the body mass and leg length of their respective subjects; this yields leg stiffness curves that are consistent and similar across all subjects.

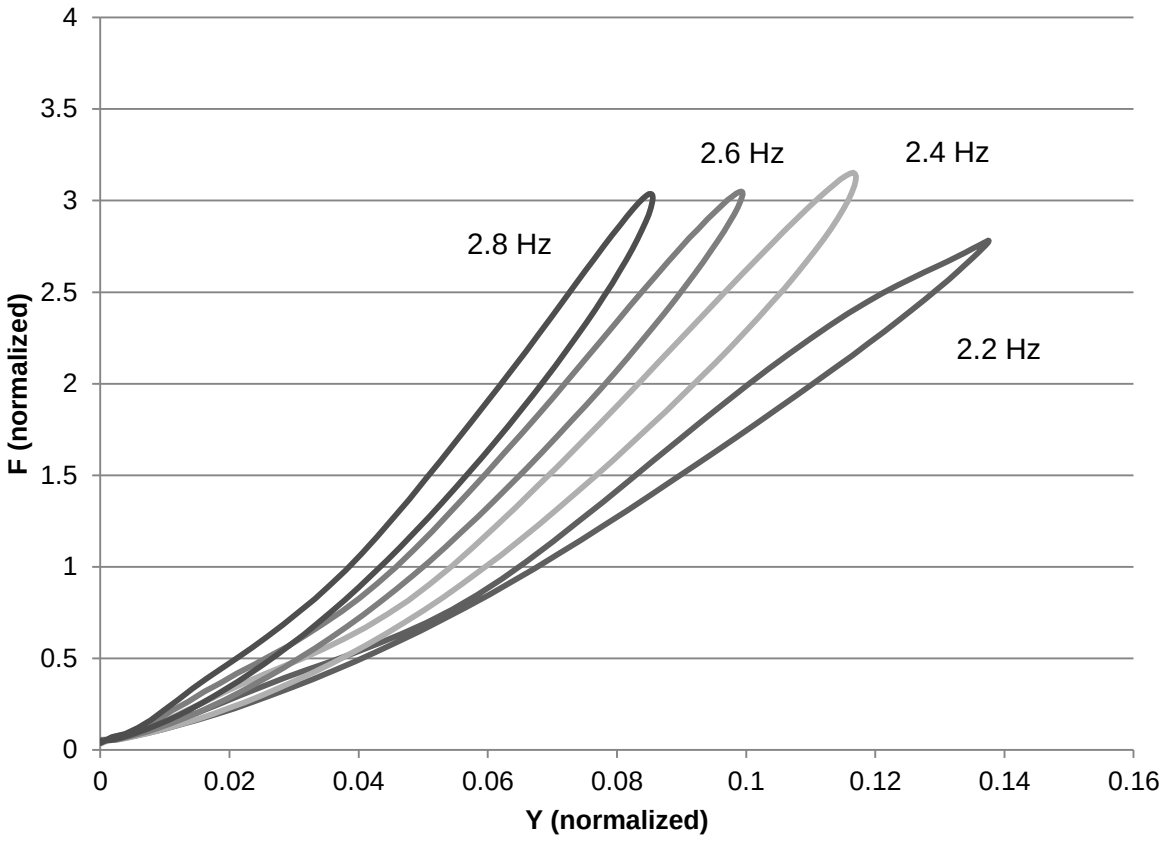

Figure 32. Force-displacement curves for all subjects hopping without the use of an exoskeleton. Force has been normalized to each subject's body mass, and displacement to leg length. When fit to linear regression models, the R^2 values of the curves range from 0.92 – 0.96. (2.2 Hz : R^2 = 0.96; 2.4Hz : R^2 = 0.93; 2.6 Hz : R^2 = 0.95; 2.8 Hz : R^2 = 0.92).

These force-displacement curves follow a recognizable shape which varies predictably with the frequency of hopping. The approximation of perfectly linear leg stiffness, made

frequently in biomechanics literature, is more accurate for lower frequencies of hopping than for higher. As might be expected, hopping at lower frequencies causes more leg deflection and a slightly lower maximum vertical force. There is also noticeable hysteresis in each curve. The upper line of each curve is made by the landing and compression of the leg, while the lower line that returns to the zero point is the extension of the leg leading up to takeoff. The area between each curve represents the energy lost during the hop.

Figure 33 shows the force-displacement data for all subjects hopping with the stiff-soft (bow spring) exoskeleton. Several similarities and differences are immediately apparent. First, the peak values of force and displacement are approximately the same when compared to Figure 32. Second, there is now a large spike that occurs immediately at impact. This is explained by the high initial stiffness of the bow spring exoskeleton, which softens once it has been initially compressed. The stiffness of the exoskeleton exceeds the leg's natural stiffness, and the exoskeleton absorbs negative work during the time interval immediately following impact. This "touchdown spike" is evidence of the role that the exoskeleton plays during hopping to absorb energy at the beginning of the stance phase, and helps to explain why the stiff-soft exoskeleton is the most effective of the three.

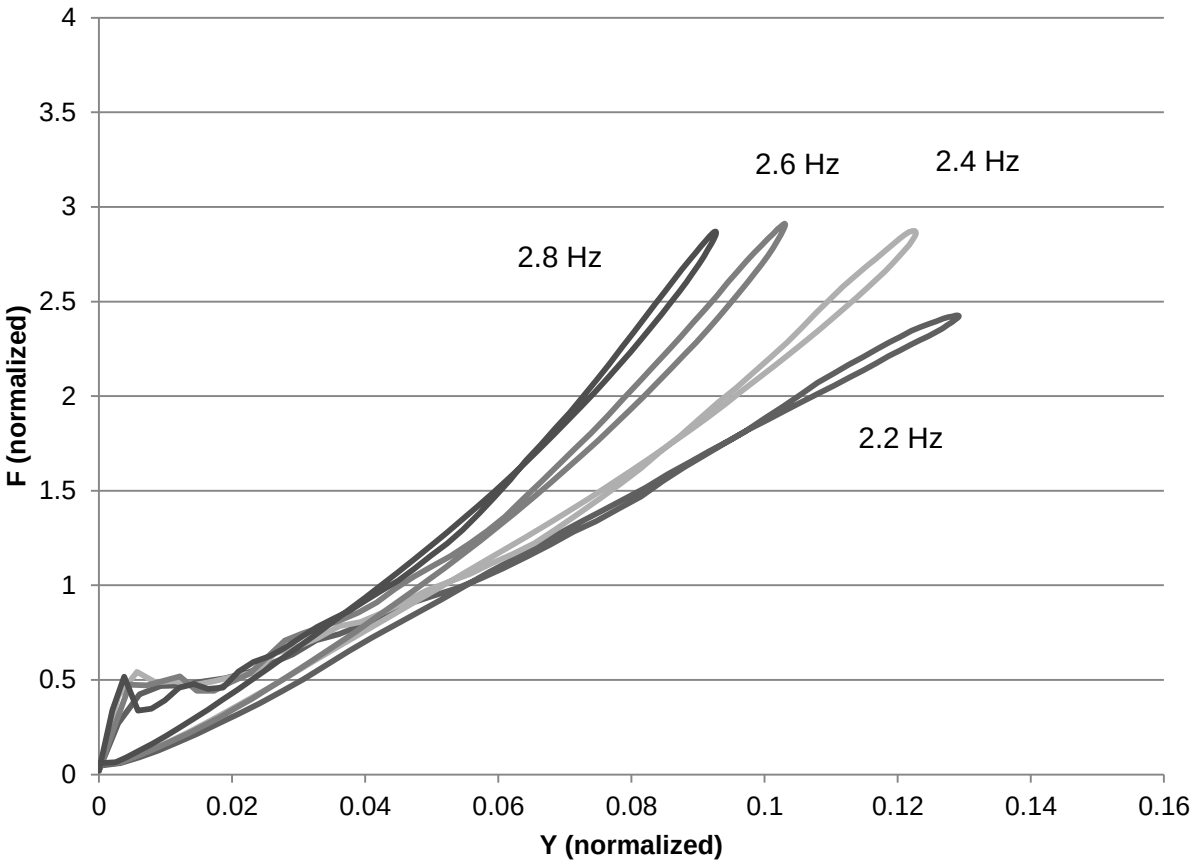

Figure 33. Force-displacement curves for all subjects using the stiff-soft (bow spring) exoskeleton. When fit to linear regression models, the R^2 values of the curves range from 0.96 – 0.99. (2.2 Hz : R^2 = 0.99; 2.4Hz : R^2 = 0.98; 2.6 Hz : R^2 = 0.96; 2.8 Hz : R^2 = 0.96). Of the overall force-displacement data sets, the stiff-soft (bow spring) curves had the highest R^2 values for linear regression curve fits.

Another difference between hopping with and without an exoskeleton is the hysteresis for each hop, which is notably reduced in the stiff-soft exoskeleton case. The explanation for this phenomenon isn't clear. It's possible that the exoskeleton, which has very little hysteresis in its compression curve (see Figure 22, Section 3.4), reduces overall energy losses by absorbing and returning energy that would otherwise be dissipated by the leg muscles. It may also be related to the presence of a semi-rigid

structure. Without an exoskeleton, the legs are free to have slightly different geometry during extension versus compression. The presence of the exoskeleton, however, may cause leg behavior to be more consistent during flexion and extension compared to hopping without an exoskeleton. The phenomenon may also be the result of a combination of these and other unknown factors.

One final characteristic of the subjects' overall stiff-soft force displacement curves is that they tend towards linearity. Aside from the initial touchdown spike, they exhibit smooth linear behavior in both impact and takeoff phases, sloping gradually upwards as frequency increases. This occurs when subjects hop without an exoskeleton, but the linearity is more pronounced with the exoskeleton present.

Figures 34 and 35 show the force-displacement curves for the linear and soft-stiff (conical) exoskeletons. When comparing the stiff-soft to the linear to the soft-stiff exoskeleton components, the touchdown spike becomes less pronounced. This makes logical sense; these latter springs are less stiff during the initial compression, and absorb less negative work at impact.

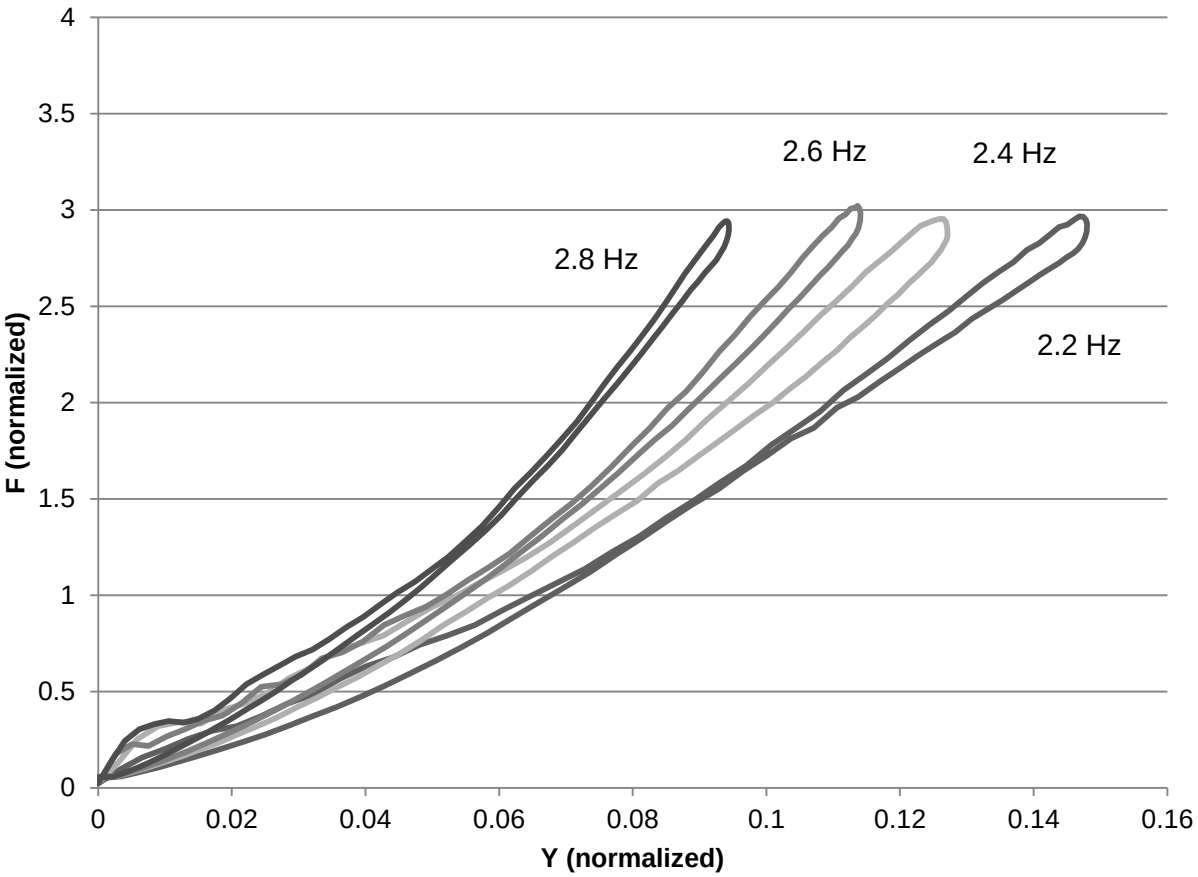

Figure 34. Force displacement curves for all subjects using the linear exoskeleton. When fit to linear regression models, the R^2 values of the curves range from 0.95 – 0.97. (2.2 Hz : R^2 = 0.97; 2.4Hz : R^2 = 0.97; 2.6 Hz : R^2 = 0.96; 2.8 Hz : R^2 = 0.95).

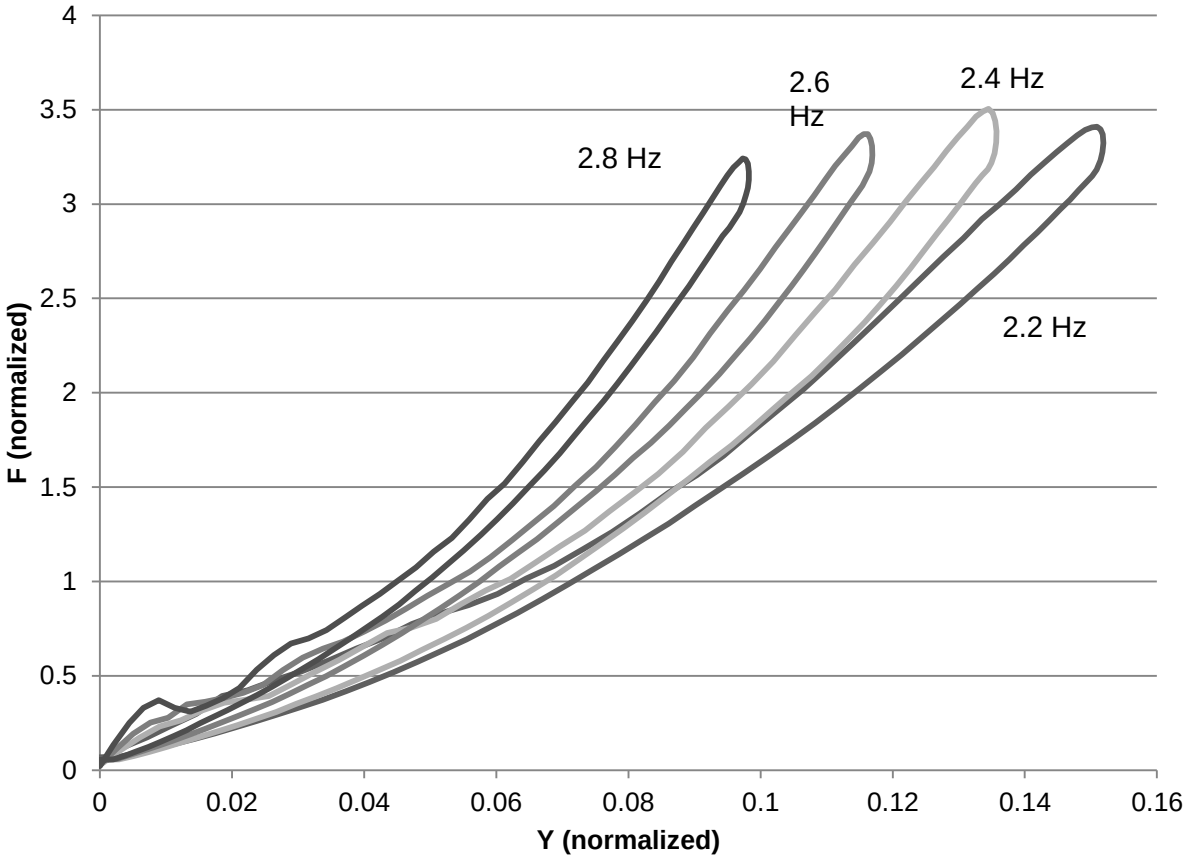

Figure 35. Force displacement curves for all subjects the using the soft-stiff (conical) exoskeleton. When fit to linear regression models, the R^2 values of the curves range from 0.93 – 0.95. (2.2 Hz : R^2 = 0.95; 2.4Hz : R^2 = 0.93; 2.6 Hz : R^2 = 0.93; 2.8 Hz : R^2 = 0.93).

The soft-stiff (conical) spring exhibits an unusual behavior: the peak force magnitudes are greater at lower frequencies than at higher frequencies. This is likely not a direct effect of hopping in the exoskeleton. The low-frequency trials with the conical springs were very difficult for all subjects, and frequently the subjects could not match the correct hopping frequency well. Often, subjects were forced to deliberately interrupt their motion in order to stay on the metronome's beat. For example, the contact time, or the duration of the subject's contact with the force plate, was recorded for each hop during the 15-second intervals. If a subject did not fully leave the force plate during the hop,

this hop was not considered in the data. At the 2.4 Hz hopping frequency, the mean contact times with the stiff-soft, linear, and soft-stiff exoskeletons were all within 0.01 seconds of the mean contact time for the no exoskeleton case (0.28 seconds). The mean hopping frequencies were similarly consistent and close to the metronome frequency. However, the contact time standard deviation of the soft-stiff case was four times greater (0.04 seconds) than the standard deviation of the no exoskeleton case and the stiff-soft exoskeleton case (0.01 seconds for each), and twice as great as the linear exoskeleton case (0.02 seconds). Using the soft-stiff exoskeleton, the subjects could not hop at a consistent frequency in the soft-stiff exoskeleton. Instead, the exoskeleton's increasing stiffness "pushed" them back upwards faster than they expected. As a result, they were continually changing their rhythm to try and match the metronome. This inconsistency resulted in erratic data for these trials, and the higher peak force may be a consequence of these issues.

Figures 31-35 provide R^2 values for linear regression models applied to each curve with an intercept at the origin. The stiff-soft force-displacement curves have the highest R^2 values, and the most linear behavior. The mean force displacement curves become more nonlinear in the less effective spring mechanisms, and the R^2 values become smaller as frequency increases. However, these data do not explain why this occurs. To examine how the spring's stiffness is affecting the leg behavior, the force-displacement curves can be compared to the Instron test data for each spring's force-displacement curve. The next section discusses the combination of these data and the results of the analysis.

5.4 Combined Instron and Force Displacement Curves

The force displacement curves generated in the previous section illustrate how the overall leg system behaves over the course of a hop. This system is the sum of two components: the legs themselves, and the exoskeleton when present. Because these components operate in parallel, the sum of their respective stiffnesses is the overall system stiffness. Therefore, subtracting the exoskeleton stiffness from the overall stiffness provides an approximation of how the leg behaves during each trial. It is important to remember that this is not a direct measurement; but rather an estimate of what is happening using the data available. The combined Instron and force-displacement data are shown in Figures 36-39.

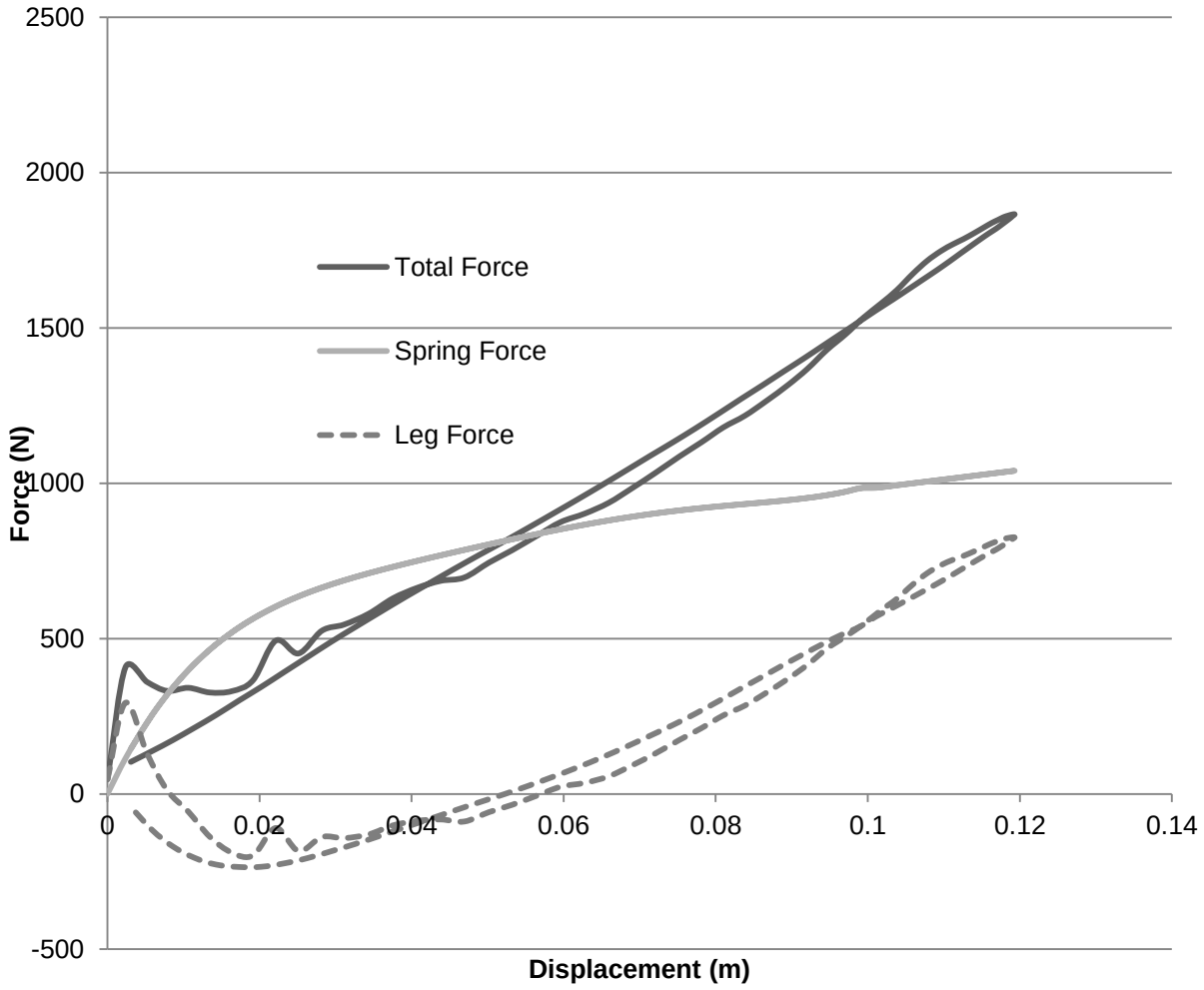

Figure 36. Combined Instron and force displacement data for Subject 1, hopping in the stiff-soft (bow spring) exoskeleton at 2.2 Hz.

Figure 36 shows the combined data for the most successful exoskeleton trial: Subject 1 hopping in the stiff-soft exoskeleton at 2.2 Hz. Subject 1 experienced a 32% reduction in net metabolic power while hopping under these conditions. The dashed line is the estimate of leg behavior. At initial impact, the stiffness of the spring dominates, and causes the sharp touchdown spike that is characteristic of the stiff-soft exoskeleton. During this phase, the force the leg must exert is minimal. Figure 36 suggests that the leg force becomes negative at impact, showing the possible limitations of this analysis

method. It’s more likely that in this phase, the exoskeleton spring is bearing all of the vertical load, and its force is compressing the soft tissues of the subject where the exoskeleton is attached to the body. As the spring is compressed further and loses stiffness, the human leg becomes the driving factor that shapes the overall stiffness. Consequently, the legs do very little of the work to absorb the impact, and dominate the effort to control the hop in general. When the spring is most compressed, leg stiffness actually closely resembles the overall stiffness curve, and is reminiscent of the gentle linear pattern seen in low-frequency hopping without an exoskeleton (Figure 32). This suggests that the most effective exoskeletons are the ones that allow the leg’s behavior to closely mimic the pattern of the no exoskeleton case, but at a reduced peak force magnitude.

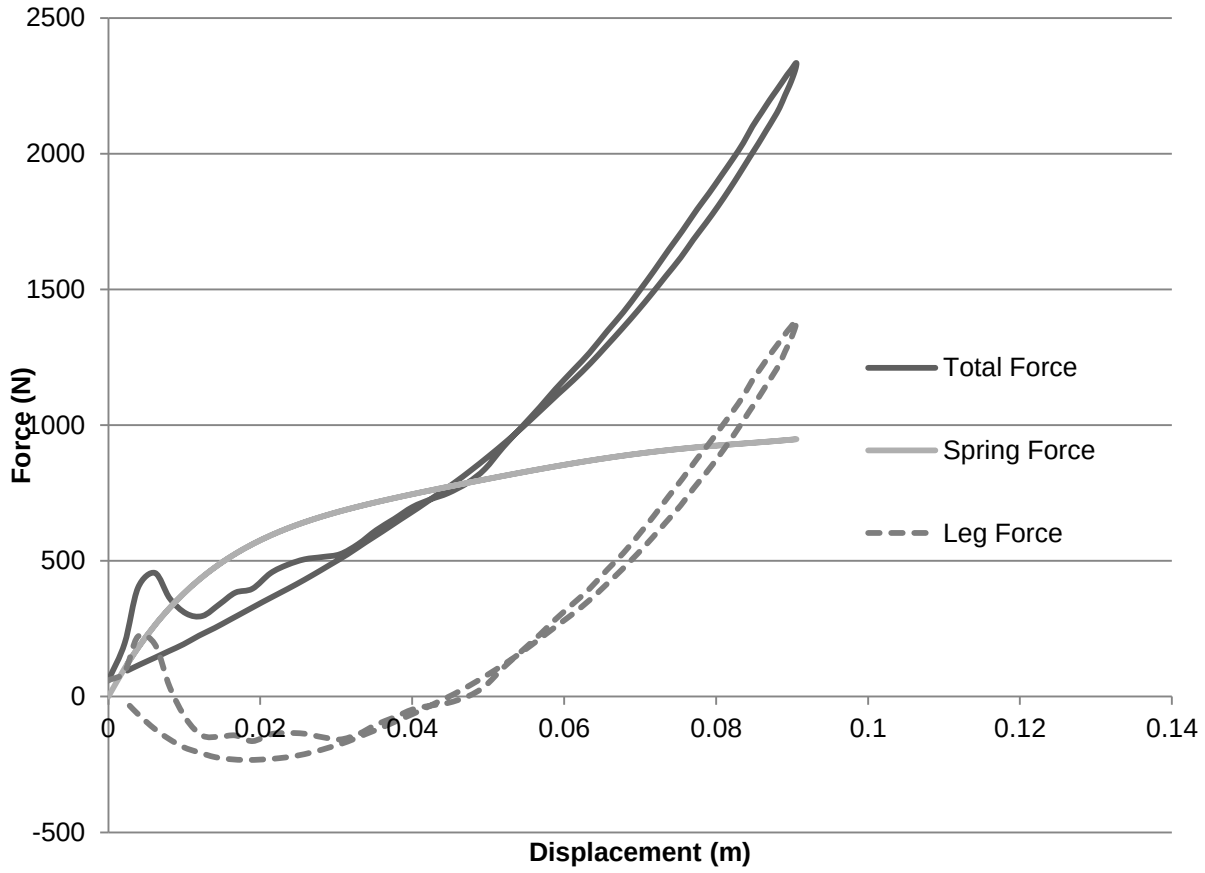

Figure 37. Combined Instron and force displacement curves for Subject 1, hopping in the stiff-soft (bow spring) exoskeleton at 2.6 Hz.

For comparison, Figure 37 shows Subject 1's least effective trial of the stiff-soft exoskeleton. At 2.6 Hz, Subject 1 experienced only a 13% reduction in metabolic power while using the exoskeleton. The impact event is similar in this case, but the higher frequency requires greater nonlinearity and increased stiffness from the leg. Instead of mirroring the overall behavior, the leg actually becomes stiffer (greater slope) than the overall system. Compared to the 2.2 Hz trial, the peak leg force in the 2.6 Hz trial is greater by approximately 600 N. The leg must exert this larger force rapidly to control the hop and maintain the overall stiffness behavior. These force-displacement data

suggest that this rapid exertion is related to the reduced effectiveness of the exoskeleton for this case.

For this step of analysis, the linear exoskeleton provides little insight. In most regards, the linear mechanism was the middle point between the soft-stiff and stiff-soft; its linearity conferred no unique benefit. For this reason, the linear exoskeleton data are omitted in this section in favor of the soft-stiff (conical) exoskeleton, which provides a more drastic comparison to the stiff-soft (bow spring) data.

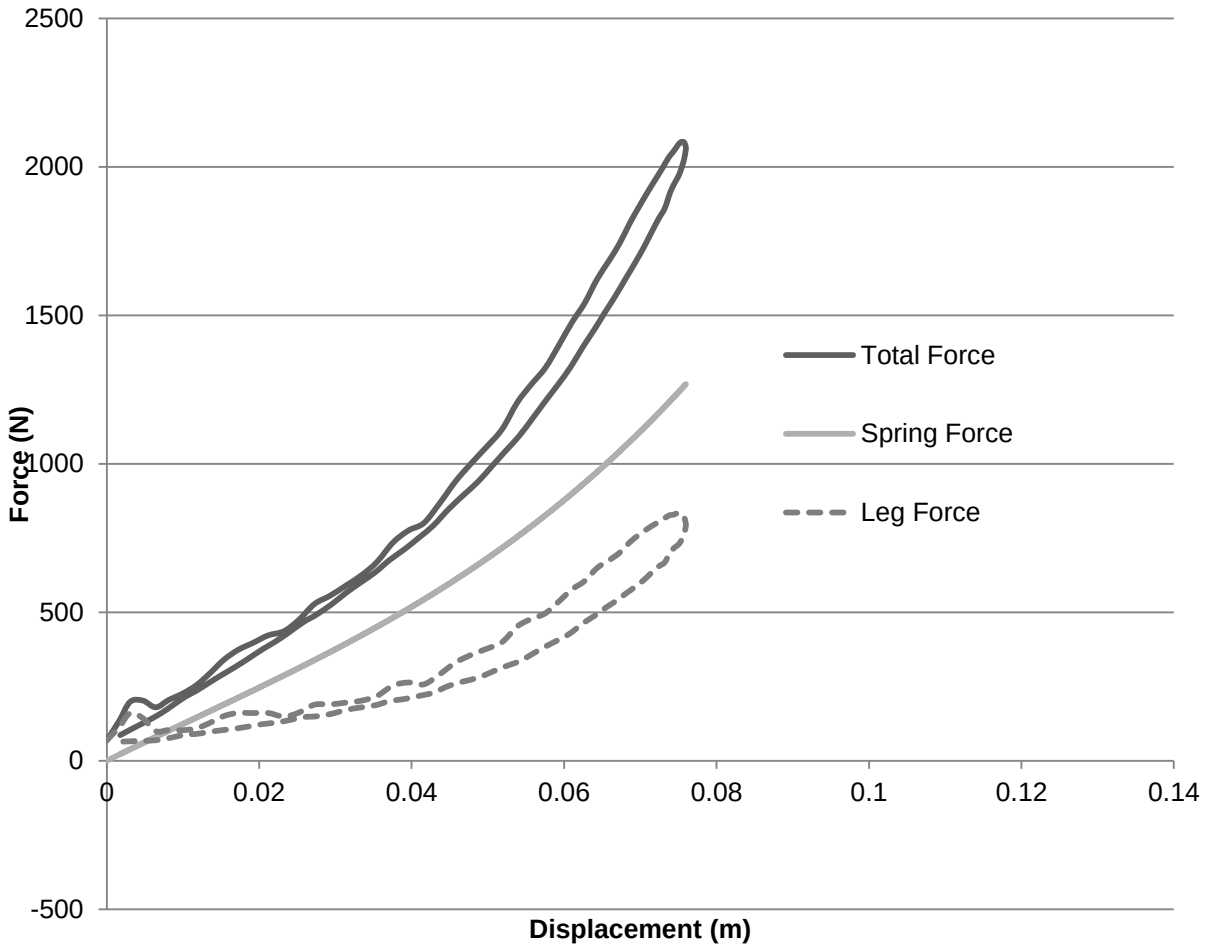

Figure 38. Combined Instron and force displacement curves for Subject 1, hopping in the soft-stiff (conical) exoskeleton at 2.8 Hz.

Figure 38 shows Subject 1's most successful trial using the soft-stiff (conical) exoskeleton. In this trial, Subject 1 experienced a 13% reduction in net metabolic power. This is the same magnitude of metabolic power reduction as the stiff-soft (bow spring) trial at 2.6 Hz, shown in Figure 37. The leg stiffness curve in Figure 38 trial mimics the stiff-soft spring case at lower frequencies, which all feature a gradually sloping stiffness and a low peak force.

A comparison of the leg behavior in Figures 37 and 38 also demonstrates the significance of the "touchdown spike." The net metabolic power for these trials was nearly identical. However, the peak force magnitude for the stiff-soft (bow spring) exoskeleton was roughly 500 Newtons greater. The other significant difference is the presence of the touchdown spike for the stiff-soft case, where the initial stiffness of the bow spring absorbed the body's landing impact. In the bow spring case, the peak leg force magnitude was ~50% greater than in the other case; however, the presence of a "touchdown spike" from the bow springs led to equivalent metabolic powers for the two cases. This supports the conclusion that both the initial and the sustained characteristics of the exoskeleton have significant effects on the device's performance.

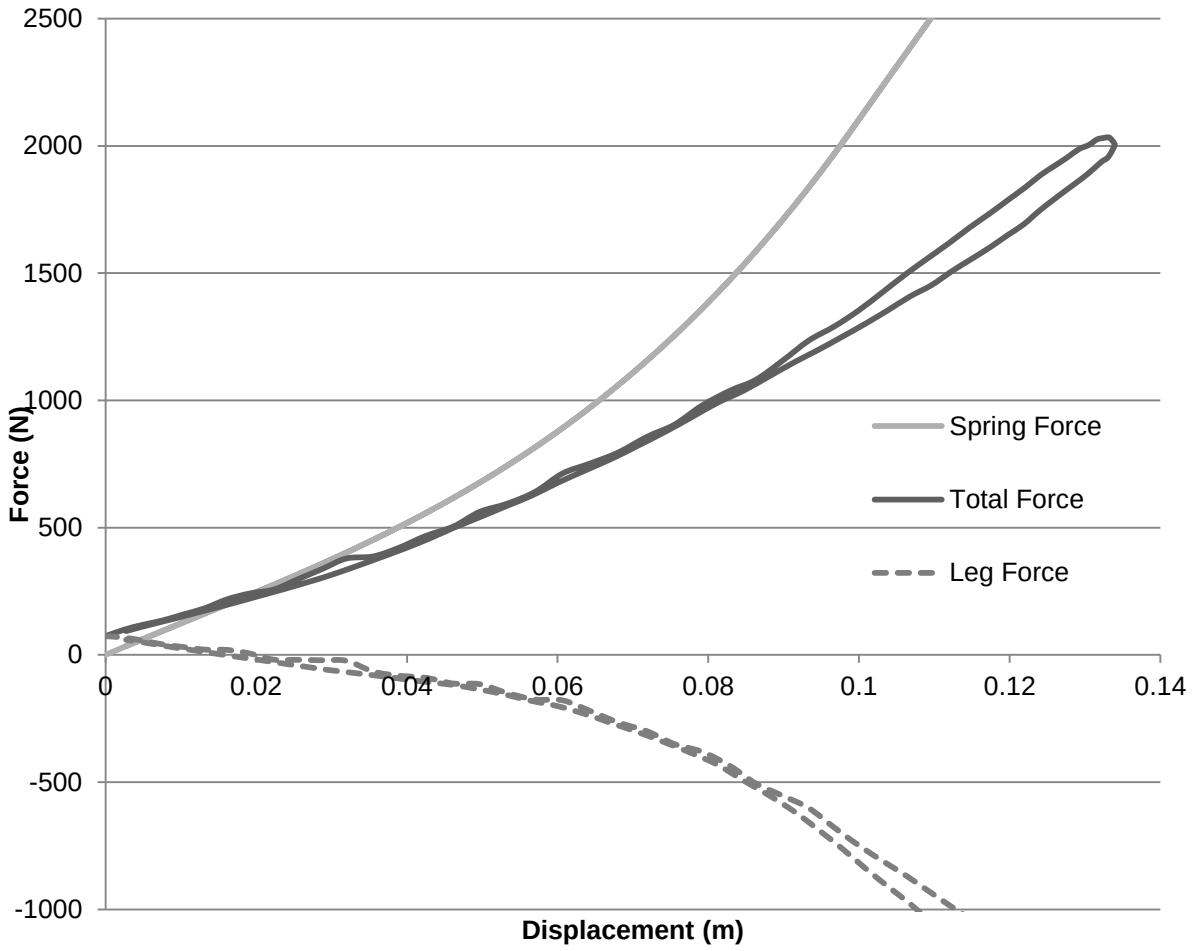

Figure 39. Combined Instron and force displacement curves for Subject 1, hopping in the soft-stiff (conical) exoskeleton at 2.2 Hz.

Figure 39 shows the counterpart to Figure 38. This is Subject 1's least effective trial of the soft-stiff (conical) exoskeleton. During this trial, Subject 1 experienced a 15% increase in metabolic power using the exoskeleton compared to the no exoskeleton case. Here, the conical springs are actually too stiff for Subject 1 to easily hop. In fact, none of the three subjects were capable of hopping consistently at 2.2 Hz using the conical spring exoskeleton. The conclusion to be drawn from this is that a spring that is stiffer than the leg requires greater effort from the person and the task is not possible to

maintain. In addition, stability may have been compromised with springs stiffer than the legs. Future research should consider less stiff soft-stiff springs.

Chapter 6: Conclusions

The bow spring exoskeleton provided subjects with the best net metabolic power results at all frequencies, reducing the metabolic power for hopping by up to 32% compared to hopping without an exoskeleton for Subject 1. The linear spring profile showed the potential to offer a metabolic benefit at higher frequencies, but the benefit it conferred was only rarely superior to that of the bow spring. Based on these data, the hypothesis that the linear spring profile would be the most effective at reducing the metabolic power for hopping was rejected. Similarly, hopping using the soft-stiff (conical) spring did reduce metabolic power at higher frequencies compared to hopping without the exoskeleton, but never to a larger extent than the other springs.

The linear spring faced one issue that likely prevented any subject from receiving its full potential benefit. The model used to select the appropriate linear stiffness for each subject (discussed in section 3.4) seemed to heavily overestimate the correct stiffness, especially for subjects of lower body mass. For every subject, the estimate was reduced by 10% to select the final spring stiffness. Even so, Subject 2 still could not hop comfortably using the linear spring selected. It was possible to reduce the stiffness of Subject 2's stiff-soft (bow spring) exoskeleton because materials were available, but a softer linear spring could not be obtained in time for Subject 2, and the results reflect this inadequacy. It is unlikely that rectifying this issue would change this study's conclusions significantly, since the other subjects' data do not suggest that a linear spring profile confers any special benefit. The linear spring generally achieved results that lay in between the results of the stiff-soft and the soft-stiff mechanisms.

The soft-stiff (conical) exoskeleton was consistently the least effective at reducing the metabolic power for hopping. One issue that the soft-stiff exoskeleton faced was the rarity of conical springs. Only one conical spring was available for testing with the correct stiffness, so there was no opportunity to tune this spring to each subject. For the other spring types, this would have been a disaster, because they needed to be chosen to allow the subject to even be able to compress them correctly; however, because the conical springs are initially soft, all subjects could comfortably compress the springs at impact. The major drawback was the lower hopping frequencies, where the natural leg stiffness is soft and near-linear. At these lower frequencies, the spring actually became too stiff to allow consistent hopping (Figure 39), and all subjects experienced difficulty matching the metronome. As the springs were compressed throughout the stance phase, they became too stiff for the leg to control the hopping motion, and the springs forced the subject back upwards more rapidly than desired.

Despite the disadvantages of the soft-stiff (conical) spring, its data proved valuable in demonstrating how the exoskeleton interacts with the user's legs. The metabolic data directly demonstrated which exoskeleton type best reduced the user's effort, but the force-displacement data helped to explain why. Based on the force displacement data, a new model was developed to explain how to design an exoskeleton stiffness profile to maximize its performance. This will be presented in the next section.

Chapter 7: Discussion

In this section, a model is presented to explain the results of the force-displacement testing. This model can be broken into two distinct regimes, during which the exoskeleton should have different goals. See Figure 40 for a visualization of this. The first regime is the impact of the body onto the ground. During this phase, an exoskeleton is most effective if it has a high initial stiffness. This phase is relatively short — approximately the first two centimeters of compression — but the force-displacement data demonstrate that it is important. The data in Figures 37 and 38 (Chapter 6) support the assertion that reducing or eliminating the rapid exertion of the leg muscles to absorb and stabilize the body's impact on the ground has a benefit equivalent to reducing the peak leg force by approximately 50%. The stiff-soft (bow spring) exoskeleton had the most pronounced impact phase benefit, with a "touchdown spike" that achieved a magnitude of approximately 50% of the subject's body weight over the first two centimeters of compression. This "50% in two centimeters" rule provides a starting point for investigating how to adjust the initial stiffness to fully take advantage of this effect, and it is recommended this be pursued in future work done on exoskeletons.

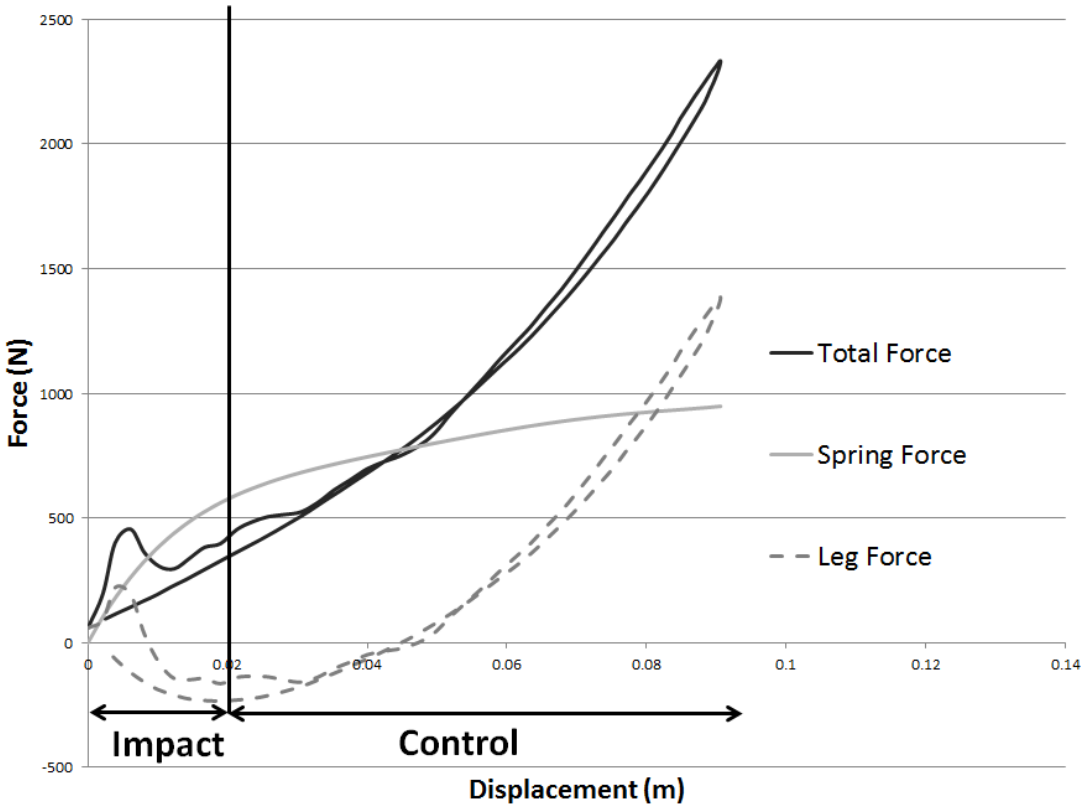

Figure 40. Visualization of the proposed model for designing an effective leg exoskeleton, showing both the impact and control regimes. The data displayed are for Subject 1, hopping in the stiff-soft exoskeleton (bow spring) at 2.6 Hz.

The second regime of the model is the control phase, during which the subject's legs play a greater role. In this phase, the exoskeleton's stiffness profile should be tuned to the frequency the user will hop at. There is no "one stiffness fits all frequencies" ideal solution because every mechanism's effectiveness depends on the hopping frequency of the trial. However, most runners run at a self-selected frequency, typically between 2.6 – 2.8 Hz (Cavagna, 1997). Competitive runners run with an even higher frequency, which can exceed 3 Hz (Daniels, 2014; Enomoto, 2008). With this information, it should be possible to design an ideal stiffness profile to confer the maximum benefit to the user (Figure 41).

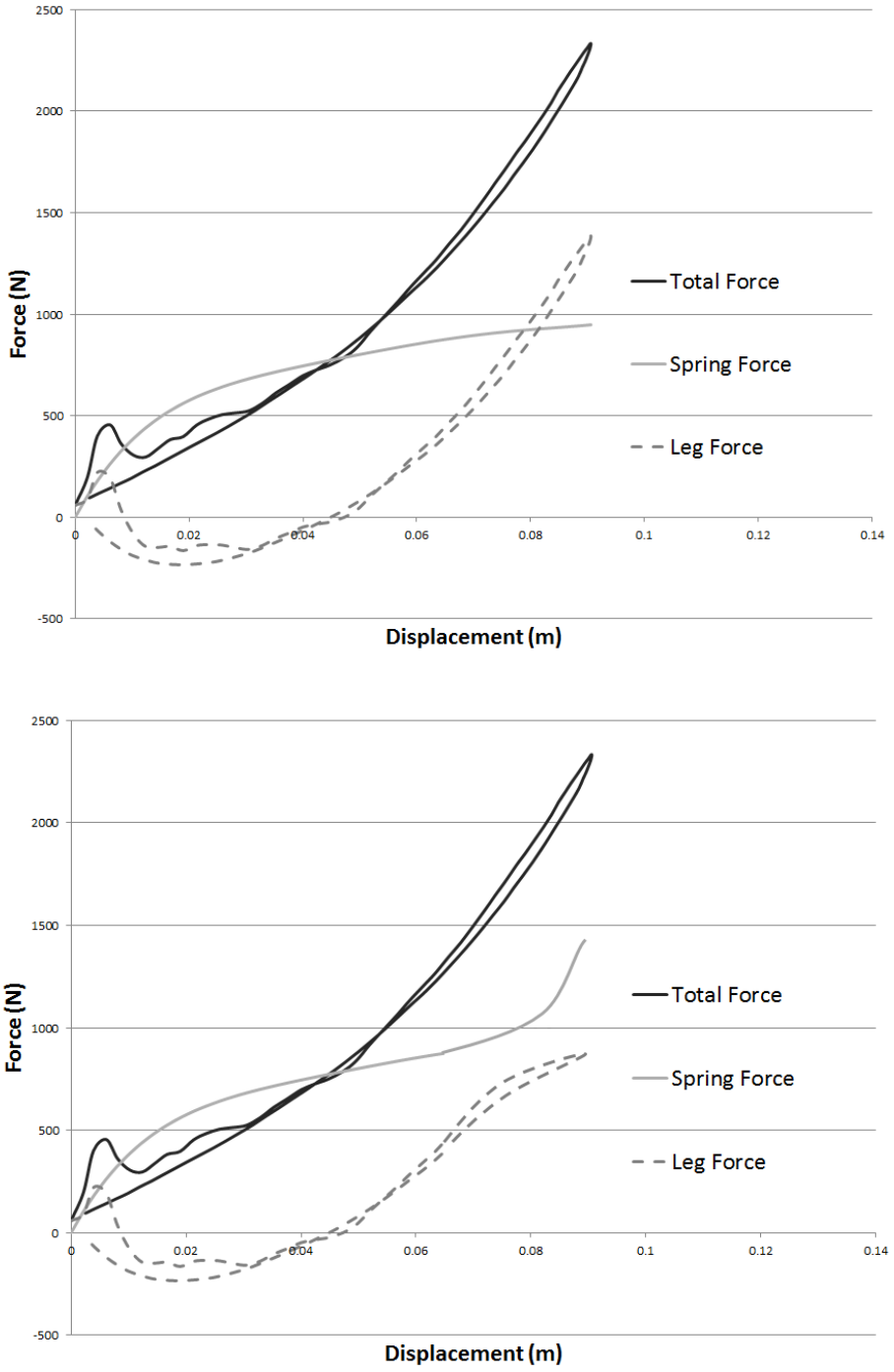

Figure 41. Illustration of how an exoskeleton's stiffness profile might be adjusted to create the desired leg behavior. The top figure shows the force-displacement data for Subject 1 hopping in the stiff-soft exoskeleton at 2.6 Hz. The lower figure shows proposed changes to the exoskeleton spring (solid gray line) that would allow the leg (dashed line) to adopt a less stiff behavior at the peak displacement.

The force-displacement results suggest that the most effective exoskeleton types in the control phase are those that provide just enough stiffness to allow the actual leg stiffness to adopt a soft, near-linear behavior (see Figure 36, Chapter 6). The peak force of this ideal stiffness profile is no more than one or two times the subject's total body weight. The stiff-soft exoskeleton was most effective because it provided a high initial stiffness, and then softened considerably to allow the legs to completely take over. At higher frequencies, though, this benefit was reduced because the overall leg behavior at higher frequencies is stiffer and more non-linear, as can be seen in Figure 32. Figure 41 shows how a stiff-soft exoskeleton might be improved in order to allow the leg to maintain a near-linear stiffness throughout the gait cycle. The leg exoskeleton which most reduced metabolic power had a stiffness profile which allowed the leg to maintain a soft, near-linear profile throughout the hop. In Figure 41, a spring profile is proposed that provides the benefits of the stiff-soft exoskeleton: a high initial stiffness which tapers off to allow the leg to control the hop. However, it also has an increasing nonlinear profile during maximum compression. This increasing stiffness at the point of maximum compression could allow the leg to maintain control of the hop without having to exert high-magnitude, non-linear loads on the ground.

Chapter 8: Future Work

In the above section, an “impact-control” model for designing effective exoskeletons was proposed. This model is supported by the data from this study, but it has not been rigorously tested and is still only a possible explanation for how an exoskeleton interacts with its user’s legs. Any future work that deliberately investigates both the impact and control phases of a hop could offer a great deal of further insight into how to design the most effective passive leg exoskeleton.

Further experimentation is not the only way to improve the leg exoskeleton, however. There are still a number of areas in which the current design could be drastically improved. Probably the most important of these is the fit of the exoskeleton to the user’s body. The primary issue is the hip frame. The current hip frame has a basic rectangular geometry, which is suitable for only some humans. In fact, most human hips are curved and do not sit comfortably in a rectangular frame. Any device for human use should be designed such that its user is comfortable using it, and wants to continue. Beyond the issue of comfort, a poorly fitting hip frame causes slop. When the body moves freely relative to the exoskeleton, that kinetic energy is not being absorbed by the exoskeleton, and the device’s effectiveness is reduced.

At the hip and ankle joints of the exoskeleton, the tolerances of the mechanical components could be improved to prevent slop and energy loss. Specifically, the axial rotation shaft in the hip joint and the uprights of the ankle joint assembly both allow

some free vertical motion. This could be avoided by redesigning the mechanism with this in mind.

The mathematical model for determining the appropriate linear spring stiffness for each subject overestimates correct values. Every subject tested thus far has required a reduction in spring stiffness from the calculated optimal value. For Subject 1, this was determined experimentally. Subject 1 tested multiple spring stiffnesses to confirm that the mathematical model was appropriate. The result was that a spring with 10% reduced stiffness from the calculated optimal value provided the greatest metabolic power reduction. For subjects with the same body mass as Subject 1, the calculated optimal spring stiffness can be likewise reduced by 10% to determine an appropriate stiffness.

However, the estimation may be less accurate for subjects with lower body mass. Subject 2, whose total body mass was significantly less than the other subjects, required a total stiffness reduction of 48% before feeling comfortable enough to use the exoskeleton. Stiffer springs made Subject 2 feel uncomfortable and out of control while using the exoskeleton. It's unclear why this is the case, but the issue should be improved for any further users for the exoskeleton. Either a new estimated stiffness model should be developed that does a better of job of accounting for the user's mass, or an experimental model can be developed that determines the correct stiffness for a user by empirical testing.

Finally, in order to make a leg exoskeleton useful for humans, it should be modified to allow running. In order to do this, the springs must be disengaged while the leg is in the air, so that the foot can be brought forward easily to begin a new step. A ratchet and pawl knee joint that replaces the rigid aluminum one used for this iteration of the exoskeleton has been designed to be incorporated into the exoskeleton. Once this has been reliably achieved, the passive-elastic exoskeleton has the potential to provide a significant health benefit to users with a wide variety of needs.

Bibliography

A. Berkeley Lower Extremity Exoskeleton
http://bleex.me.berkeley.edu/research/exoskeleton/bleex/
Image retrieved 11/31/2015

B. Cyberdyne HAL for Medical Use (Lower Limb Type)
http://www.cyberdyne.jp/english/products/LowerLimb_medical.html
Image retrieved 11/31/2015

Works Cited

1. Biewener, A A. "Muscle function in vivo: a comparison of muscles used for elastic energy savings versus muscles used to generate mechanical power." *American Zoologist* 38.4 (1998): 703-717.

2. Biewener, A A, D D Konieczynski, and R V Baudinette. “In Vivo Muscle Force-Length Behavior During Steady-Speed Hopping in Tammar Wallabies.” *The Journal of Experimental Biology 201* (1998): 1681–1694.

3. Biewener, A A, and T J Roberts. “Muscle and Tendon Contributions to Force, Work, and Elastic Energy Savings: A Comparative Perspective.” *Exercise and Sport Sciences Reviews* 28.3 (2000): 99–107.

4. Blickhan, R. “The Spring-Mass Model for Running and Hopping.” *Journal of Biomechanics* 22 (1989): 1217–1227.

5. Brockway, J M. “Derivation of Formulae Used to Calculate Energy Expenditure in Man.” *Human Nutrition. Clinical Nutrition* 41 (1987): 463–471.

6. Brooks, G A et al. *Exercise Physiology: Human Bioenergetics and its Applications.* Mountain View, CA: Mayfield Publishing, 2000.

7. Browning, R C, J R Modica, et al. “The Effects of Adding Mass to the Legs on the Energetics and Biomechanics of Walking.” *Medicine & Science in Sports & Exercise* 39.3 (2007): 515–525.

8. Brughelli, M, and J Cronin. “A Review of Research on the Mechanical Stiffness in Running and Jumping: Methodology and Implications.” *Scandinavian Journal of Medicine & Science in Sports* 18.4 (2008): 417–426.

9. Bullimore, S R., and J F Burn. “Ability of the Planar Spring-Mass Model to Predict Mechanical Parameters in Running Humans.” *Journal of Theoretical Biology* 248.4 (2007): 686–695.

10. Cavagna, G A. “Force Platforms as Ergometers.” *Journal of Applied Physiology* 39.1 (1975): 174–179.

11. Cavagna, G A, N C Heglund, and C R Taylor. "Mechanical work in terrestrial locomotion: two basic mechanisms for minimizing energy expenditure." *American Journal of Physiology-Regulatory, Integrative and Comparative Physiology* 233.5 (1977): R243-R261.

12. Cavagna, G A, M Mantovani, et al. “The Resonant Step Frequency in Human Running.” Pflügers Archiv : *European Journal of Physiology* 434.6 (1997): 678–84.

13. Cavagna, G A, N C Heglund, and C R Taylor. “Mechanical Work in Terrestrial Locomotion: Two Basic Mechanisms for Minimizing Energy Expenditure.” *American Journal of Physiology - Regulatory, Integrative and Comparative Physiology* 233 (1977): R243–R261.

14. Cavanagh, A R. Biomechanics of Distance Running. Champaign, IL: Human Kinetics Books, 1990.

15. Cavanagh, P R, and K R Williams. "The effect of stride length variation on oxygen uptake during distance running." *Medicine and Science in Sports and Exercise* 14.1 (1981): 30-35.

16. Cenciarini, M, and A M Dollar. “Biomechanical Considerations in the Design of Lower Limb Exoskeletons.” *2011 IEEE International Conference on Rehabilitation Robotic*s (2011): 1–6.

17. Collins, Steven H., M B Wiggin, and G S Sawicki. “Reducing the Energy Cost of Human Walking Using an Unpowered Exoskeleton.” *Nature* 522.7555 (2015): 212–215.

18. Daniels, Jack. *Daniels’ Running Formula – 3rd Edition*. Champaign, IL: Human Kinetics, 2014.

19. Davidson, P R, and D M Wolpert. “Widespread Access to Predictive Models in the Motor System: A Short Review.” *Journal of Neural Engineering* 2.3 (2005): S313–S319.

20. Dick, J, Edwards E. “Human Bipedal Locomotion Device.” *U.S. Patent 5,016,869* (1991).

21. Enomoto, Y, H Kadono, et al. “Biomechanical Analysis of the Medalists in the 10,000 Metres at the 2007 World Championships in Athletics.” *New Studies in Athletics* 3 (2008): 61-66.

22. Farley, C T, R Blickhan, et al. “Hopping Frequency in Humans: A Test of How Springs Set Stride Frequency in Bouncing Gaits.” *Journal of Applied Physiology* 71.6 (1991): 2127–2132.

23. Farley, C T, H H Houdijk, et al. “Mechanism of Leg Stiffness Adjustment for Hopping on Surfaces of Different Stiffnesses.” *Journal of Applied Physiology* 85.3 (1998): 1044–55.

24. Farley, C T, and D P Ferris. “Biomechanics of Walking and Running: Center of Mass Movements to Muscle Action.” *Exercise and Sport Sciences Reviews* 26.1 (1998): 253–285.

25. Farley, C T, J Glasheen, and T A McMahon. “Running Springs: Speed and Animal Size.” *The Journal of Experimental Biology* 185 (1993): 71–86.

26. Farley, C T, and O González. “Leg Stiffness and Stride Frequency in Human Running.” *Journal of Biomechanics* 29.2 (1996): 181–186.

27. Farley, C T, and D C Morgenroth. “Leg Stiffness Primarily Depends on Ankle Stiffness during Human Hopping.” *Journal of Biomechanics* 32.3 (1999): 267–273.

28. Farris, D J, B D Robertson, and G S Sawicki. “Elastic Ankle Exoskeletons Reduce Soleus Muscle Force but Not Work in Human Hopping.” *Journal of Applied Physiology* 115.5 (2013): 579–585.

29. Farris, D J, and G S Sawicki. “Human medial gastrocnemius force-velocity behavior shifts with locomotion speed and gait.” *Proc Natl Acad Sci U S A 109.* (2012): 977-982.

30. Ferris, D P, and C T Farley. “Interaction of Leg Stiffness and Surfaces Stiffness during Human Hopping.” *Journal of Applied Physiology* 82.1 (1997): 15–22.

31. Ferris, D P, M Louie, and C T Farley. “Running in the Real World: Adjusting Leg Stiffness for Different Surfaces.” *Proceedings of the Royal Society B: Biological Sciences* 265.1400 (1998): 989–994.

32. Ferris, D P, Z A Bohra, et al. “Neuromechanical Adaptation to Hopping with an Elastic Ankle-Foot Orthosis.” *Journal of Applied Physiology* 100.1 (2006): 163–170.

33. Franz, J R., N E. Lyddon, and R Kram. “Mechanical Work Performed by the Individual Legs during Uphill and Downhill Walking.” *Journal of Biomechanics* 45.2 (2012): 257–262.

34. Grabowski, A M, and H M Herr. “Leg Exoskeleton Reduces the Metabolic Cost of Human Hopping*.” Journal of Applied Physiology* 107.3 (2009): 670–678.

35. Herr, H. “Exoskeletons and Orthoses: Classification, Design Challenges and Future Directions.” *Journal of NeuroEngineering and Rehabilitation* 6.1 (2009): 21.

36. Herr, H. “Shoe and foot prosthesis with bending beam spring structures.” *US Patent 5,701,686* (1997).

37. Hobara, H, K Kanosue, and S Suzuki. “Changes in Muscle Activity with Increase in Leg Stiffness during Hopping.” *Neuroscience Letters* 418.1 (2007): 55–59.

38. Holt, N C, T J Roberts, and G N Askew. “The Energetic Benefits of Tendon Springs in Running: Is the Reduction of Muscle Work Important?” *Journal of Experimental Biology* 217.24 (2014): 4365–4371.

39. Hunter, I, and G A Smith. “Preferred and Optimal Stride Frequency, Stiffness and Economy: Changes with Fatigue during a 1-H High-Intensity Run.” *European Journal of Applied Physiology* 100.6 (2007): 653–661.

40. Kawamoto, H, S Lee, et al. “Power Assist Method for HAL-3 Using EMG-Based Feedback Controller.” *SMC’03 Conference Proceedings. 2003 IEEE International Conference on Systems, Man and Cybernetics.* (2003): 1648–1653.

41. Kerdok, Amy E, A A Biewener, et al. “Energetics and Mechanics of Human Running on Surfaces of Different Stiffnesses.” *Journal of Applied Physiology* 92.2 (2002): 469–478.

42. Krishnaswamy, P, E N Brown, and H M. Herr. “Human Leg Model Predicts Ankle Muscle-Tendon Morphology, State, Roles and Energetics in Walking.” *PLoS Computational Biology* 7.3 (2011): e1001107.

43. Lichtwark, G A. “In Vivo Mechanical Properties of the Human Achilles Tendon during One-Legged Hopping.” *Journal of Experimental Biology* 208.24 (2005): 4715–4725.

44. Magnusson, S P, M V Narici, et al. “Human Tendon Behaviour and Adaptation, in Vivo.” *The Journal of Physiology* 586 (2008): 71–81.

45. Malcolm, P, W Derave, et al. “A Simple Exoskeleton That Assists Plantarflexion Can Reduce the Metabolic Cost of Human Walking.” *PLoS ONE* 8.2 (2013): e56137.

46. McMahon, T A, G Valiant, and E C Frederick. “Groucho Running.” *Journal of Applied Physiology* 62 (1987): 2326–2337.

47. McMahon, T A, and G C Cheng. “The Mechanics of Running: How Does Stiffness Couple with Speed?” *Journal of Biomechanics* 23 (1990): 65–78.

48. Mooney, L M, E J Rouse, and H M Herr. “Autonomous Exoskeleton Reduces Metabolic Cost of Human Walking during Load Carriage.” *Journal of NeuroEngineering and Rehabilitation* 11.1 (2014): 80.

49. Moritz, C T, and C T Farley. “Human Hoppers Compensate for Simultaneous Changes in Surface Compression and Damping.” *Journal of Biomechanics* 39.6 (2006): 1030–1038.

50. Moritz, C T, and C T Farley. “Human Hopping on Damped Surfaces: Strategies for Adjusting Leg Mechanics.” *Proceedings of the Royal Society B: Biological Sciences* 270.1525 (2003): 1741–1746.

51. Moritz, C T, and C T Farley. “Human Hopping on Very Soft Elastic Surfaces: Implications for Muscle Pre-Stretch and Elastic Energy Storage in Locomotion.” *Journal of Experimental Biology* 208.5 (2005): 939–949.

52. Roberts, T J. “The Integrated Function of Muscles and Tendons during Locomotion.” *Comparative Biochemistry and Physiology - A Molecular and Integrative Physiology* 133.4 (2002): 1087–1099.

53. Taylor, C R, N C Heglund, and G M Maloiy. “Energetics and Mechanics of Terrestrial Locomotion. I. Metabolic Energy Consumption as a Function of Speed and Body Size in Birds and Mammals.” *The Journal of Experimental Biology* 97.1970 (1982): 1–21.

54. Teunissen, L P J, A M Grabowski, and R Kram. “Effects of Independently Altering Body Weight and Body Mass on the Metabolic Cost of Running.” *The Journal of Experimental Biology* 210.Pt 24 (2007): 4418–4427.

55. Westerterp, K R. “Physical Activity and Physical Activity Induced Energy Expenditure in Humans: Measurement, Determinants, and Effects.” *Frontiers in Physiology* 4.April (2013): 1–11.

56. Zoss, A, and H Kazerooni. “Design of an Electrically Actuated Lower Extremity Exoskeleton.” *Advanced Robotics* 20.9 (2006): 967–988.

57. Zoss, A, H Kazerooni, and A Chu. “On the Mechanical Design of the Berkeley Lower Extremity Exoskeleton (BLEEX).” *2005 IEEE/RSJ International Conference on Intelligent Robots and Systems, IROS* 11.2 (2005): 3132–3139.

Appendix A: MATLAB Code

K_{leg} Script

```
% This script interprets a .txt file containing force plate data and
% integrates to determine the overall leg stiffness using known data about
% the patient. It then returns a normalized set of force vs. displacement, as
% well as a plot of the data.

% This script WILL NOT WORK if the hopping frequency is less than 2.0 Hz.
% If it is to be used at less than 2 Hz, the size of the A and F arrays
% must be changed to allow for longer hopping periods. CTRL + F "500" to
% find instances of this.

% NOTE: This script relies on a file naming convention that has the initials
of the
% hopping subject first, in capitals.

clc
clear all

% Initialize the text files to be read and written.

filenameIn = uigetfile('*.txt');
Forces = load(filenameIn);%load('20140404 3Hz sample1.txt','\t')
%f = input('State hopping frequency of trial: ');
%m = input('State mass of subject, in kg: ');

subject = filenameIn(1:2);
if upper(subject) == 'JK'
    m = 76.5;
    L = .914;
elseif upper(subject) == 'AG'
    m = 58.5;
    L = .813;
elseif upper(subject) == 'JN'
    m = 73.5;
    L = .978;
end


sampling_freq = 1000;            % sampling Freq
dt = 1E-3;               % time
%L = input('State leg length of subject, in m: ');
F_raw = Forces(:,3) * 4.4482;    % hange lb to N. Update this if the wrong
column is being used.
F_adj = F_raw- min(F_raw(1:2000)); % Calibrate to minimum force

if (min(F_raw(1:2000)) > 6) || (min(F_raw(1:2000)) < -5)
    fprintf('Warning: force plate calibration may be off')
end
```

```
A_raw = (F_adj-9.81*m)./m;        % m/s^2
freq_start = 10000;

raw_start = 1;          % Remove portions of hops at start and end
raw_end = 15000;
while F_adj(raw_start) > 10    % to account for possibility of calibration
error
    raw_start = raw_start +1;
end
raw_start = raw_start + 5; % was 20

while F_adj(raw_end) <= 10      % eliminate last fill numbers, cut-off hop
    raw_end = raw_end -1;
end
while F_adj(raw_end) > 10
    raw_end = raw_end -1;
end
raw_end = raw_end - 5;

A_full = A_raw(raw_start:raw_end);
F_full = F_adj(raw_start:raw_end);

n = 20; % number of hops sampled
A = zeros(500,n);
F = zeros(500,n);
Y_new = zeros(100,n);
F_new = zeros(100,n);
start_locations = zeros(n,1);
end_locations = zeros(n,1);
starts = zeros(1,n);

% Locate starts and ends of hops
% The j loop is the rough cut, that identifies about where the hops begin
% and end.

ind_above=find(F_full>150);
j=1;
for i=2:(length(ind_above))
    if (ind_above(i)-ind_above(i-1))>1
        to(j)=ind_above(i-1);
        td(j)=ind_above(i);
        j=j+1;
    end
end
f_td = td;
f_to = to;
% Find actual toe-offs and touch-downs
steps=n;
k=1;
while k<=length(td)
    while F_full(f_td(k))>80
        f_td(k)=f_td(k)-1;
    end
    k=k+1;
end
```

```
f_td = unique(f_td);
td=f_td(1:steps+1);

k=1;
while k<=length(to)
    while F_full(f_to(k))>80
        f_to(k)=f_to(k)+1;
    end
    k=k+1;
end

f_to = unique(f_to);
to=f_to(1:steps+1);

if td(1)<to(1)
    to=to(1:steps);
else
    to=to(2:(steps+1));
end

for i = 1:n
    A_hop_vector = A_full(td(i):to(i));
    F_hop_vector = F_full(td(i):to(i));
    A(1:length(A_hop_vector),i) = A_hop_vector;     % Separate runs into
columns
    F(1:length(F_hop_vector),i) = F_hop_vector;
end


time = (1:1:length(F)) /1000;
V_unmod = cumtrapz(time, A);                % Numerical integration of A

for j= 1:n                          % Set average velocity to 0 over hop
    V(:,j) = V_unmod(:,j) - mean(V_unmod(1:to(j)-td(j)+2,j));
end

% The following for loop fills in zeroes for velocity when there is no
% force being applied to the plate. Because velocity is zero until that
% point, it does not change the position integral.

for i = 1:n
    j = to(i)-td(i)+2;
    while j <= length(V)
        V(j,i) = 0;
        j=j+1;
    end
end

Y = -1 * cumtrapz(time, V);              % Find vertical distance by
integrating V

for i = 1:n
    j = to(i)-td(i)+2;
```

```
    while j <= length(Y)
        Y(j,i) = 0;
        j=j+1;
    end
end


p = 100;                          % Desired interval length
Y_vector_length = to - td(1:n);
for ind = 1:n
    q = Y_vector_length(ind);
    Y_new(:,ind) = resample(Y(1:q,ind),p,q,0,1);
    F_new(:,ind) = resample(F(1:q,ind),p,q,0,1);
end


Y_avg = mean(Y_new.');
F_avg = mean(F_new.');
Y_norm = Y_avg / L;
F_norm = F_avg / (m*9.81);
% figure(7)
% plot(Y_avg,F_avg);
% title('Normalized force compared to normalized displacement');
Output_matrix = cat(4,Y_norm.',F_norm.',Y_avg.',F_avg.');

for i = 1:n-1
    period_actual(i) = (to(i+1)-to(i))/sampling_freq;
    contact_time(i) = (to(i)-td(i))/sampling_freq;
    aerial_time(i) = (td(i+1)-to(i))/sampling_freq;
end

% These adjustments filter contact and aerial times for the incorrect
% values that occur when the start and end locations do not provide a
% good understanding of the hopping frequency (for example, if the subject
% didn't leave the force plate entirely).
period_mean = mean(period_actual);


aerial_time_adj = aerial_time(aerial_time>.006);
contact_time_adj = contact_time(contact_time>(((period_mean*1000)-
100)/sampling_freq));

t_c = mean(contact_time_adj);
t_a = mean(aerial_time_adj);

% period_actual_adj = aerial_time_adj + contact_time_adj;
% hopping_frequency = 1/(mean(period_actual_adj));

period = t_c + t_a;
hopping_frequency = 1/period;
% This is the operation that removes unwanted "bad" hops from the time
% calcs
```

```
% Breaks down k_leg chart based on spring stiffness, using regression and
% extrapolation to simulate spring stiffness curves. The Spring_coeff
% vectors are the coefficients of the regression equations for the
% nonlinear springs.

% This section now multiplies modeled spring force by 2 to correctly
% simulate both legs.
if upper(subject) == 'JK'
    if findstr(upper(filenameIn), 'STIFFSOFT') > 1
        Spring_type = 'Stiff-soft';
        Spring_coeff = [4.2721321358E-07 -1.2714756734E-04 1.4575129584E-02 -
8.2363337658E-01 2.5989479890E+01];
        for x = 1:length(Y_avg)
            Y_avg_mm(x) = Y_avg(x) * 1000;
            if Y_avg(x) <= 0.1
                F_spring(x) = 2*(Spring_coeff(1) * Y_avg_mm(x)^5 +
Spring_coeff(2) * Y_avg_mm(x)^4 + Spring_coeff(3) * Y_avg_mm(x)^3 +
Spring_coeff(4) * Y_avg_mm(x)^2 + Spring_coeff(5) * Y_avg_mm(x)^1);
            else
                F_spring(x) = 2*(1.5061 * Y_avg_mm(x) + 340.37);
            end
        end

    elseif findstr(upper(filenameIn), 'LINEAR') > 1
        Spring_type = 'Linear';
        for x = 1:length(Y_avg)
            F_spring(x) = 2* (6.2468 * Y_avg(x) * 1000);
        end

    elseif findstr(upper(filenameIn), 'SOFTSTIFF') > 1
        Spring_type = 'Soft-stiff';
        Spring_coeff = [6.43254843E-04  -2.27402644E-02  6.36096144E+00];
        for x = 1:length(Y_avg)
            Y_avg_mm(x) = Y_avg(x)*1000;
            if Y_avg(x) <= 0.1
                F_spring(x) = 2*(Spring_coeff(1) * Y_avg_mm(x)^3 +
Spring_coeff(2) * Y_avg_mm(x)^2 + Spring_coeff(3) * Y_avg_mm(x)^1);
            else
                F_spring(x) = 2*(20.767 * Y_avg_mm(x) - 1024.2);
            end
        end
    end
elseif upper(subject) == 'AG'
    if findstr(upper(filenameIn), 'STIFFSOFT') > 1
        Spring_type = 'Stiff-soft';
        Spring_coeff = [-1.0241881481E-05 2.5956715210E-03  -2.4231756472E-01
1.0913572763E+01];
        for x = 1:length(Y_avg)
            Y_avg_mm(x) = Y_avg(x) * 1000;
            if Y_avg(x) <= 0.1
                F_spring(x) = 2*(Spring_coeff(1) * Y_avg_mm(x)^4 +
Spring_coeff(2) * Y_avg_mm(x)^3 + Spring_coeff(3) * Y_avg_mm(x)^2 +
Spring_coeff(4) * Y_avg_mm(x)^1);
            else
```

```
                F_spring(x) = 2*(.7305 * Y_avg_mm(x) + 171.68);
            end
        end
    elseif findstr(upper(filenameIn), 'SOFTSTIFF') > 1
        Spring_type = 'Soft-stiff';
        Spring_coeff = [6.43254843E-04  -2.27402644E-02  6.36096144E+00];
        for x = 1:length(Y_avg)
            Y_avg_mm(x) = Y_avg(x)*1000;
            if Y_avg(x) <= 0.1
                F_spring(x) = 2*(Spring_coeff(1) * Y_avg_mm(x)^3 +
Spring_coeff(2) * Y_avg_mm(x)^2 + Spring_coeff(3) * Y_avg_mm(x)^1);
            else
                F_spring(x) = 2*(20.767 * Y_avg_mm(x) - 1024.2);
            end
        end
    end
end

F_leg = F_avg - F_spring;

figure('Color','white')
plot(Y_avg,F_avg,Y_avg,F_spring,Y_avg,F_leg);
%title([subject ' ' Spring_type ' spring at '
num2str(round(hopping_frequency*10)/10) ' Hz.']);
xlabel('Y (m)');ylabel('F
(N)');legend('Total','Spring','Leg','Location','Northwest');
limits=[0 0.14 -1000 2500];axis(limits);



% %filenameIn_red = input('Input desired name of output file: ','s');
filenameIn_red = strrep(filenameIn, '.txt', '');
filenameOut = strcat(filenameIn_red,' hop data', '.txt');
fid = fopen(filenameOut, 'w');              % Open the file
if fid >= -1                              % If the file name is valid
    fprintf(fid, '%s\r\n','Mean contact time (s): ');
    fprintf(fid, '%f\r\n',t_c);
    fprintf(fid, '%s\r\n','Mean aerial time (s): ');
    fprintf(fid, '%f\r\n',t_a);
    fprintf(fid, '%s\r\n','Mean hopping frequency (s): ');
    fprintf(fid, '%f\r\n',hopping_frequency);
    fprintf(fid, '%s\t %s\t %s\t %s\r\n', 'Y(norm)','F(norm)','Y(m)','F(N)');
    fclose(fid);
end
dlmwrite(filenameOut,Output_matrix,'-append', 'newline', 'pc',
'delimiter','\t');
```

Appendix B: Exoskeleton Bill of Materials

Part Name	Exoskeleton Part #	External Part Source & Part #
Axial Rotation Shaft	1	-
Abduction Collar	2	-
Linch Pin Plate	3	-
Hip Flexion Plate	4	-
R12 Bearing	5	
Bearing Collar	6	-
Frame Bar / T Bar	7	-
Hip Plate	8	-
Bearing Cap	9	-
Nylon Thrust Bushing	10	McMaster-Carr #2797T2
# 8 x 7/8" Machine Screw	11	McMaster-Carr #90273A198
#8 x 1/2" Machine Screw	12	McMaster-Carr #90910A777
Retaining Ring	13	McMaster-Carr #97633A170
Hip Linch Pin	14	McMaster-Carr #98416A019
Knee Joint	15	-
Spring Steel Platform	16	-
Spring Deflection Joint	17	-
Ankle Joint Plate	18	-
Ankle Joint Riser	19	-
Telescoping Outer Rod	20	-
Telescoping Inner Rod	21	-
Inner Rod Collar	22	-
Inner Spring Plate	23	-
Outer Rod Collar	24	-

Outer Spring Plate	25	-
Axial Rotation Attachment	26	-
Nylon Sleeve Bushing	27	McMaster-Carr #6389K117
Bow Spring Fiberglass Rod	28	-
Linear Coil Spring (Subject 1 & 3)	29	W.B. Jones Spring Co. #C96-250-256
Linear Coil Spring (Subject 2)	30	McMaster-Carr #96485K156
Conical Coil Spring	31	Gibson Athletic SB-60001 Coil Spring 8”
Hip Joint Assembly	32	-
Hip Frame Assembly	33	-
Shoe Attachment Assembly	34	-
Coil Spring Assembly	35	-
Flanged Nylon Bushing	36	McMaster-Carr #6389K552
¼-20 x 0.50” Set Screw	37	McMaster-Carr #92845A129

Appendix C: Cost Spreadsheet

Item	Cost	Quantity	Net Cost
8" x 8" x 3/8" Al plate	$14.82	1	$14.82
2" Round Al Extruded	$17.54	1	$17.54
2.25" Round Al Extruded	$22.20	1	$22.20
2.5" Round Al Extruded	$27.41	1	$27.41
8-32 7/8" Machine Screw	$4.93	1	$4.93
8-32 3/4" Machine Screw	$3.58	1	$3.58
Linch Pin	$2.09	2	$4.18
Retaining Ring for 3/8" Shaft, 10 pack	$8.36	1	$8.36
3/8" Nylon Thrust Bearing	$1.27	4	$5.08
1/2"-13 x 1" Machine Screw, 10 pack	$5.93	1	$5.93
R12 Ball Bearing	$3.99	2	$7.98
Shipping, item 18	$7.02	1	$7.02
Waterjet cut	$100.00	1	$100.00
6061 Al 2" Square 10-12" length	$21.54	1	$21.54
4130 Steel 12x12x.125" sheet	$27.36	1	$27.36

6061 Al drawn tube, 1" OD .125" wall, 2 ft long	$15.76	1	$15.76
6061 Al 2" Cylinder 10-12" length	$15.89	1	$15.89
6061 Al 0.875"x0.12"x0.635" round 24" length	$18.09	2	$36.18
6061 Al 0.625" x 0.125" x 0.375" round 24" length	$20.15	2	$40.30
6061 Al 0.625" x 0.125" x 0.375" round 24" length	$13.84	2	$27.68
McMaster Jumbo Steel Compression Spring, 10" 42 lb/in	$18.63	2	$37.26
Gibson vault non-linear conical spring	$11.00	2	$22.00
		TOTAL	**$473.00**

Appendix D: CAD Documentation

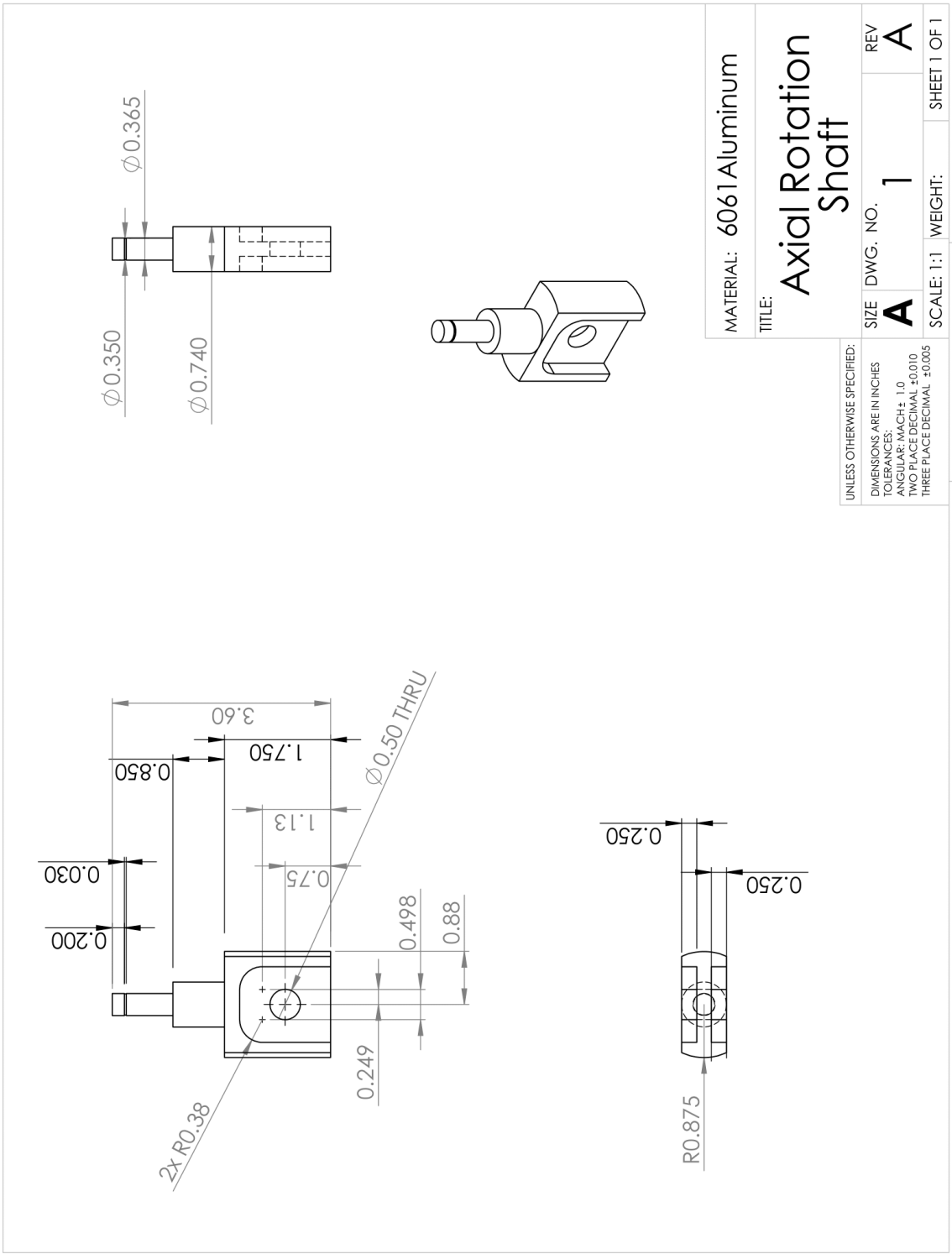

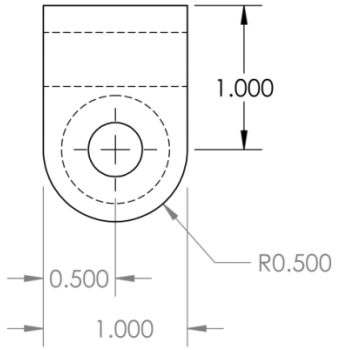

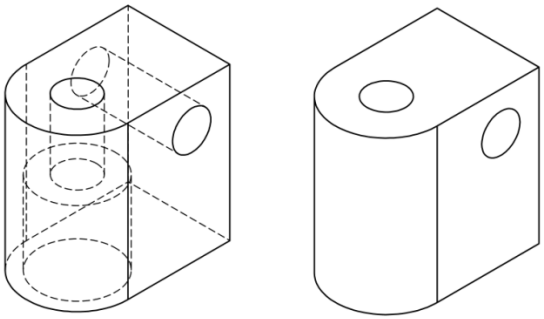

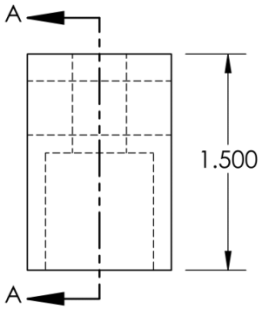

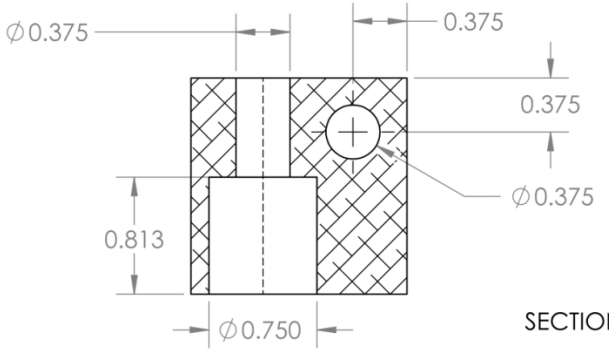

SECTION A-A

MATERIAL:	6061 Aluminum
TITLE:	Abduction Collar
UNLESS OTHERWISE SPECIFIED:	
DIMENSIONS ARE IN INCHES TOLERANCES: ANGULAR: MACH± 1.0 TWO PLACE DECIMAL ±0.010 THREE PLACE DECIMAL ±0.005	
SIZE: A	DWG. NO.: 2
REV: A	
SCALE: 1:1	WEIGHT:
SHEET 1 OF 1	

5 3 2 1

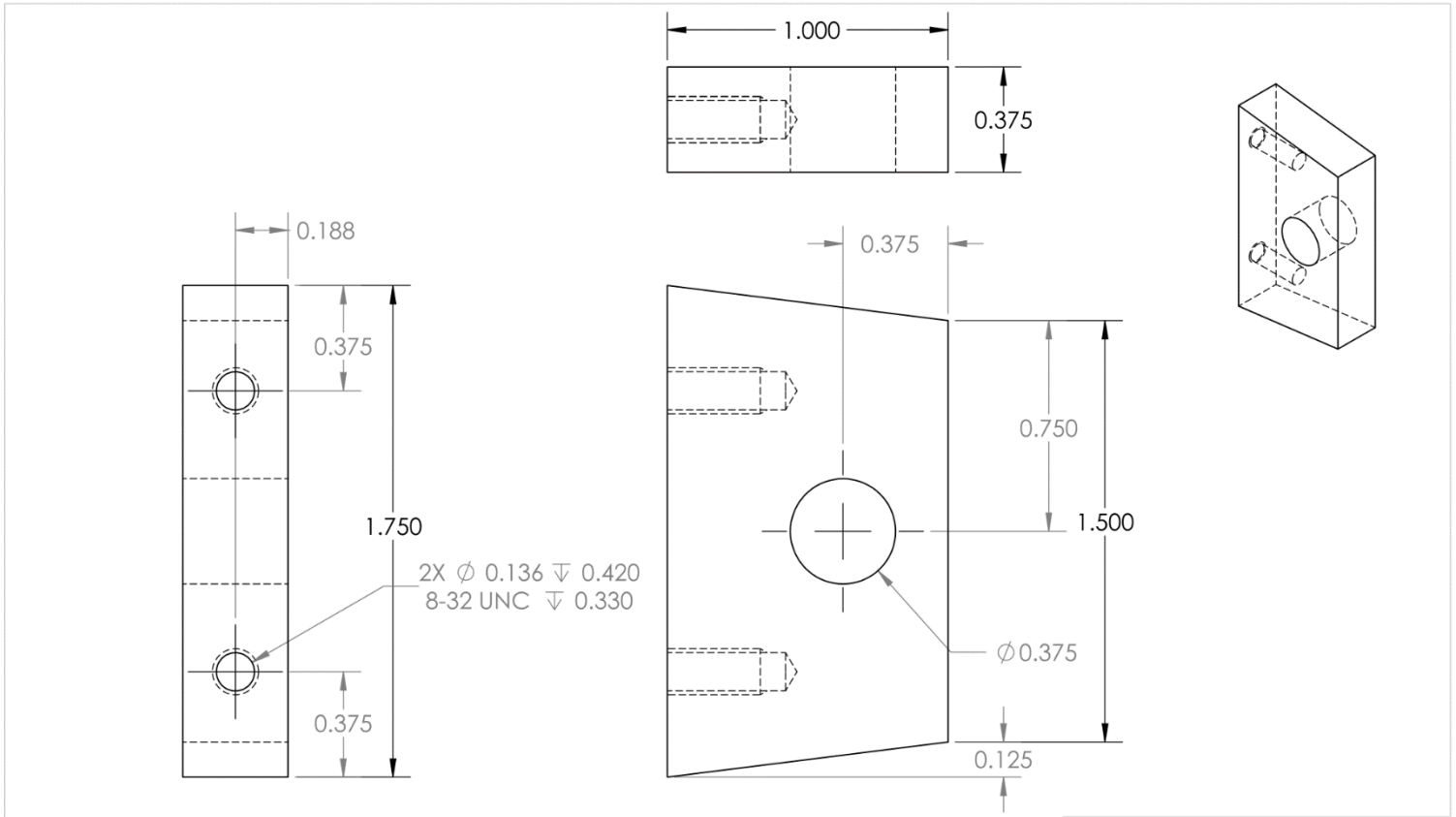

MATERIAL:	6061Aluminum
TITLE:	Linch Pin Plate

UNLESS OTHERWISE SPECIFIED:

DIMENSIONS ARE IN INCHES
TOLERANCES:
ANGULAR: MACH± 1.0
TWO PLACE DECIMAL ±0.010
THREE PLACE DECIMAL ±0.005

SIZE	DWG. NO.	REV
A	3	A

SCALE: 2:1	WEIGHT:	SHEET 1 OF 1

5 3 2 1

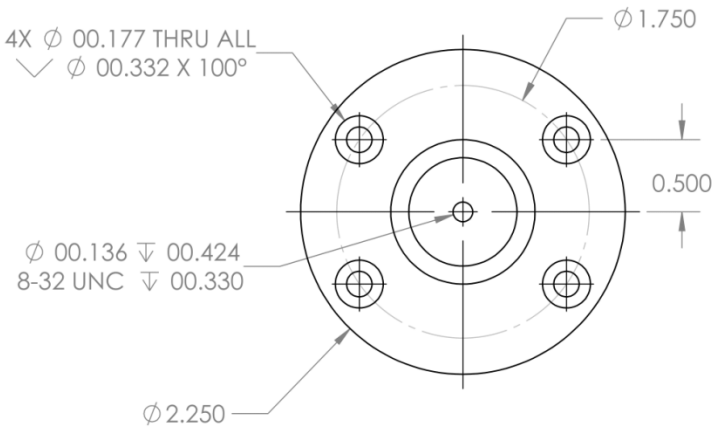

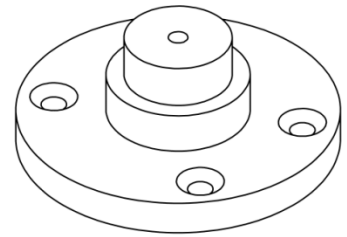

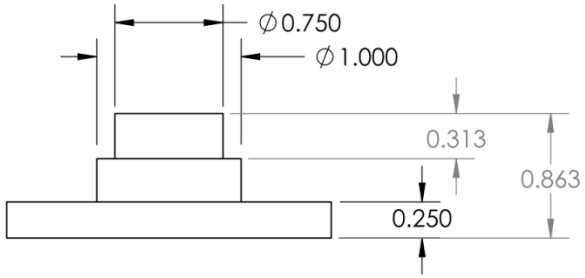

MATERIAL: 6061Aluminum			
TITLE: Hip Flexion Plate			
UNLESS OTHERWISE SPECIFIED: DIMENSIONS ARE IN INCHES TOLERANCES: ANGULAR: MACH± 1.0 TWO PLACE DECIMAL ±0.010 THREE PLACE DECIMAL ±0.005	SIZE A	DWG. NO. 4	REV A
	SCALE: 1:1	WEIGHT:	SHEET 1 OF 1

5 3 2 1

SECTION A-A
SCALE 1 : 1

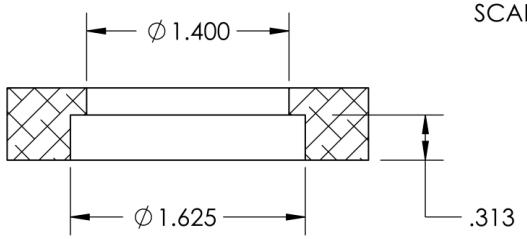

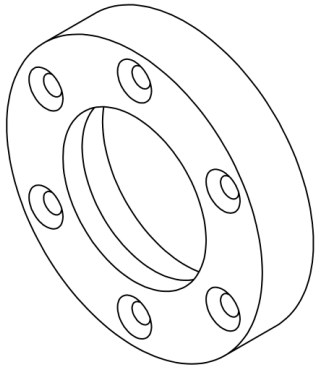

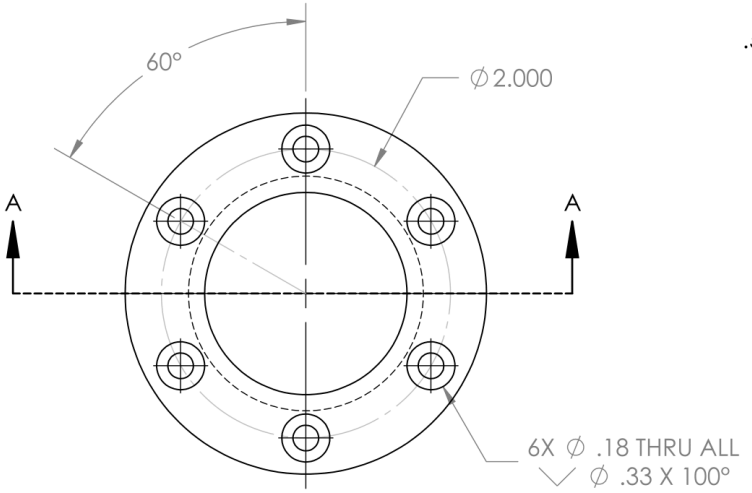

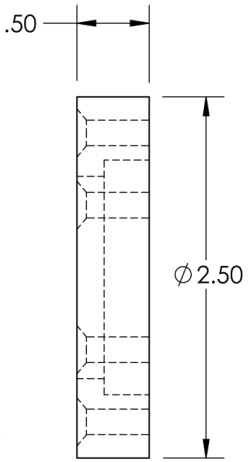

MATERIAL: Aluminum

TITLE:
Bearing Collar

UNLESS OTHERWISE SPECIFIED:

DIMENSIONS ARE IN INCHES
TOLERANCES:
ANGULAR: MACH± 1.0
TWO PLACE DECIMAL ±0.010
THREE PLACE DECIMAL ±0.005

SIZE	DWG. NO.	REV
A	6	B

SCALE: 1:1 | WEIGHT: | SHEET 1 OF 1

5 3 2 1

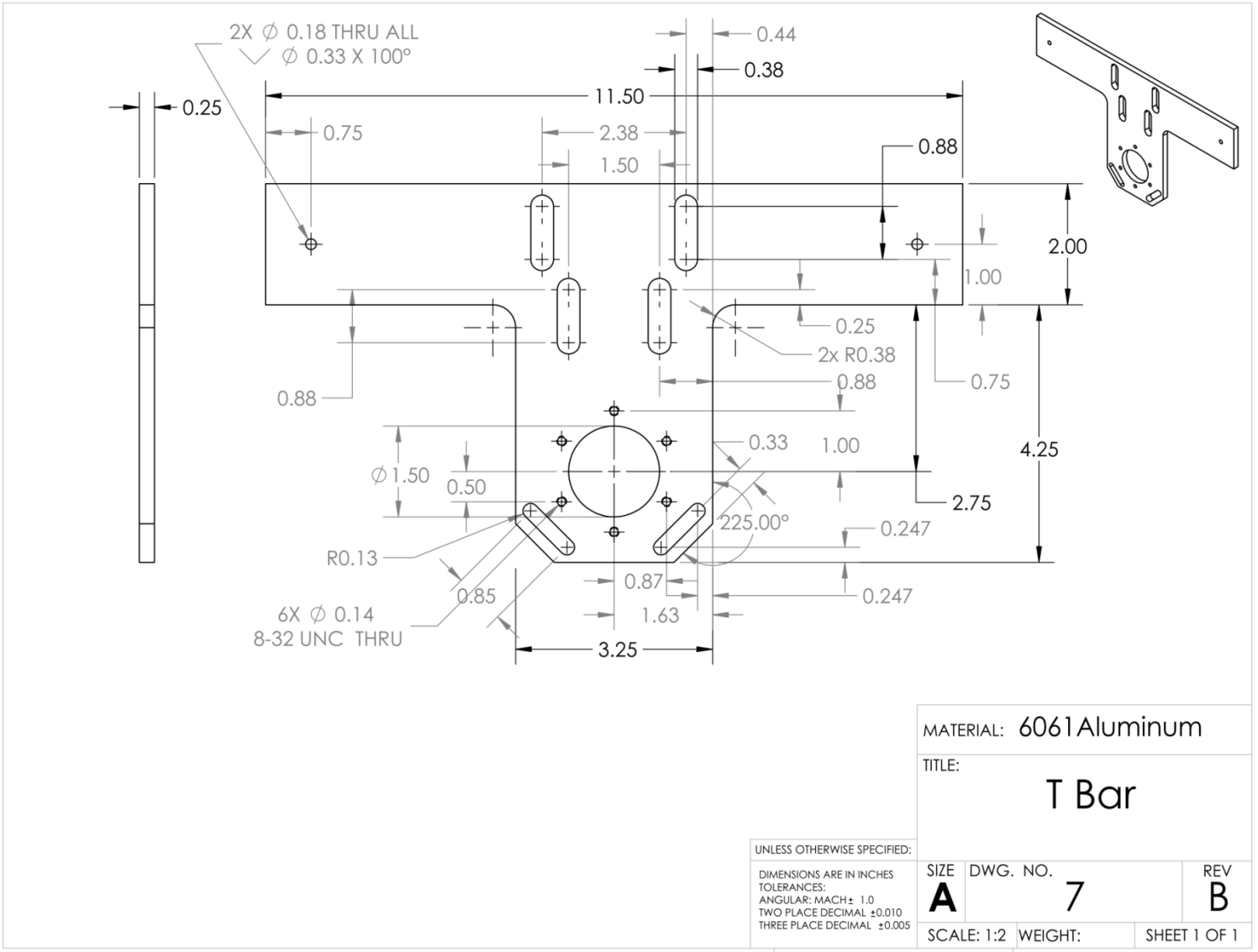

MATERIAL:	6061Aluminum
TITLE:	T Bar
UNLESS OTHERWISE SPECIFIED:	
DIMENSIONS ARE IN INCHES TOLERANCES: ANGULAR: MACH± 1.0 TWO PLACE DECIMAL ±0.010 THREE PLACE DECIMAL ±0.005	
SIZE: A	DWG. NO.: 7
REV: B	
SCALE: 1:2	WEIGHT:
SHEET 1 OF 1	

5 3 2 1

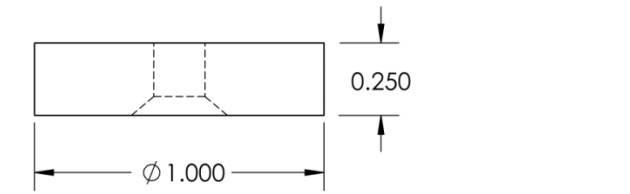

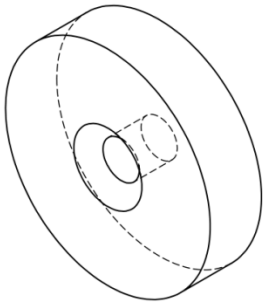

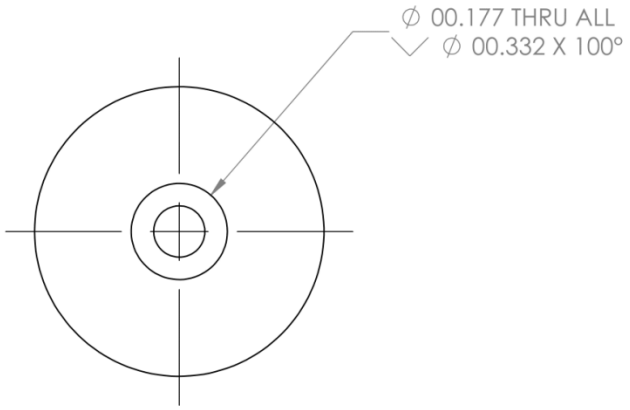

MATERIAL: 6061Aluminum		
TITLE: Bearing Cap		
UNLESS OTHERWISE SPECIFIED: DIMENSIONS ARE IN INCHES TOLERANCES: ANGULAR: MACH ± 1.0 TWO PLACE DECIMAL ±0.010 THREE PLACE DECIMAL ±0.005	SIZE A / DWG. NO. 9 / REV A	
	SCALE: 2:1	WEIGHT: / SHEET 1 OF 1

5 3 2 1

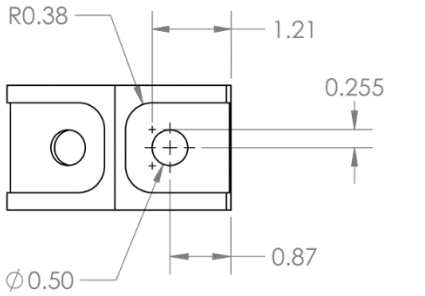

Sides are Mirrored about vertex

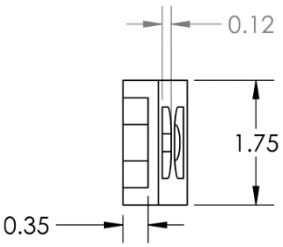

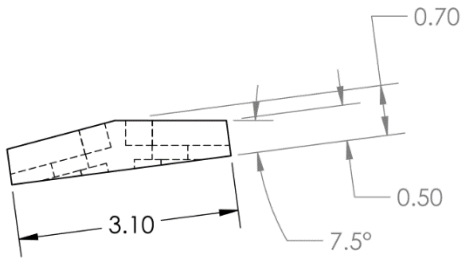

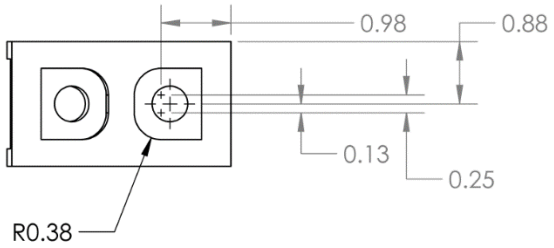

MATERIAL: 6061 Aluminum		
TITLE: Knee Joint		
UNLESS OTHERWISE SPECIFIED:		
DIMENSIONS ARE IN INCHES TOLERANCES: ANGULAR: MACH± 1.0 TWO PLACE DECIMAL ±0.010 THREE PLACE DECIMAL ±0.005	SIZE A / DWG. NO. 15	REV B
	SCALE: 1:2 / WEIGHT:	SHEET 1 OF 1

5 3 2 1

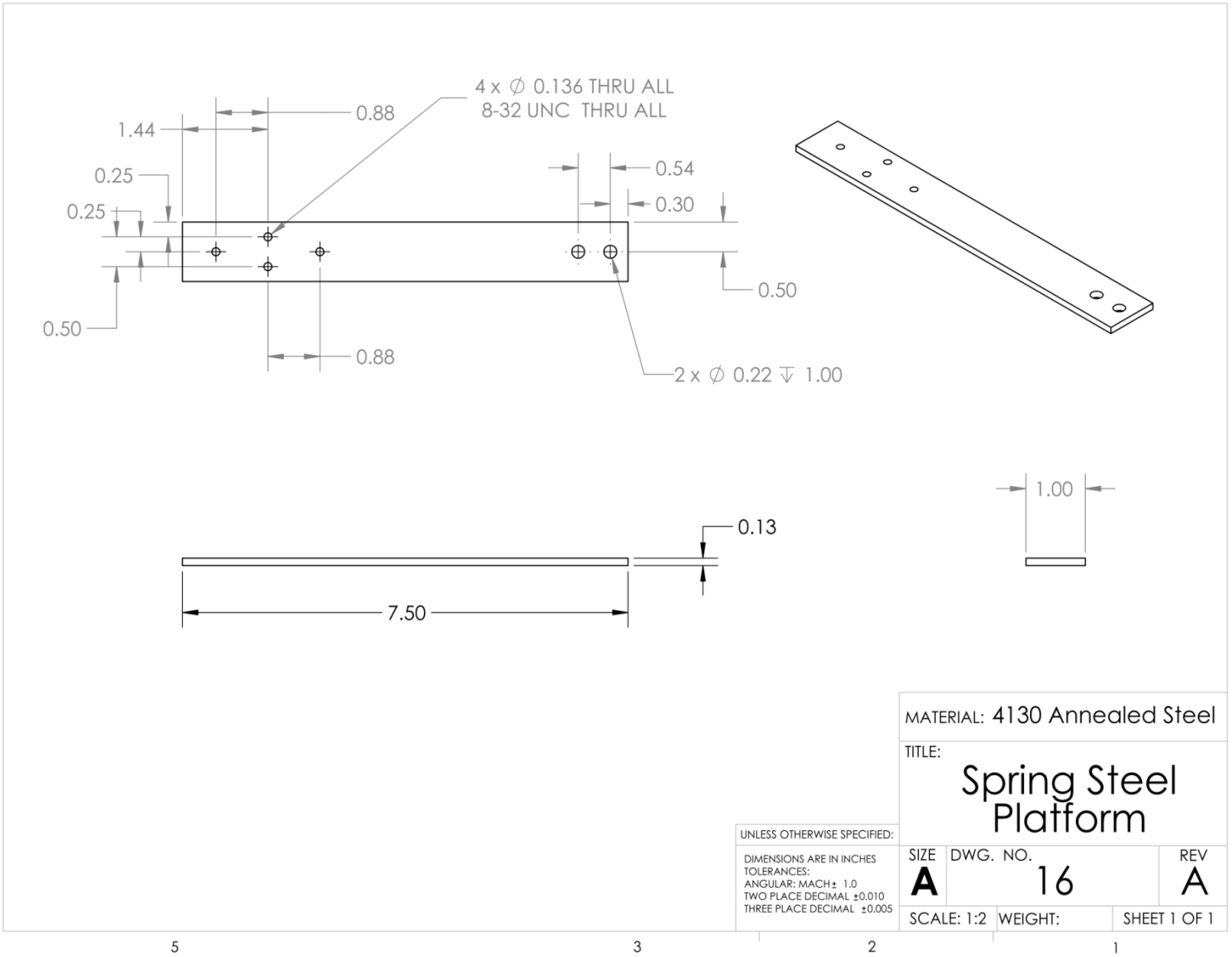
4 x ∅ 0.136 THRU ALL
8-32 UNC THRU ALL
0.88
1.44
0.25
0.25
0.54
0.30
0.50
0.50
0.88
2 x ∅ 0.22 ↧ 1.00
1.00
0.13
7.50
MATERIAL: 4130 Annealed Steel
TITLE:
Spring Steel Platform
UNLESS OTHERWISE SPECIFIED:
DIMENSIONS ARE IN INCHES
TOLERANCES:
ANGULAR: MACH± 1.0
TWO PLACE DECIMAL ±0.010
THREE PLACE DECIMAL ±0.005
SIZE
A
DWG. NO.
16
REV
A
SCALE: 1:2
WEIGHT:
SHEET 1 OF 1
5
3
2
1

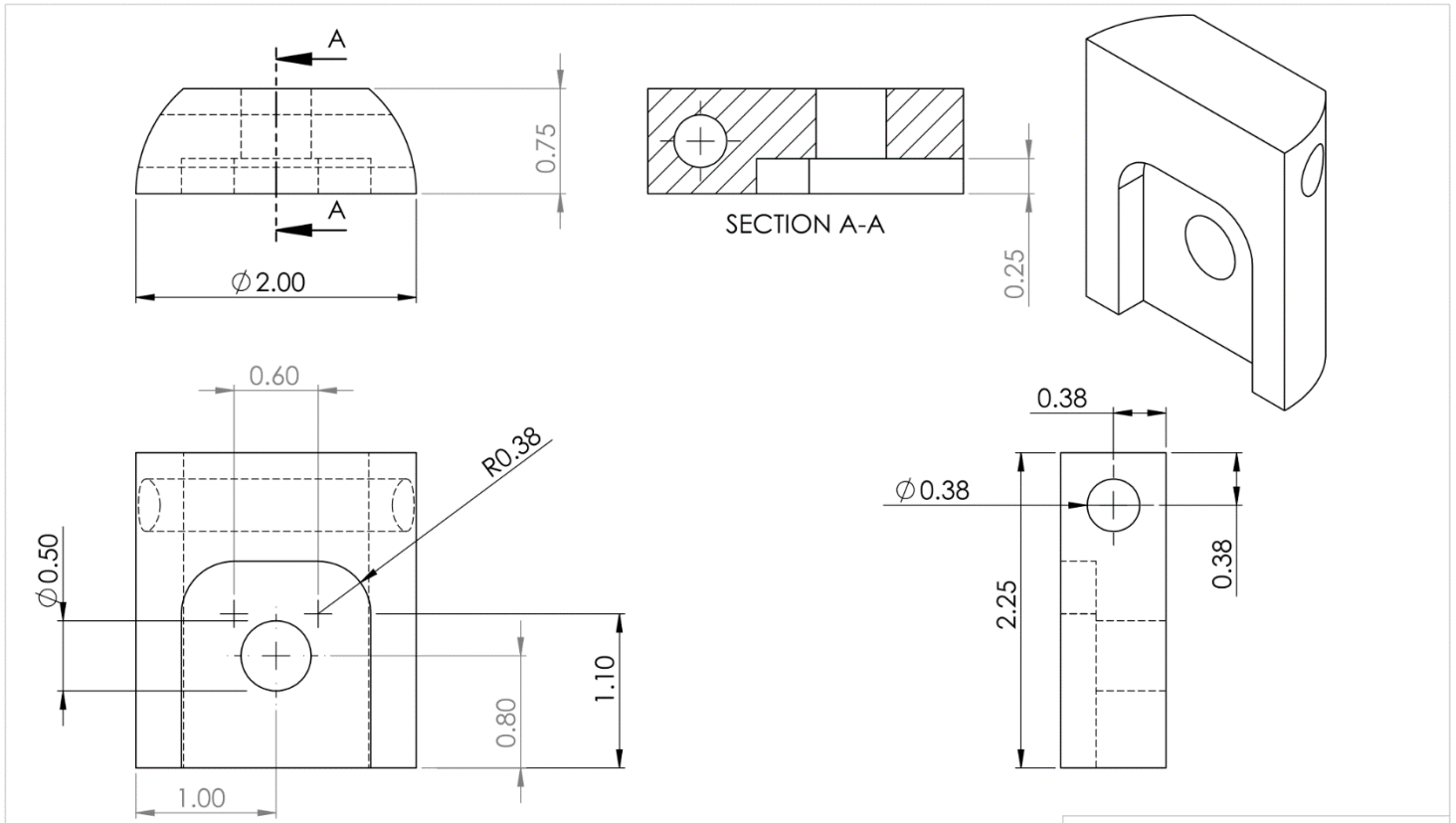
A
A
0.75
⌀2.00
SECTION A-A
0.25
0.60
R0.38
⌀0.50
1.10
0.80
1.00
0.38
⌀0.38
2.25
0.38
MATERIAL: 6061Aluminum
TITLE:
Spring
Deflection Joint
UNLESS OTHERWISE SPECIFIED:
DIMENSIONS ARE IN INCHES
TOLERANCES:
ANGULAR: MACH ± 1.0
TWO PLACE DECIMAL ±0.010
THREE PLACE DECIMAL ±0.005
SIZE
A
DWG. NO.
17
REV
A
SCALE: 1:1
WEIGHT:
SHEET 1 OF 1
5
3
2
1

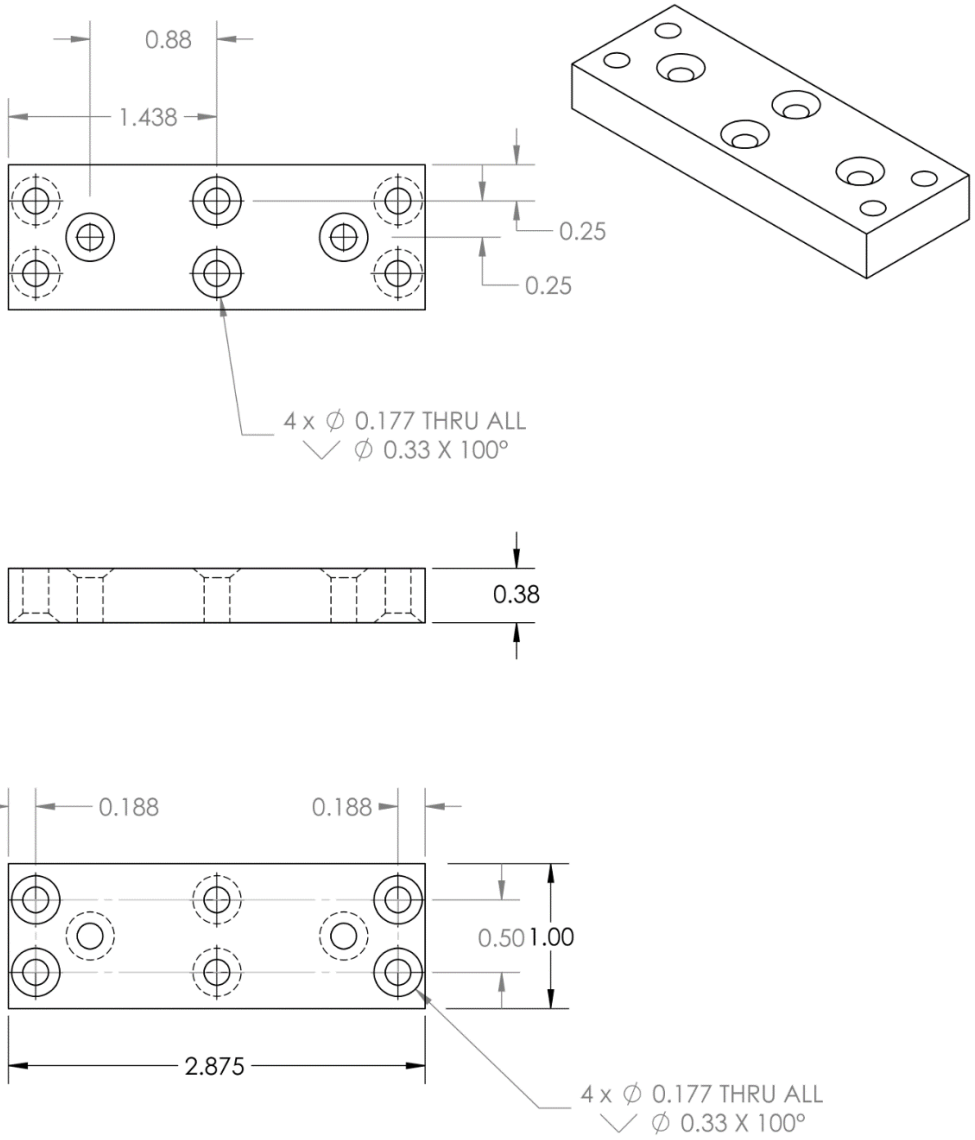

MATERIAL: 6061 Aluminum

TITLE:

Ankle Joint Plate

UNLESS OTHERWISE SPECIFIED:

DIMENSIONS ARE IN INCHES
TOLERANCES:
ANGULAR: MACH ± 1.0
TWO PLACE DECIMAL ±0.010
THREE PLACE DECIMAL ±0.005

SIZE	DWG. NO.	REV
A	18	B
SCALE: 1:2	WEIGHT:	SHEET 1 OF 1

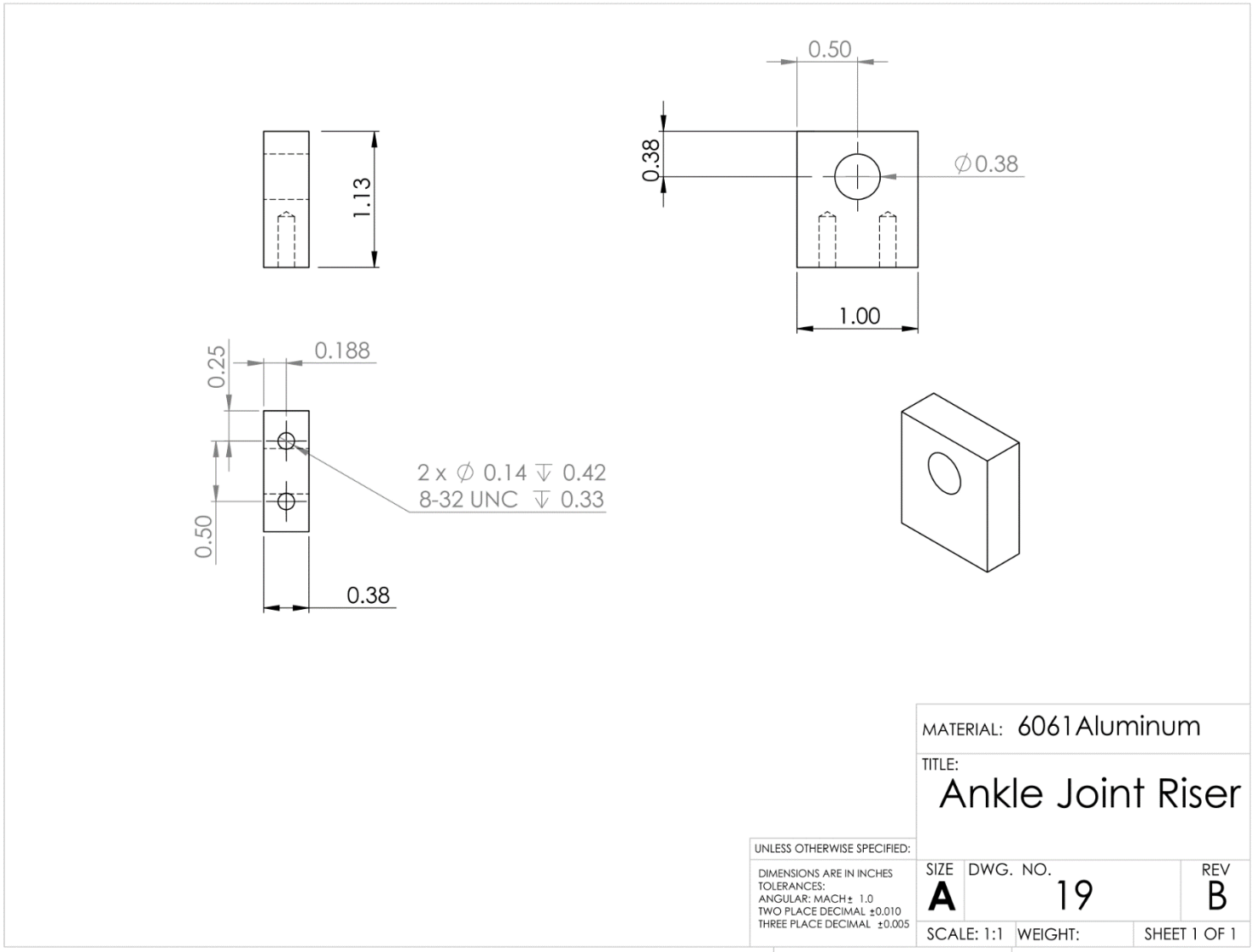
0.50
0.38
∅0.38
1.00
1.13
0.188
0.25
2 x ∅ 0.14 ↧ 0.42
8-32 UNC ↧ 0.33
0.50
0.38
MATERIAL: 6061 Aluminum
TITLE:
Ankle Joint Riser
UNLESS OTHERWISE SPECIFIED:
DIMENSIONS ARE IN INCHES
TOLERANCES:
ANGULAR: MACH ± 1.0
TWO PLACE DECIMAL ±0.010
THREE PLACE DECIMAL ±0.005
SIZE
A
DWG. NO.
19
REV
B
SCALE: 1:1
WEIGHT:
SHEET 1 OF 1
5
3
2
1

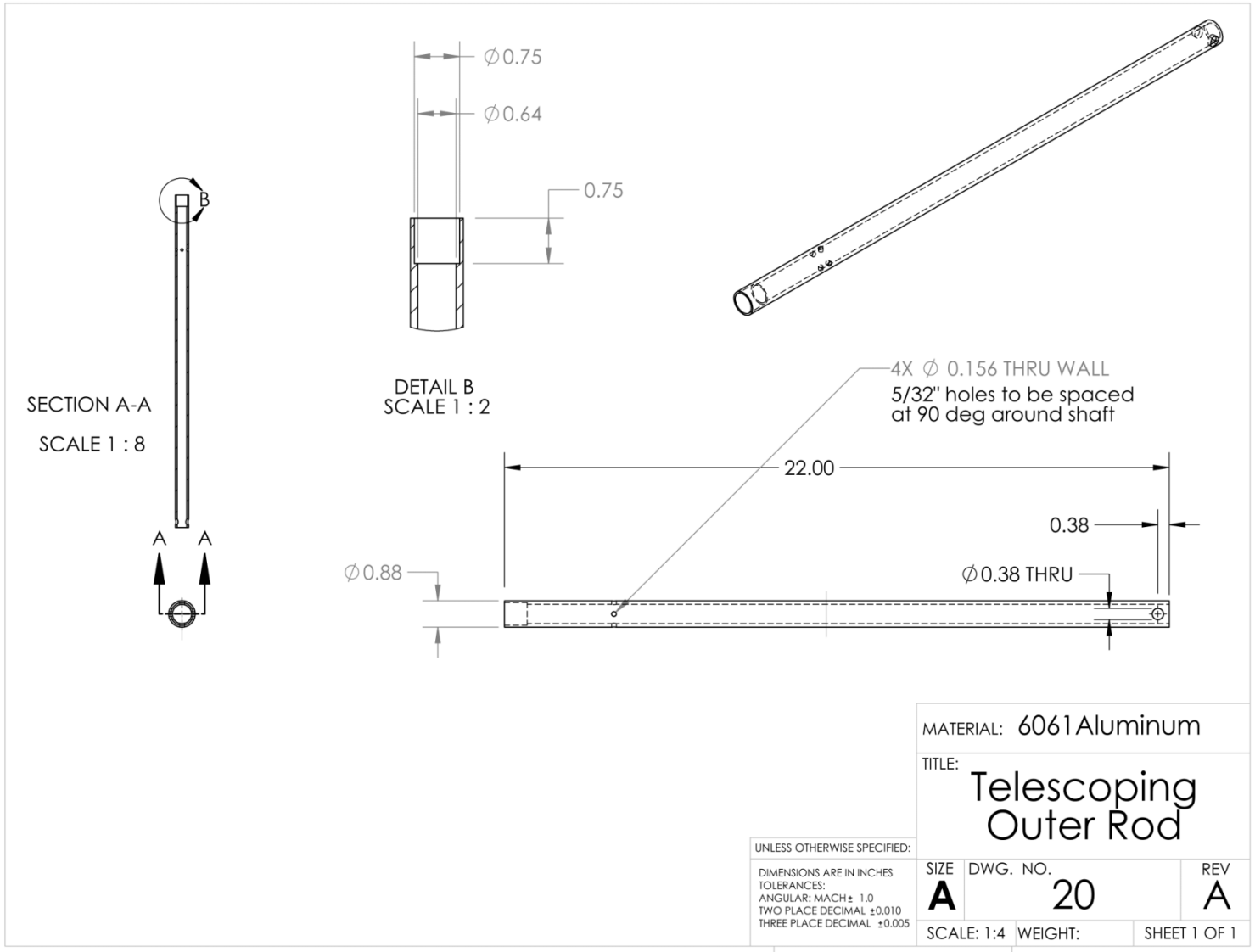
∅0.75
∅0.64
0.75
B
SECTION A-A
SCALE 1 : 8
A
A
DETAIL B
SCALE 1 : 2
4X ∅ 0.156 THRU WALL
5/32" holes to be spaced
at 90 deg around shaft
22.00
0.38
∅0.88
∅0.38 THRU
MATERIAL: 6061Aluminum
TITLE:
Telescoping
Outer Rod
UNLESS OTHERWISE SPECIFIED:
DIMENSIONS ARE IN INCHES
TOLERANCES:
ANGULAR: MACH± 1.0
TWO PLACE DECIMAL ±0.010
THREE PLACE DECIMAL ±0.005
SIZE
A
DWG. NO.
20
REV
A
SCALE: 1:4
WEIGHT:
SHEET 1 OF 1
5
3
2
1

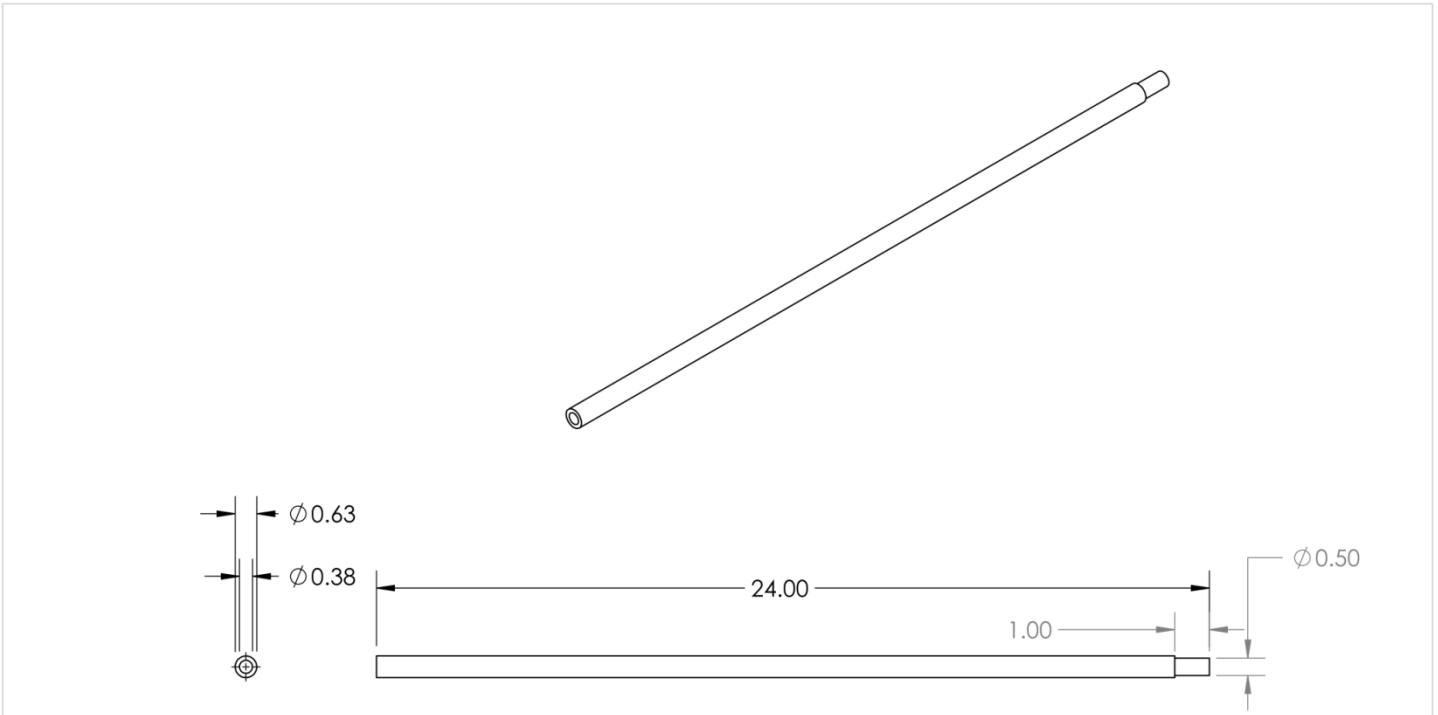

MATERIAL:	6061 Aluminum
TITLE:	Telescoping Inner Rod
UNLESS OTHERWISE SPECIFIED:	
DIMENSIONS ARE IN INCHES TOLERANCES: ANGULAR: MACH ± 1.0 TWO PLACE DECIMAL ±0.010 THREE PLACE DECIMAL ±0.005	
SIZE: A	DWG. NO. 21
REV: A	
SCALE: 1:4	WEIGHT:
SHEET 1 OF 1	

5 3 2 1

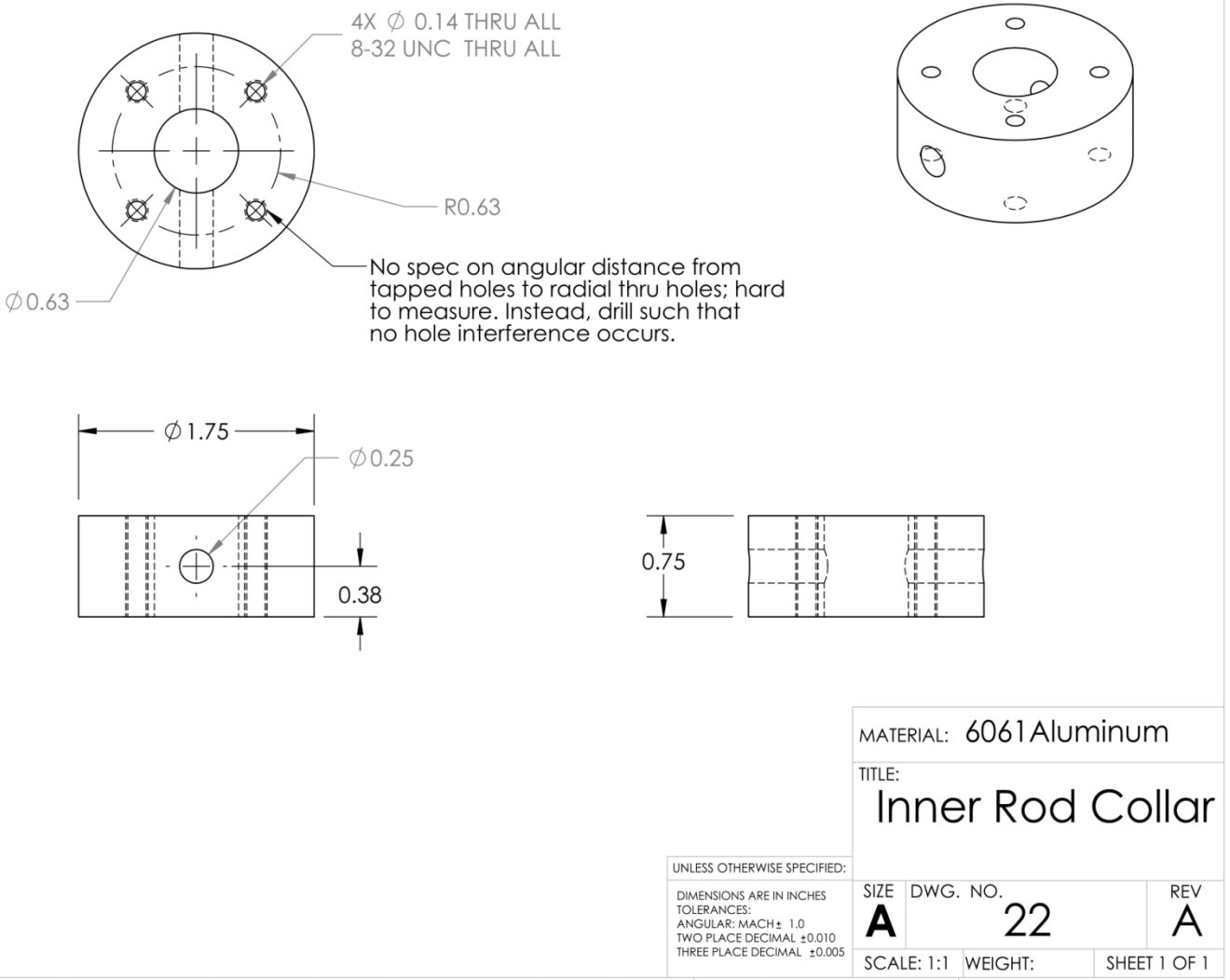
4X ∅ 0.14 THRU ALL
8-32 UNC THRU ALL
R0.63
∅0.63
No spec on angular distance from tapped holes to radial thru holes; hard to measure. Instead, drill such that no hole interference occurs.
∅1.75
∅0.25
0.38
0.75
MATERIAL: 6061Aluminum
TITLE:
Inner Rod Collar
UNLESS OTHERWISE SPECIFIED:
DIMENSIONS ARE IN INCHES
TOLERANCES:
ANGULAR: MACH ± 1.0
TWO PLACE DECIMAL ±0.010
THREE PLACE DECIMAL ±0.005
SIZE
A
DWG. NO.
22
REV
A
SCALE: 1:1
WEIGHT:
SHEET 1 OF 1
5
3
2
1

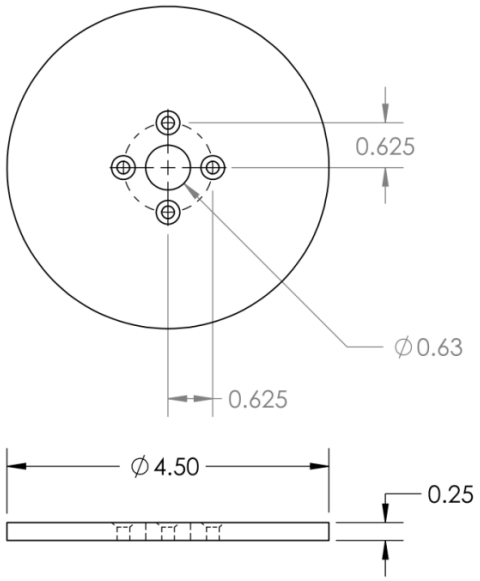

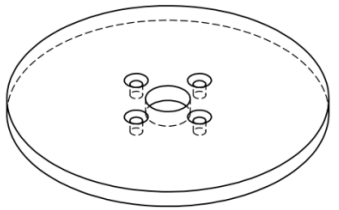

MATERIAL: 6061 Aluminum		
TITLE: Inner Spring Plate		
UNLESS OTHERWISE SPECIFIED: DIMENSIONS ARE IN INCHES TOLERANCES: ANGULAR: MACH ± 1.0 TWO PLACE DECIMAL ±0.010 THREE PLACE DECIMAL ±0.005	SIZE A / DWG. NO. 23	REV A
	SCALE: 1:2 / WEIGHT:	SHEET 1 OF 1

5 3 2 1

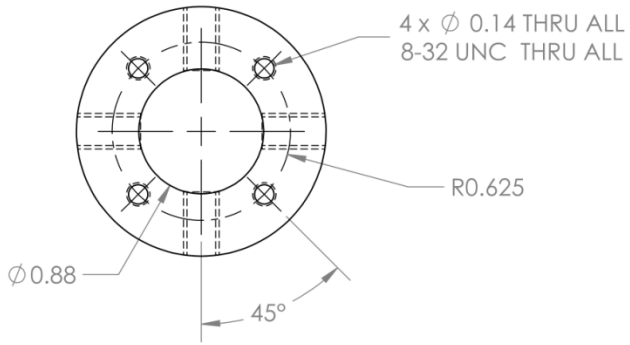

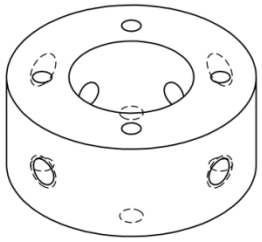

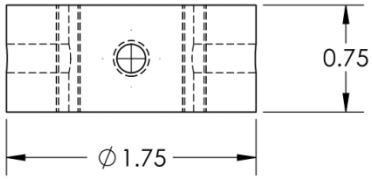

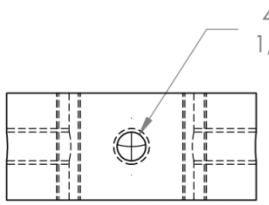

MATERIAL: 6061 Aluminum		
TITLE: Outer Rod Collar		
UNLESS OTHERWISE SPECIFIED: DIMENSIONS ARE IN INCHES TOLERANCES: ANGULAR: MACH ± 1.0 TWO PLACE DECIMAL ±0.010 THREE PLACE DECIMAL ±0.005	SIZE A / DWG. NO. 24	REV A
	SCALE: 1:1 / WEIGHT:	SHEET 1 OF 1

5 3 2 1

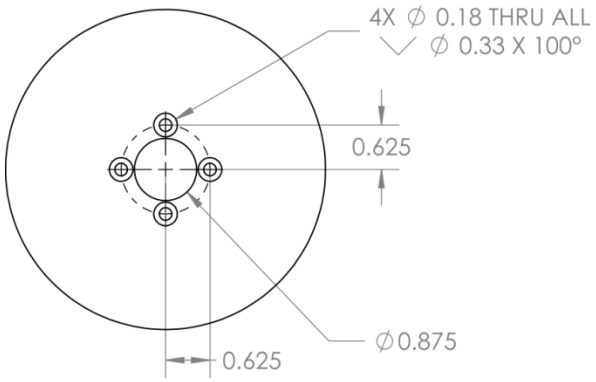

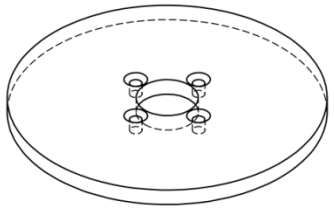

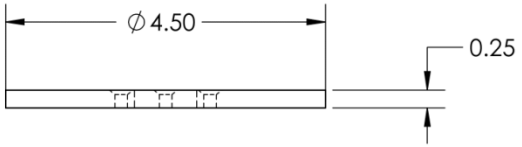

MATERIAL: 6061 Aluminum			
TITLE: Outer Spring Plate			
UNLESS OTHERWISE SPECIFIED:	SIZE	DWG. NO.	REV
DIMENSIONS ARE IN INCHES TOLERANCES: ANGULAR: MACH ± 1.0 TWO PLACE DECIMAL ±0.010 THREE PLACE DECIMAL ±0.005	A	25	A
	SCALE: 1:2	WEIGHT:	SHEET 1 OF 1

5 3 2 1

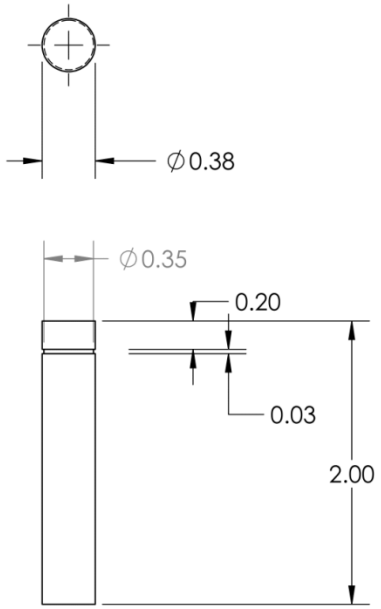

This small piece is adhered inside the upper end of the inner telescoping rod (part #21)using epoxy for metal surfaces. The grooved end should protrude from the rod 1.00".

MATERIAL: 6061Aluminum

TITLE:

Axial Rotation Attachment

UNLESS OTHERWISE SPECIFIED:

DIMENSIONS ARE IN INCHES
TOLERANCES:
ANGULAR: MACH ± 1.0
TWO PLACE DECIMAL ±0.010
THREE PLACE DECIMAL ±0.005

SIZE	DWG. NO.	REV
A	26	A

SCALE: 1:1	WEIGHT:	SHEET 1 OF 1

5 3 2 1

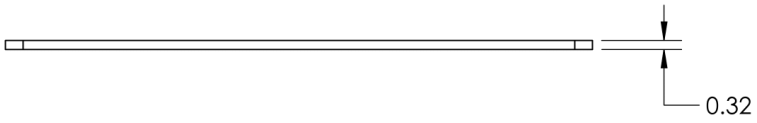

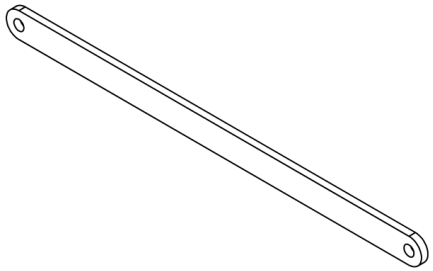

The length dimension is varied according to the leg length of the wearer. A range of springs between 14.50 and 19.50 inches, at one-inch intervals, sufficed for the study.

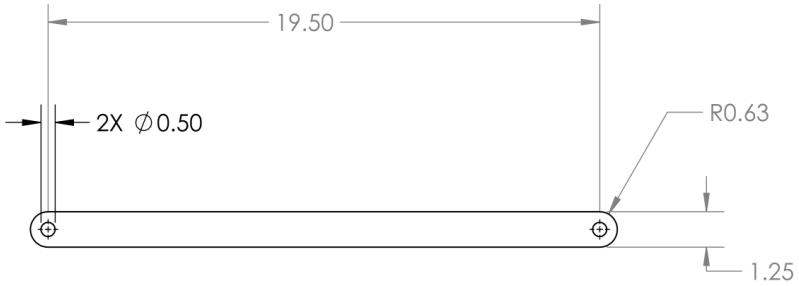

MATERIAL:	GC-67-UB Fiberglass
TITLE:	Bow Spring
UNLESS OTHERWISE SPECIFIED:	
DIMENSIONS ARE IN INCHES TOLERANCES: ANGULAR: MACH± 1.0 TWO PLACE DECIMAL ±0.010 THREE PLACE DECIMAL ±0.005	
SIZE: A	DWG. NO. 28
REV: A	
SCALE: 1:5	WEIGHT:
SHEET 1 OF 1	

5 3 2 1

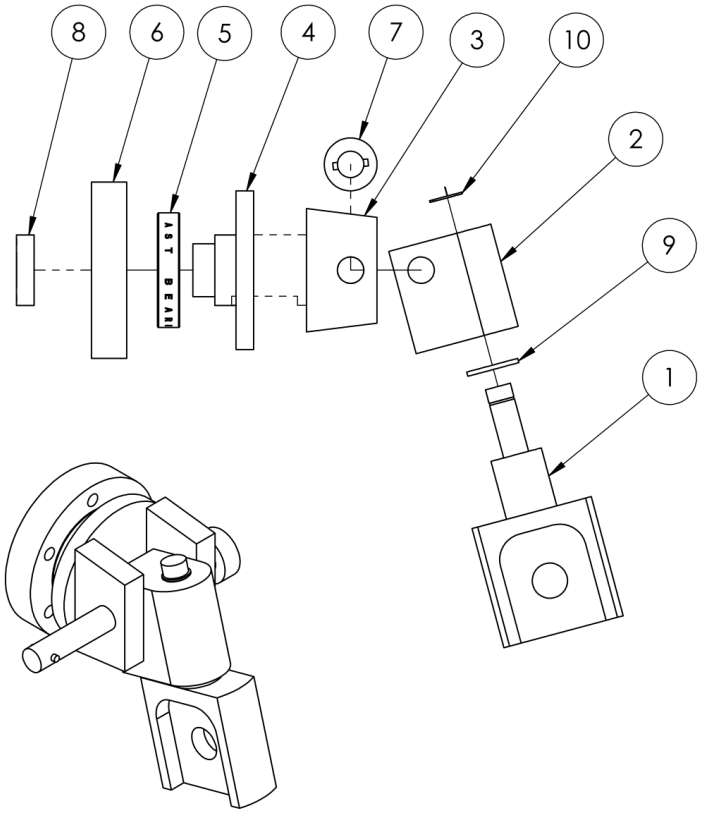

ITEM NO.	PART NUMBER	DESCRIPTION	QTY.
1	1	Axial Rotation Shaft	1
2	2	Abduction Collar	1
3	3	Linch Pin Plate	2
4	4	Hip Flexion Plate	1
5	5	R12 Bearing	1
6	6	Bearing Collar	1
7	98416A019	Linch Pin	1
8	9	Bearing Cap	1
9	2797T2	Nylon Thrust Bearing	1
10	97633A170	Retaining Ring	1

UNLESS OTHERWISE SPECIFIED:

DIMENSIONS ARE IN INCHES
TOLERANCES:
ANGULAR: MACH ± 1.0
TWO PLACE DECIMAL ±0.010
THREE PLACE DECIMAL ±0.005

MATERIAL: -

TITLE:

Hip Joint Assembly

SIZE	DWG. NO.	REV
A	32	B

SCALE: 1:1 | WEIGHT: | SHEET 1 OF 1

5 3 2 1

ITEM NO.	PART NUMBER	DESCRIPTION	QTY.
1	7	T-Bar	2
2	10	Inner Frame Rod	2
3	11	Outer Frame Rod	2
4	12	Outer Frame Interference Plug	2
5	32	Hip Joint Assembly	2
6	90273A198	#8 x 7/8" Machine Screw	4
7	90910A777	#8-32 x 3/4" Button Head Screw	12

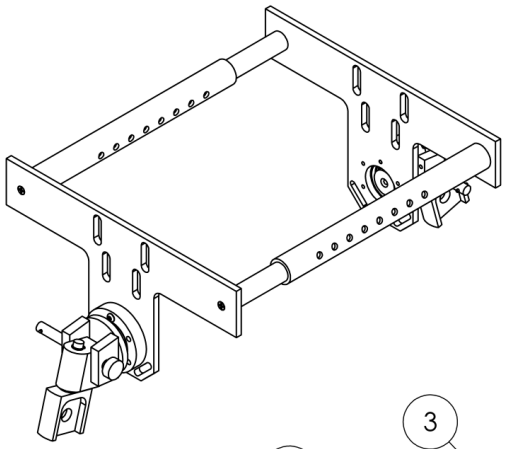

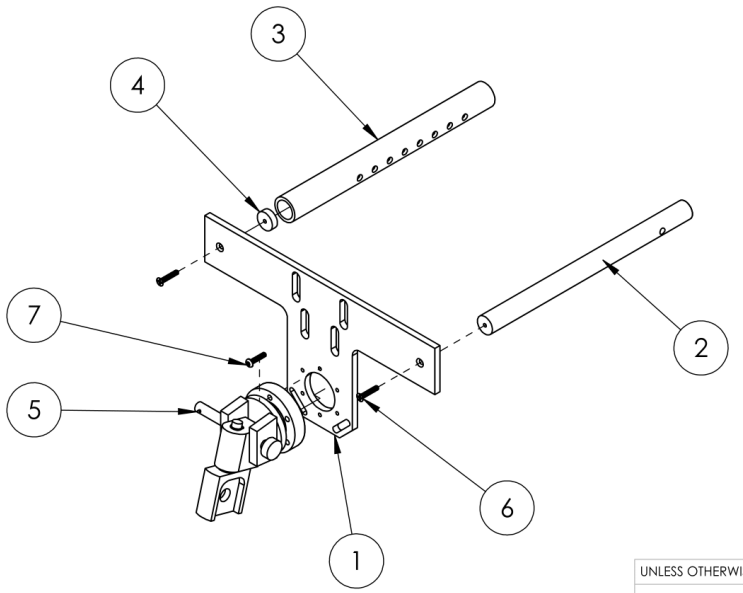

UNLESS OTHERWISE SPECIFIED:

DIMENSIONS ARE IN INCHES
TOLERANCES:
ANGULAR: MACH ± 1.0
TWO PLACE DECIMAL ±0.010
THREE PLACE DECIMAL ±0.005

MATERIAL: -

TITLE:

Hip Frame Assembly

SIZE	DWG. NO.	REV
A	33	B

SCALE: 1:5 | WEIGHT: | SHEET 1 OF 1

5 3 2 1

ITEM NO.	PART NUMBER	DESCRIPTION	QTY.
1	14	Spring Deflection Joint	1
2	15	Ankle Flexion Riser	2
3	16	Ankle Flexion Plate	1
4	17	Spring Steel Platform	1
5	98416A019	Linch Pin	1

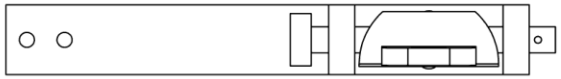

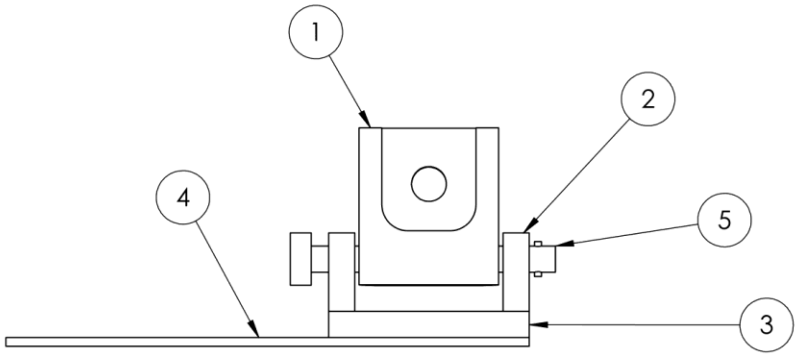

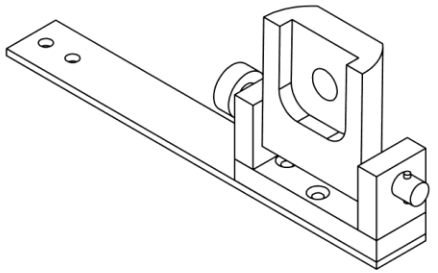

MATERIAL: -

TITLE:
Shoe Attachment Assembly

UNLESS OTHERWISE SPECIFIED:

DIMENSIONS ARE IN INCHES
TOLERANCES:
ANGULAR: MACH± 1.0
TWO PLACE DECIMAL ±0.010
THREE PLACE DECIMAL ±0.005

SIZE	DWG. NO.	REV
A	34	B

SCALE: 1:2	WEIGHT:	SHEET 1 OF 1

5 3 2 1

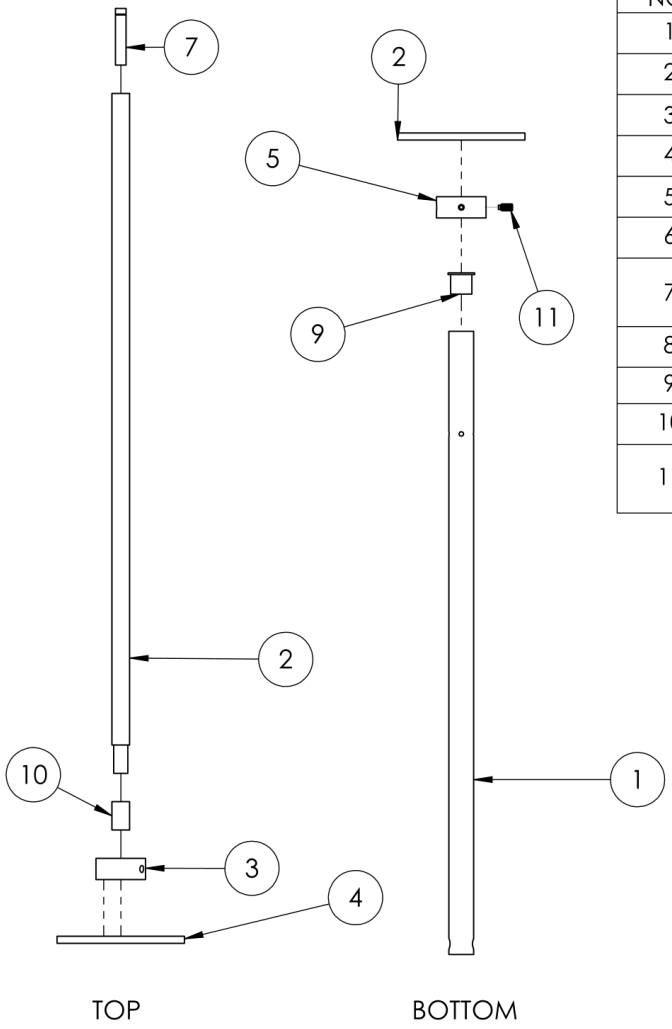

ITEM NO.	PART NUMBER	DESCRIPTION	QTY.
1	20	Telescoping Outer Rod	1
2	21	Telescoping Inner Rod	1
3	22	Inner Rod Collar	1
4	23	Inner Spring Plate	1
5	24	Outer Rod Collar	1
6	25	Outer Rod Spring Plate	1
7	26	Axial Rotation Attachment	1
8	29	Compression Spring	1
9	6389K552	Flanged Nylon Bearing	1
10	6389K117	Nylon Sleeve Bearing	1
11	92845A129	1/4-20 x 1/2" Dog End Set Screw	4

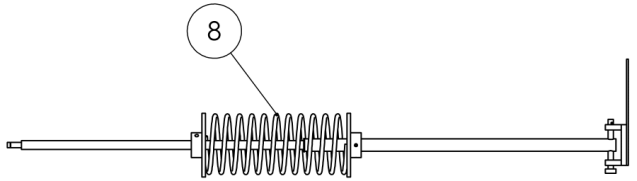

MATERIAL: -

TITLE: Coil Spring Assembly

UNLESS OTHERWISE SPECIFIED:

DIMENSIONS ARE IN INCHES
TOLERANCES:
ANGULAR: MACH± 1.0
TWO PLACE DECIMAL ±0.010
THREE PLACE DECIMAL ±0.005

SIZE	DWG. NO.	REV
A	35	A

SCALE: 1:5 | WEIGHT: | SHEET 1 OF 1

5 3 2 1